

**Geotechnical Properties and Flow Behavior of Fine Coal
Refuse under Static and Impact Loading**

OSM Project S12AC20022

Final Report

**Yao Yu, Ph.D.
Research Assistant**

**David Zeng, Ph.D.
Frank H. Neff Professor and Chairman**

**Dept. of Civil Engineering
Case Western Reserve University
10900 Euclid Avenue
Cleveland, Ohio 44106-7201, USA
Phone: 216-368-2923; Email: xxz16@case.edu**

And

**Peter R. Michael, PG
Geologist
US Office of Surface Mining Reclamation and Enforcement
Appalachian Regional Office
3 Parkway Center
Pittsburgh, PA 15220, USA
Phone: 412-937-2867; Email: pmichael@osmre.gov**

June 30, 2015

TABLE OF CONTENTS

LIST OF TABLES	IV
LIST OF FIGURES	VI
ACKNOWLEDGMENTS	XI
ABSTRACT.....	XII
NOTATION.....	XIII
Chapter 1 INTRODUCTION	1
1.1 Background.....	1
1.2 Review of Tailings Dams.....	2
1.3 Review of Flow Failure of Tailings Dams.....	7
1.4 Review of Breakthrough of Impounded Coal Refuse into Underground Mine.	11
1.5 Review of Flow Failure Prevention for Coal Waste Impoundments	13
1.6 Research Objectives.....	16
1.7 Outline of the Report	16
Chapter 2 GEOTECHNICAL PROPERTIES OF COAL WASTE SLURRY.....	18
2.1 Introduction.....	18
2.2 Sample Collection and Preparation.....	18
2.3 Geotechnical Properties of Coal Waste Slurry	19
2.3.1 Particle Size Distribution	20
2.3.2 Specific Gravity	24
2.3.3 Atterberg Limits Tests	24
2.3.4 Consolidation Tests.....	29
2.3.5 Permeability Tests.....	42

2.3.6	Triaxial Tests	49
2.3.7	Viscosity Tests	62
2.4	Conclusions.....	74

Chapter 3 ANALYSIS OF FLOW BEHAVIOR OF COAL WASTE SLURRY BY SMALL SCALE MODEL TESTS.....78

3.1	Introduction.....	78
3.1.1	Review of Rheological Models.....	79
3.1.2	Determine Rheological Parameters of Bingham Plastic Flow.....	82
3.2	Model Preparations and Test Procedures.....	84
3.2.1	Flume Tests under Static Loading	84
3.2.2	Flume Test under Impact Loading	86
3.3	Test Results and Analysis under Static Loading.....	88
3.3.1	Representation of Coal Waste Slurry by Bingham Plastic Model.....	95
3.3.2	Estimation of Flow Regime	104
3.3.3	Velocity Profile	109
3.3.4	Relationship between Flow Velocity and Viscosity	111
3.4	Test Results and Analysis under Impact Loading.....	113
3.5	Conclusions.....	118

Chapter 4 ANALYSIS OF FLOW BEHAVIOR OF COAL WASTE SLURRY BY CENTRIFUGE MODEL TESTS121

4.1	Introduction.....	121
4.1.1	Review of Geotechnical Centrifuge Test.....	122

4.1.2	Scaling Law	123
4.2	Facilities and Instrumentation.....	129
4.2.1	Centrifuge	129
4.2.2	Pore Pressure Transducers	132
4.2.3	Flow Container for Centrifuge Test.....	132
4.3	Model Preparations and Test Procedures.....	137
4.4	Test Results and Analysis under Static Loading.....	138
4.5	Test Results and Analysis under Impact Loading.....	144
4.6	Evaluation of Slurry Cell as a Countermeasure.....	151
4.6.1	Review of Coal Refuse Slurry Cells	151
4.6.2	Centrifuge Model Preparations	152
4.6.3	Test Results and Analysis	154
4.7	Conclusions.....	155
 Chapter 5 CONCLUSIONS AND RECOMMENDATIONS		158
5.1	Introduction.....	158
5.2	Summary of Conclusions.....	159
5.2.1	Geotechnical Properties of Impounded Coal Refuse	159
5.2.2	Flow Behavior of Impounded Coal Refuse under Static Loading.....	161
5.2.3	Flow Behavior of Impounded Coal Refuse under Impact Loading.....	163
5.2.4	Effectiveness of Slurry Cells as a Countermeasure	164
5.3	Recommendations for Future Studies.....	165
 REFERENCES.....		168

LIST OF TABLES

Table 2-1 Summary of laboratory tests conducted on coal waste slurry	21
Table 2-2 Summarized results of specific gravity test.....	23
Table 2-3 Summarized results of Atterberg limit tests	28
Table 2-4 Comparison of Compression Index C_c and Swelling Index C_s	38
Table 2-5 Compression index C_c for different types of soils (Widodo and Ibrahim, 2012)40	
Table 2-6 Typical ranges of permeability for various soils	48
Table 2-7 Typical cohesion value for different soil groups (after Lindeburg, 2003)	60
Table 2-8 Typical viscosity values of various materials (after Mezger, 2002)	64
Table 2-9 Range table of each spindle under different velocities (unit: cp).....	69
Table 2-10 Recorded viscosities of KY samples with different water content (unit: cp). 72	
Table 2-11 Recorded viscosities of WV samples with different water content (unit: cp) 73	
Table 3-1 Reference summary of published researches on the impact loading (after Charlie, 1988)	87
Table 3-2 Variation of flow velocities of KY sample with water content and slope angle (Unit: m/sec).....	90
Table 3-3 Variation of flow velocities of WV sample with water content and slope angle (Unit: m/sec).....	90
Table 3-4 Recorded travel distance and flow depth in the midstream of KY sample	91
Table 3-5 Recorded travel distance and flow depth in the midstream of WV sample	91
Table 3-6 Determination of shear rate from rotational speed	97

Table 3-7 Recorded viscosities of KY sample at different water content and shear rate .	98
Table 3-8 Recorded viscosities of WV samples at different water content and shear rate	99
Table 3-9 Determination of critical Reynolds number for KY sample	105
Table 3-10 Determination of critical Reynolds number for WV sample.....	106
Table 3-11 Determination of flow regime for KY sample	107
Table 3-12 Determination of flow regime for WV sample.....	108
Table 3-13 The summarized test results of KY sample under impact loading ($\alpha = 30^\circ$)	115
Table 3-14 The summarized test results of WV sample under impact loading ($\alpha = 30^\circ$)	116
Table 4-1 Scaling relationship for centrifuge test (N: scaling factor)	127
Table 4-2 Pore Pressure Transducer PDCR81 (Source: GE Sensing).....	132
Table 4-3 Comparison of liquid limit with critical water content in centrifuge tests	141
Table 4-4 Recorded travel distance and flow depth of two samples in the centrifuge tests	141
Table 4-5 Determination of flow regime in the centrifuge tests.....	144
Table 4-6 The summarized results of centrifuge tests under impact loading ($\alpha = 30^\circ$)..	147
Table 4-7 The summarized results of centrifuge tests with slurry cells ($\alpha = 30^\circ$).....	154

LIST OF FIGURES

Figure 1-1 Overview of a typical coal waste tailings dams (Michael et al., 2013)	3
Figure 1-2 Three construction methods for embankment (after Zeng, 2003).....	4
Figure 1-3 Disposal of fine refuse in impoundment (after Zeng, 2003).....	7
Figure 1-4 Failure of impoundment in Buffalo Creek area	9
Figure 1-5 Slurry impoundment basin and adjacent coal mine workings (after NRC, 2002)	11
Figure 1-6 Breakthrough failure occurred at the Big Branch slurry impoundment in Martin County, KY in 2000 (after MSHA, 2001)	12
Figure 2-1 Slurry sample collected from coal preparation plant	19
Figure 2-2 Particle size distribution curve for KY sample and WV sample	22
Figure 2-3 Liquid limit test on coal refuse sample (the groove has closed 12.7mm).....	25
Figure 2-4 Relationship between water content and blow number N for KY sample (Liquid Limit $w_L = 38.1$).....	26
Figure 2-5 Relationship between water content and blow number N for WV sample (Liquid Limit $w_L = 42.5$).....	27
Figure 2-6 Plastic limit test on coal refuse sample	27
Figure 2-7 Plasticity chart to use for the Unified Soil Classification System	29
Figure 2-8 Consolidation spring analogy (Anonymous, 2007)	30
Figure 2-9 Consolidometer used in consolidation test.....	33
Figure 2-10 An example plot of dial reading vs. log time in minute.....	33
Figure 2-11 Summarized results of coefficients of consolidation C_v for KY sample	35

Figure 2-12 Summarized results of coefficients of consolidation C_v of WV Sample	36
Figure 2-13 Void ratio vs. pressure for KY samples with different initial water content	38
Figure 2-14 Void ratio vs. pressure for WV samples with different initial water content	39
Figure 2-15 Compressibility of mine tailings as a function of void ratio (Qiu and Segoo, 1998)	39
Figure 2-16 A schematic diagram of constant-head permeability test (after Hanson et al., 2013)	43
Figure 2-17 A schematic diagram of constant-head permeability test (after Chang et al., 2013)	45
Figure 2-18 Falling-head permeability test apparatus	46
Figure 2-19 Comparison of permeability test results of two samples	47
Figure 2-20 Direct shear apparatus	51
Figure 2-21 Triaxial chamber with external LVDT and load cell (FHWA, 2007).....	52
Figure 2-22 Mohr stress circles and developed strength envelope	53
Figure 2-23 Prepared test sample and triaxial chamber for triaxial tests.....	55
Figure 2-24 Example of Mohr stress circles for UU triaxial test.....	56
Figure 2-25 Variation of undrained shear strength with water content	57
Figure 2-26 Results of consolidated-drained (CD) tests for KY sample	58
Figure 2-27 Results of consolidated-drained (CD) tests for WV sample	58
Figure 2-28 Variation of Φ' with water content for two samples.....	61
Figure 2-29 Shear flow by using Two-Plates-Model (after Vlachopoulos, 2003)	63
Figure 2-30 a) U-tube viscometer; b) Falling sphere viscosity.....	66
Figure 2-31 Schematic diagram of rotational viscometer (after Anonymous, 2012)	67

Figure 2-32 Structure of NDJ-8S digital rotary viscometer: (1) Level indicator (2) LCD (3) Housing (4) Protection bracket (5) Base (6) Operation key (7) Rotor connector (8) Rotor (9) Level adjustment knob.....	68
Figure 2-33 Four types of spindles of NDJ-8S digital rotary viscometer.....	69
Figure 2-34 Example plot of viscosity vs. time (water content=40%, rotational speed=6rpm)	71
Figure 2-35 Water content vs. viscosity of KY sample under different rotational speeds	73
Figure 2-36 Water content vs. viscosity of WV sample under different rotational speeds	74
Figure 3-1 Basic models of rheological behavior (after Kawatra et al., 1995).....	80
Figure 3-2 Pseudo-Bingham Plastic Model (after Krizek, 2004)	84
Figure 3-3 Small-scale model for flow study under static loading.....	85
Figure 3-4 Small-scale model test for flow study under impact loading.....	86
Figure 3-5 Example of the variation of flow velocity with distance for KY sample at initial water content of 80%	89
Figure 3-6 The flows of KY sample at different water content (w) and slope angle (α)..	92
Figure 3-7 The flows of WV sample at different water content (w) and slope angle (α)..	93
Figure 3-8 Comparison of variations of viscosities with rotational speed at 50% and 80% example water content	94
Figure 3-9 Comparison of flow velocity of two coal refuse samples varying with initial water content and slope angle.....	95
Figure 3-10 Sketch of cylindrical spindle rotating in the tested fluid.....	96
Figure 3-11 Variation of viscosity with shear rate for KY coal refuse sample (23°C) .	100
Figure 3-12 Variation of viscosity with shear rate for WV coal refuse sample (23°C)..	100

Figure 3-13 Determination of flow parameters of Bingham Plastic model (KY coal refuse sample, w=80%).....	101
Figure 3-14 Bingham Plastic model for KY samples at different water content.....	102
Figure 3-15 Bingham Plastic model for WV samples at different water content.....	103
Figure 3-16 Schematic of flow configuration (De Kee et al., 1990)	109
Figure 3-17 Comparison of flow profile at different water content (WV sample).....	110
Figure 3-18 The relationship between flow velocity and viscosity of KY sample.....	112
Figure 3-19 The relationship between flow velocity and viscosity of WV sample.....	112
Figure 3-20 Results of impact loading tests on KY sample under different compressive strains ($\alpha =30^\circ$, w=48%).....	116
Figure 3-21 Results of impact loading tests on WV sample under different compressive strains ($\alpha =30^\circ$).....	117
Figure 4-1 Gravity effects in prototype and model (after Schofield, 1980)	125
Figure 4-2 CWRU geotechnical centrifuge	130
Figure 4-3 Cross-sectional view of CWRU centrifuge (after Figueroa et al., 1998).....	131
Figure 4-4 Rigid box on the CWRU geotechnical centrifuge.....	131
Figure 4-5 The design drawing of model container for centrifuge test (unit: cm)	133
Figure 4-6 The flow container in the centrifuge test.....	134
Figure 4-7 Actuator used in the centrifuge test.....	135
Figure 4-8 Design of centrifuge model test under impact loading	137
Figure 4-9 Centrifuge test results for two coal slurry samples	140
Figure 4-10 Flow of KY coal refuse sample in the centrifuge tests	142
Figure 4-11 The centrifuge model test under impact loading.....	145

Figure 4-12 Flow of coal refuse in the centrifuge tests under impact loading ($\alpha = 30^\circ$) 148

Figure 4-13 Recorded pore water pressure under impact loading 150

Figure 4-14 Coal refuse slurry cells (after Wu et al., 2003; and Michael et al. 2010) ... 152

Figure 4-15 Centrifuge model with coarse refuse build cells 153

Figure 4-16 Recorded pore water pressure under impact loading by using slurry cells. 155

ACKNOWLEDGMENTS

The authors would like to acknowledge the financial support to this study by Office of Surface Mining (OSM) through Grant S12AC20022, without which the work in this report would have been impossible. We would also like to thank the guidance and support of the project manager, Mr. Peter Michael of OSM, throughout the project.

The opinions expressed in this report are those of the authors and do not represent the official policies of the funding agency.

Geotechnical Properties and Flow Behavior of Coal Refuse under Static and Impact Loading

ABSTRACT

Millions of tons of coal waste are produced every year and stored in the coal waste slurry impoundments. Since impounded slurry waste has high water content and low shear strength an inadequately designed or constructed impounding structure is susceptible to the flow failure via a breach of its embankment following static or dynamic impact loading. In other cases a flow failure may occur in the form of a breakthrough into an adjacent or subjacent underground mine. Both types of failure endanger public safety and health, property, and natural ecosystems. They may result from several factors including poor embankment construction or a weak or coal barrier between an impoundment basin and an underground mine. They always result from impounded slurry that remains flowable because of insufficient consolidation to resist the effects of static or dynamic forces. To date there has been no comprehensive study on the geotechnical and rheological properties of impounded coal waste slurry, and the mechanisms that cause and sustain slurry flow.

In this study the geotechnical properties and flow behavior of impounded coal refuse under static and impact loading is assessed by using a range of standard laboratory tests, and small-scale model and centrifuge model experiments. In addition, the construction of slurry cells as a countermeasure to flow-failure potential was evaluated in the centrifuge model experiments. The combined results provide a better understanding of coal waste slurry flowability and consequent failure potential of coal waste impoundments. It is concluded that using liquid limit as the maximum allowable water content is an appropriate, conservative option for preventing flow failure during the construction and expansion of an impounding facility. Implications for design and recommendations for further study are proposed.

NOTATION

a	cross-sectional area of standpipe
A	cross-sectional area of soil mass through which flow q takes place
B	Skempton's pore pressure parameter
c	cohesion of soil
c_s	shape factor
c_u	undrained shear strength
C_c	compression index
C_s	swelling index
C_v	coefficient of consolidation
d	hydraulic radius in the open channel
D_s	effective grain diameter
e	void ratio
e_0	initial void ratio
F_f	flow factor
G_s	specific gravity
h	total head difference across the flow path of length L
H_{dr}	maximum drainage path
He	Hedstrom number
h_1	hydraulic head across soil sample at the begin of test ($t=0$)

h_2	hydraulic head across soil sample at the end of test
i	hydraulic gradient
I_p	plasticity index
k	hydraulic conductivity
KY	coal refuse sample collected from Kentucky
L	length of sample or flow path that produces the head difference h
m_v	coefficient of volume change
N	scaling factor
q	quantity of fluid flow in a unit time
\bar{q}	deviator stress
Re	Reynolds number
Re_c	critical Reynolds number
t	time required to get V volume
t_{50}	time elapsed at 50 percent consolidation
T_v	time factor
u	excessive pore water pressure
v	flow velocity
V	collected volume of water
WV	coal refuse sample collected from West Virginia
W_n	water content
w_L	liquid limit
w_p	plastic limit

α	slope angle
σ	normal stress on the plane of shearing
σ_3	confining pressure
σ_t	total vertical stress
τ	shear stress
τ_f	shear strength at failure
τ_y	yield stress
ϕ	friction angle of soil
γ_w	unit weight of pore fluid
$\dot{\gamma}$	shear rate or velocity gradient
η	viscosity of fluid
η_p	plastic viscosity
ν	kinematic viscosity
ρ	density of liquid

INTRODUCTION

1.1 Background

Despite the growing availability of alternative energy resources, coal still plays an important role in domestic energy consumption. In the U.S., nearly 90 percent of the produced coal was burned in the power plant and accounted for more than 36 percent of electric power generation in 2015 (US Energy Information Administration, 2015).

In order to comply with specifications limiting ash-producing impurities, coal is processed before it is transported to power plants. Consequently, millions of tons of coal refuse are produced in the U.S. every year and stored in impoundments or refuse piles in the coal producing states. Hundreds of coal waste impoundments have been built in the past few decades.

Coal waste slurry impoundments are common structures in the coal fields. They are characterized by slurried fine refuse hydraulically placed into an impoundment basin controlled by an embankment generally comprised of compacted coarse refuse. The fine refuse, with particle sizes similar to that of silt, has very low engineering strength and permeability. Full consolidation of the material may take many years. The properties of fine refuse slurry can result in flow failure of an impoundment under static loading or dynamic disturbance if the embankment is not well constructed, coal barriers or rock strata between an impoundment basin and an underground mine are too thin or weak, or pillars of subjacent mine workings are unable to withstand the overburden load.

Flow failure of coal waste and non-coal waste slurry impoundments has been documented many times in the past several decades. The failed structures released large

quantities of coal waste causing loss of life, property damage, and catastrophic ecological degradation.

There is insufficient information about the engineering properties of the impounded fine coal refuse, especially the material's flow behavior. From an extensive literature review on the flow properties of slurried coal waste and like materials, Michael et al. (2005) found that they could not ensure that all or most of the impounded material was non-flowable even several years post reclamation. They stated that there was even greater uncertainty concerning the nature of slurry flow, such as its speed and distance of travel in response to various degrees of stress. This project entails a comprehensive study of the geotechnical properties and flow behavior of coal refuse under static and dynamic impact loading. It evaluates response mechanisms of slurry samples to induced loads using laboratory tests, and small-scale and centrifuge model experiments.

1.2 Review of Coal Waste Impoundments

Coal waste, also called fine or coarse refuse, gob, and tailings, are a byproduct of coal mining and processing. The composition of waste is primarily dependent on the composition of the run-of-mine coal and the method of coal extraction. The processing typically includes removing extraneous materials, crushing and grinding, sizing, blending coal from several locations, and mineral concentration {National Research Council (NRC), 2002}.

The coal waste is separated into coarse refuse (grain sizes ranging from 0.1mm to 70mm) and fine refuse (grain sizes ranging from 0.001mm or less to 20mm). One common type of coal waste impoundment, called the cross-valley impoundment, includes an embankment made of

relatively dry, compacted coarse refuse and a basin or pool containing slurried fine refuse. An overview of a cross-valley impoundment is shown in Figure 1-1.



Figure 1-1 Overview of a typical coal waste slurry impoundment

Coarse refuse is generally too wet to be used in constructing the toe of the embankment. The embankment is constructed in multiple layers or “stages” of coarse refuse to accommodate additions of fine refuse slurry into the impoundment basin. The height of an impoundment embankment can reach up to three hundred meters (1000 feet).

Following the completion of a starter embankment, there are three different construction methods applied to coal waste impoundments as shown in Figure 1-2, which are the downstream, upstream, and centerline methods. The stability of a coal waste impoundment is partly dependent on which construction method is used. The selection among them at a particular impoundment site depends on project budget, supply of coarse vs. fine refuse, available land area, and potential safety and environmental hazards. A description of the characteristics of the three construction methods follows:

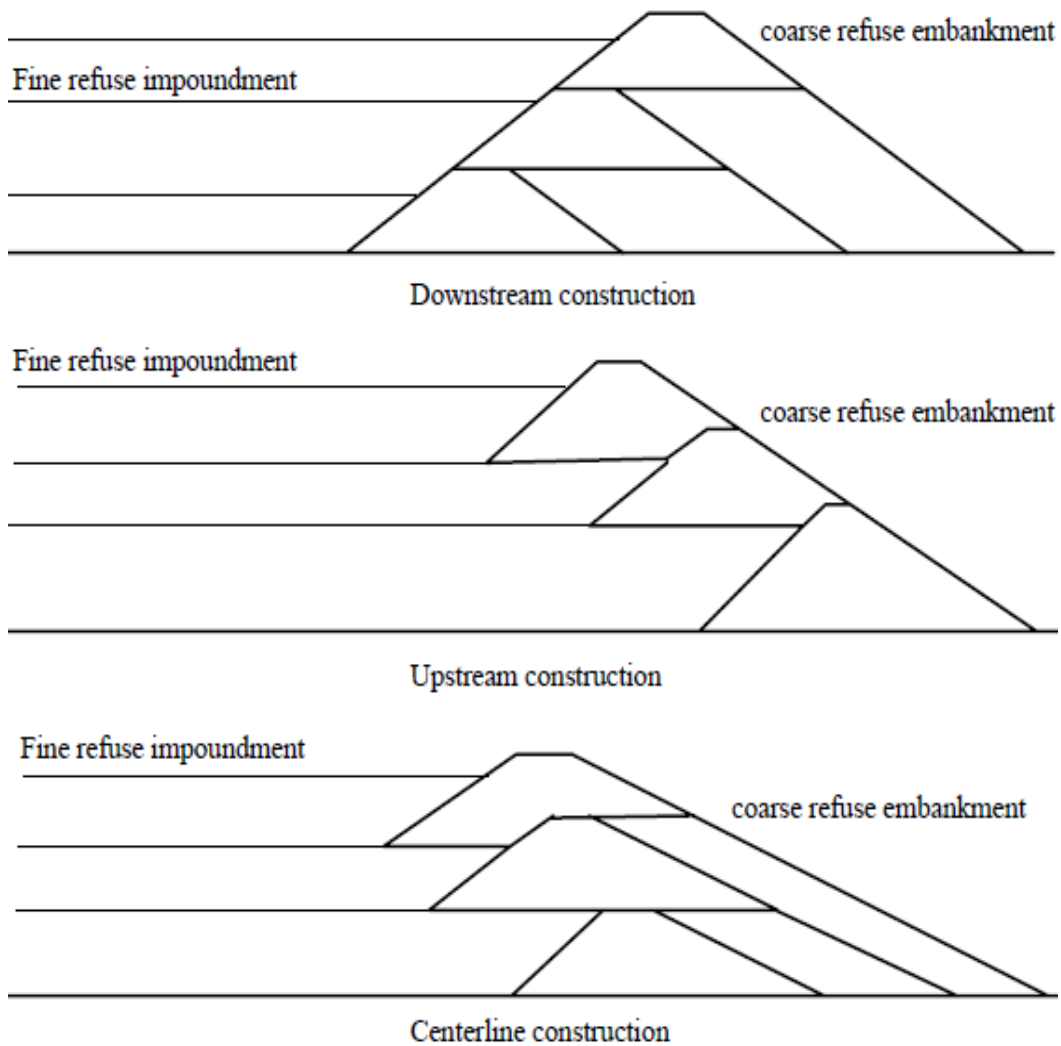


Figure 1-2: Three coarse refuse embankment construction methods (after Zeng, 2003)

Downstream Method

The downstream method is least commonly employed for the construction of an impoundment embankment. In this type of construction method, each stage is not placed on previously discharged fine refuse. The crest and toe of the embankment is moved downstream with each stage. Since none of the stages are underlain by wet and geotechnically weak fine refuse, the downstream method generally results in the most stable structure among the construction methods. However, this method requires a large volume of coarse refuse. It also requires more downstream land area which may or may not be available to the impoundment operator depending on the cooperation of land owners and regulatory allowances and restrictions.

Upstream Method

In the upstream method, the fine refuse beach at the upstream edge of the embankment crest becomes part of the foundation for each construction stage. In contrast to the downstream method, the embankment crest is moved upstream with each stage and the embankment downstream toe remains in place. This construction method requires less coarse refuse and disturbs less land area downstream. However, its important disadvantage stems from the low-strength and low-permeability fine refuse that comprises much of the embankment. The significance of the condition of the fine refuse material is emphasized by the NRC (2002): “Under static loading conditions, the ultimate embankment height will depend on the strength of the consolidated fine refuse within the zone of shearing, the steepness of the downstream slope of the embankment, and the location of the phreatic surface within the embankment. Under seismic loading, the stability of the embankment depends on the potential of the consolidated

fine refuse to liquefy”. It is important to add that the impounded fine refuse comprising part of the embankment should never be considered sufficiently consolidated for stability purposes in the absence of testing and analysis.

Centerline Method

Centerline method of impoundment embankment construction is a compromise between the upstream and downstream methods. As seen in Figure 1-2, each stage of the embankment is raised by symmetrically adding coarse refuse in both the upstream and downstream directions, resulting in the crest elevation rising along a vertical centerline. The impounded fine refuse comprises part of the embankment but to a lesser degree in comparison with one constructed upstream. Consequently the general stability of centerline embankments falls in between those constructed by the downstream and upstream methods.

The stability of impoundment designs is evaluated by using identical procedures and criteria applied to water dams (Wilson and Marsal, 1979; and U.S. Army Corps of Engineers, 1982). However, the average unit weight of fine refuse slurry is much greater than that of water. At the same time, the flowability of slurry is less than that of water. Therefore, impoundments retaining fine refuse slurry (especially those constructed by the upstream method) are quite different from dams retaining water but still deserve great care in their design, construction, and maintenance.

1.3 Review of Embankment Flow Failures

With the completion of each stage of the embankment, additional slurried fine refuse is pumped into the impoundment (see Figure 1-3). A large amount of water is required to avoid blockages as the material is piped from the processing plant to the impounding facility. When impounded, the fine refuse consolidates as pore water is drained from the matrix and grains become more compact under the weight of the material. Because of the initial high water content and low permeability of the material, the consolidation process can occur over several months to a few years. Studies documenting slow consolidation effects in coal waste slurry and other kinds of slurried waste have been reviewed by Zeng (1998) and Michael et al. (2005 and 2008).



Figure 1-3: Disposal of fine refuse in impoundment (after Zeng, 2003)

According to the National Inventory of Dams, there are more than 700 coal waste impoundments in the U.S. The Federal Emergency Management Agency classifies 241 of these

to have high hazard potential.¹ Government regulatory agencies such as the Office of Surface Mining Reclamation and Enforcement (OSMRE) and the Mine Safety and Health Administration (MSHA) require comprehensive stability analyses in the design of all impoundments and dams holding more than 20 acre-feet of fluid.

The principal method of evaluating embankment stability is the slope stability analysis under the static and dynamic loading. One of the critical factors in the stability analysis is the engineering strength properties of a structure's constituent materials. With respect to embankments built with upstream and centerline methods, this includes flowability of impounded fine refuse under static load and its potential for liquefaction under dynamic load. Fine refuse has different properties from most natural soils in terms of granular fabric, unit weight, and mineral composition. Experiments at several sites by Huang and Li (1987) have shown that the non-plastic fraction of fine refuse comprises more than 50% of its total material.

The problem of instability in various kinds of mining waste, including coal refuse, was first documented by Casagrande (1950). After studying several case histories of such failure he concluded that, "chemical and mining wastes consisting of flour-sized material are usually deposited hydraulically in very loose condition. Although they may appear stable behind some of the flimsiest dikes and in some cases supported only by a thin wall of the same material which has dried along the slopes, they are extremely sensitive to disturbance and constitute treacherous conditions which in some instances have caused disastrous flow slides with much loss of life and property."

¹ Facilities with high hazard potential are those that, upon structural failure, could reasonably be expected to cause loss of human life as well as serious damage to houses, industrial and commercial buildings, important utilities, highways, and railroads.

The most well-known flow failure of a coal waste impoundment in the U.S. occurred in the Appalachian coal field at Buffalo Creek in West Virginia on February 26, 1972. As shown in Figure 1-4, the impoundment was built on top of a thick layer of wet, loose sludge. It suddenly collapsed during a rainstorm. A flood of 500,000 cubic meters of black refuse and water was released into the valley below. 118 people were confirmed dead and 7 were reported missing. In addition, 1121 were injured and over 4000 were left homeless (Engineering News-Record, 1972). Another impoundment embankment failure occurred at Ages Creek in Kentucky in 1981. According an OSMRE report, fresh coal waste was dumped into the impoundment pool at midnight prior to the event. An eye witness claimed to have felt a stress wave during the dump that may have triggered the failure.



Figure 1-4: Failure of impoundment in Buffalo Creek area

The International Workshop on Seismic Stability of Tailings Dams sponsored by National Science Foundation and MSHA and organized by Prof. Zeng was held at Case Western Reserve University in 2003. Prof. Idriss (2003) presented a keynote lecture in the workshop and indicated that there have been more than 15 cases of liquefaction-induced failure of tailings dams in the past 40 years. Dobry and Alvarez (1967) reported widespread tailings dam failures during earthquakes in Chile. For instance, the EL Cobre dams were almost completely destroyed during the 1965 earthquake. More than 2 million tons of tailings flowed into the valley, traveled 12 km in a few minutes, destroyed part of the town of EL Cobre, and killed more than 200 people. The major cause of the failures was believed to be slope instability as a result of soil liquefaction. A similar failure occurred during the Central Chile Earthquake of March 3, 1985. Failures with similar patterns were also reported in Japan by Ishihara (1992).

Thacker et al. (1988) and Zeng (2003) conducted experimental studies on the mechanical properties of coal refuse and demonstrated that excess pore water pressure can build up in fine refuse under cyclic shear stress. Jayapalan et al. (1983a, 1983b) studied the failure mechanism and the resulting displacement of coal waste impoundments due to the liquefaction of fine refuse via theoretical analysis and small-scale model tests that subjected simulated impoundments to 1.0 g acceleration. The liquefied coal refuse was treated as a heavy viscous fluid. Zeng et al. (1998a, 1998b, 1998c) studied the seismic stability of tailings dam by using centrifuge model tests and found that the upstream embankment model deformed the most, thereby exhibiting the lowest stability under earthquake loading. In addition, they performed a number of Standard Penetration Test measurements and laboratory tests on fine refuse collected from a tailings dam in eastern Kentucky. It was confirmed that the fine refuse was a silt-like powder with low plasticity and high potential to be liquefied under earthquake loading. Al-Hussaini et al. (1981)

performed centrifuge model tests with varying geometrics and properties of coal refuse and confirmed that positive seepage control can help stabilize impoundments.

1.4 Review of Breakthrough of Impounded Coal Refuse into Underground Mine

In addition to the embankment failure, another issue that has concerned OSMRE and MSHA for many years is the potential of breakthrough of impounded coal waste slurry into underground mines. A schematic illustrating the relationship between an impoundment and adjacent and subjacent underground mines is provided in Figure 1-5.

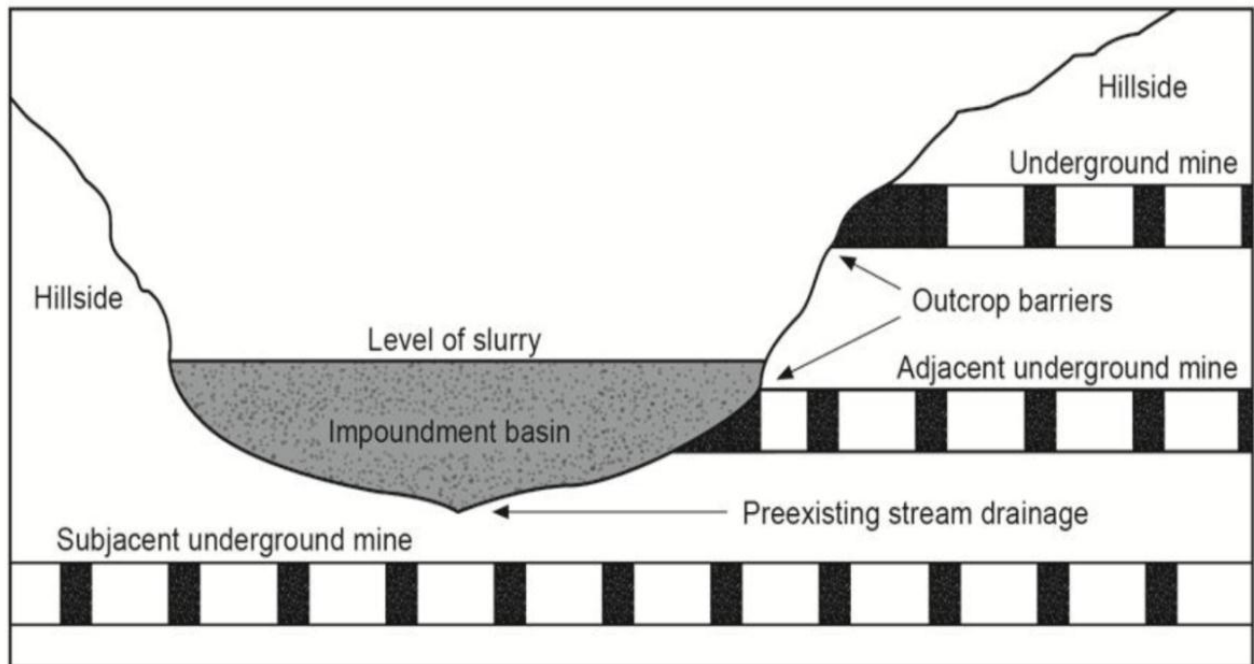


Figure 1-5: Slurry impoundment basin and adjacent and subjacent coal mine workings (after NRC, 2002)

In 1996, there was an underground mine breakthrough at the Miller Cove slurry impoundment. According to the report by Michalek et al. (1996), approximately 2.75 inches of rain had fallen in the area about one and a half hours before the event. Approximately one million gallons of coal waste materials were released into Gin Creek through an abandoned mine

(Michalek et al., 1996). When the fine refuse beach was excavated near the site of the breakthrough, it was found that the leak occurred in an area where mine maps indicated a coal barrier to the mine at least 25 feet wide. Investigators concluded that hydrostatic pressure from the slurry had expanded the cracks in the coal and initiated a piping-type failure.

A more devastating breakthrough occurred at the Big Branch slurry impoundment in Martin County, Kentucky in 2000 (Figure 1-6). An estimated 306 million gallons of coal slurry was released into a nearby underground coal mine and 260 gallons escaped the mine and flowed into nearby creeks and rivers causing tremendous environmental damages. No lives were lost from this accident. However, in the words of the NRC (2002) “...the release killed aquatic life along the Tug Fork of the Big Sandy River and its tributaries. Public water supplies were disrupted when communities along the rivers in both Kentucky and West Virginia shut down water plants to prevent contamination. American Electric Power had to close its massive generating plant, and numerous properties and residences were damaged.”

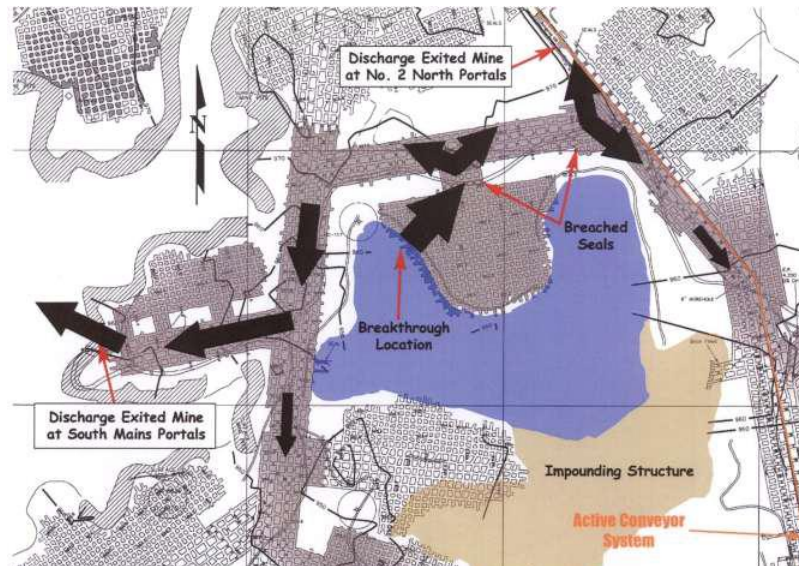


Figure 1-6: Breakthrough failure occurred at the Big Branch slurry impoundment in Martin County, KY in 2000 (after MSHA, 2001)

At the request of Congress, the NRC (2002) performed an investigation on coal waste impoundment breakthrough potential. It examined current regulations and engineering practices pertinent to the breakthrough issue; and identified effective measures to prevent breakthroughs, including methods to identify and locate underground mines relative to the impoundment and techniques to maximize coal utilization and consequently reduce coal refuse production. Studies specifically addressing the background and causes of the Martin County breakthrough were performed by MSHA (2001), OSMRE (2002), Thacker (2002) and Hagerty et al. (2004). Michael et al. (2005) performed an extensive literature review of investigations into the rheology of coal waste slurry and other kinds of impounded mine tailings. Finally, OSMRE (2011) provides a comprehensive overview of factors that must be considered by impoundment operators and regulatory authorities in the interest in breakthrough prevention. All of those publications recognize that breakthroughs can occur when the presence and location of nearby underground mines are not adequately investigated and impounded slurry is not sufficiently consolidated under increasing static loads or during dynamic disturbances.

1.5 Review of Flow Failure Prevention for Coal Waste Impoundments

Engineering recommendations and in-depth investigations on mitigation measures have been proposed in the past few decades regarding embankment failures and impoundment basin breakthroughs. Dewatering and densification of impounded fine refuse were suggested by the NRC (2002), Shinavski (2006), and Michael et al. (2010). Decant systems and spillways were recommended by MSHA (2009) in order to control water accumulation in the impoundment pool. Michael and Chavel (2008) assessed the effect of capping and reclaiming coal waste slurry

impoundments on breakthrough potential. They recognized that the weight of cap material above flowable fine refuse slurry could induce a breakthrough against a weak mine barrier, however, they concluded that the capping and reclamation process has the net effect of minimizing breakthrough potential by dewatering the slurry prior to capping and constructing drainage structures that prevent future water infiltration into the reservoir.

Other means of flow-failure prevention pertain to the kind of structures used to store coal waste. Two of these are mentioned below:

Incised Pond

An incised pond is a small impoundment commonly used for the temporary or emergency disposal of fine coal refuse. It has been widely used in the Midwest regions where surface mining is primarily conducted on flat topography. The pool surface in an incised pond is typically below the ground surface. Since there is no embankment, a breach type flow failure is not a concern with these structures but, conceivably, an underground mine breakthrough is possible. Since storage volume comparable to that of a large cross-valley or diked² impoundment would require extensive excavation producing fill material to be stored elsewhere, this structure is not regarded as an effective solution to flow-failure potential.

Slurry Cells

The concept of slurry cell is to reduce the total capacity of flowable material to a level that is consistent with a low-hazard-potential MSHA classification. The impoundment is constructed with a number of individual cells with the designed slurry storage capacity of less than 20 acre-feet. Each cell is small and self-contained and can be designed according to the

² A diked impoundment is one in which an embankment or series of embankments completely surround the slurry pool or basin. Diked impoundments commonly occur in flat to gently sloped topography. However, they can evolve from cross-valley impoundments in steep-sloped terrain when natural abutments formed by valley side slopes are not high enough to contain the volume of slurry deposited in the pool.

strength properties of the coarse refuse separating the cells and forming the main embankment (NRC, 2002). Coarse refuse dikes containing the cells facilitate fine-refuse dewatering. Another advantage is that they would reduce the availability of flowable material in the event of a breach or breakthrough. Whether slurry cells are employed depends on the ratio of coarse-to-fine refuse to be stored and cost of construction.

Combined Refuse Piles

Combined refuse piles are non-impounding facilities and consist of fine coal refuse that has been dewatered and combined with coarse refuse. Provided that measures are taken to maintain low moisture content, flow failure from this type of facility is not a concern. However, the control of water content for effective compaction is a common challenge. Constructing a combined refuse pile that holds a volume of fine refuse comparable to the storage capacity of a cross-valley or diked impoundment is an expensive way of avoiding flow failures.

Other proposed methods for reducing impoundment flow-failure potential were recognized by Michael et al. (2010). They include mixing coarse refuse or mine spoil in with the fine refuse slurry to increase permeability and thus accelerate consolidation, and combining polymers instead of water with fine refuse to facilitate pipe transport. The authors of this report are not aware of any instances where these technologies have been put to productive use in the coal mining and reclamation industry. Finally, older impoundments with impounded fine refuse containing sufficiently high BTUs can be eliminated by re-mining.

The authors expect that storage of slurried fine refuse in impoundments will continue into the future. Given the ever-present danger of impoundment flow failure it is important that the flow characteristics of fine coal refuse slurry be well understood.

1.6 Research Objectives

In this study, a comprehensive investigation was performed on geotechnical properties and flow behavior of impounded coal refuse under static and impact loading using laboratory tests, small-scale model tests, and centrifuge model tests. A working hypothesis is that the flow behavior of fine coal refuse is critically controlled by water content. This study evaluates the relationships between water content of the material, its engineering properties, and rheological characteristics in terms of velocity and distance of flow (as measured in the lab). The potential advantage of using slurry cells to minimize flow failure was also assessed. A second hypothesis is that the liquid limit can be treated as the critical water content at which the slurry will flow.

The objectives of this study also include but are not limited to the following:

- To better understand the mechanism of fine refuse slurry flow;
- To explore the applicability of existing flow models to fine coal refuse;
- To begin developing a database of geotechnical properties and flow behavior of fine coal refuse for future studies.
- To provide engineering recommendations on the design and construction of slurry impoundments so as to prevent flow failure.

1.7 Outline of the Report

Chapter 1 introduces different types of coal waste impoundments. A literature review is also performed on the case histories of embankment-breach and underground-mine-breakthrough flow failure of impoundments and potential measures and techniques to reduce the risk of flow failure.

Chapter 2 studies geotechnical properties of impounded coal refuse by performing a range of laboratory tests. The measured soil properties include particle size distribution, Atterberg limits, specific gravity, coefficient of consolidation, compression index, hydraulic conductivity, shear strength, and viscosity. The variations of these parameters with initial water content are investigated.

Chapter 3 performs comprehensive investigation on the flow behavior of coal refuse by small-scale model tests. The flow characteristics of coal slurry with different water content are analyzed under static loading and impact loading. A standard flow model is proposed as the one most applicable to the flow behavior of coal refuse slurry. The model is employed to obtain a deeper understanding of the rheological properties of the material and the mechanisms of flow failure.

Chapter 4 describes a group of centrifuge tests used to analyze the flow behavior of coal refuse in a high stress field. The test data is compared with those of the small-scale model tests to validate the results of both procedures. The proposed countermeasure of using slurry cells is also evaluated in the centrifuge model tests.

Chapter 5 summarizes the significant findings and conclusions of this research, along with plans and recommendations for future work.

GEOTECHNICAL PROPERTIES OF COAL WASTE SLURRY

2.1 Introduction

The understanding of geotechnical properties of coal waste slurry is of fundamental importance to the investigation of flow behavior of the material as well as the engineering design and construction of slurry impoundments. Fine coal refuse is a mixture of many different substances including coal, rock fragments and soil particles separated from saleable coal (Osborne, 1988). The physical properties of coal waste slurry may be quite variable due to the mineralogy of the coal impurities and the coal preparation process. One of the most important objectives of this project is to study the relationship between moisture content and the geotechnical properties of the fine coal refuse which might influence its flow behavior under static and impact loading.

2.2 Sample Collection and Preparation

The fine coal refuse slurry samples used in this research project were collected from two coal refuse slurry impoundments in the Appalachian region (located in Kentucky and West Virginia). The coal slurry samples obtained from Kentucky and West Virginia are henceforth designated as “KY” and “WV” samples, respectively.

Both samples of fine refuse were collected directly from the coal preparation plant located near the entrance of the mine. A sample collected at the processing facility is representative of the material that is pumped up the mountain and hydraulically placed in the impoundment.

The coal slurry samples were taken directly from the pipeline by catching the slurry in buckets (Figure 2-1) at the processing plant before it was transported to the impoundment. The

initial water content was extremely high and too wet to be tested. The buckets of slurry suspension were placed at rest for periods of time varying from two days to two weeks before testing. The settled refuse could then be used to prepare samples with different initial water contents (or initial void ratios). In order to prepare samples with relatively lower water contents, excess water was removed by spinning the coal slurry in a centrifuge.



Figure 2-1 Slurry sample collected from coal preparation plant

2.3 Geotechnical Properties of Coal Waste Slurry

The geotechnical properties of coal waste slurry were determined by a group of laboratory tests performed in the Department of Civil Engineering at Case Western Reserve University, Cleveland, OH. The tests included index tests, (particle size analysis by mechanical and hydrometer methods, Atterberg limits, and specific gravity), consolidation, permeability, triaxial strength, and viscosity. A summary of the tests conducted is shown in Table 2-1. All the laboratory tests were performed strictly in accordance with ASTM standardized procedures,

which are commonly used by the geotechnical engineering community, so as to ensure the consistency and comparability of the results. Some of the tests were performed multiple times on other specimens taken from the same samples in order to check for repeatability. Each type of test has its purpose, advantages, and limitations. Combined results of these tests can provide information regarding the flowability of coal refuse.

Table 2-1 Summary of laboratory tests conducted on coal waste slurry

Lab. Tests	ASTM Standard	Soil Properties Measured
Sieve Test & Hydrometer Tests	D421; D422; D423	Particle size distribution
Specific Gravity Tests	D854	Specific gravity G_s
Atterberg Limits Tests	D4318	Liquid limit; Plastic limit; Plastic index
Consolidation Tests	D2435	Coefficient of consolidation; Compressive index;
Permeability Tests	D2434; D5084	Coefficient of permeability
Triaxial Tests	D7181; D2850	Cohesion; Internal friction angle
Viscosity Tests	D1084; D2556; D4402; D5018	Relationship between water content and viscosity

2.3.1 Particle Size Distribution

Introduction

Particle size distribution is one of the most significant properties affecting the strength, compressibility, and dynamic resistance of the impounded coal refuse. Wakeley and Peterson (2004) indicated that other factors include the material's mineralogy, grain size, and grain shape, all of which are connected to the geological setting of the mined area. Since coal refuse is derived from cyclothem sedimentary rock it is relatively rich in clay minerals and clay sized particles. Justice (1997) performed a particle size analysis of coal slurry and found that more than 70% of fine refuse particles were within the silt size range, resulting in a coefficient of

uniformity C_u between 11 and 34. The values of C_u indicated that the slurry was composed of a moderate to narrow range of particle sizes. Ferrini et al. (1984), Round and Hessari (1985), Logos and Nguyen (1996), and Boylu et al. (2004) pointed out that the rheological behavior of coal-waste slurry had close relationships to mean particle size, particle size distribution and particle shape.

The particle size distribution of fine coal refuse was determined in this study by following the ASTM standardized procedures for sample preparation (D421), sieve analysis for coarse particles (D422), and hydrometer tests for fine particles (D422). An oven-dried coal refuse sample weighing approximately 300g was washed under tap water through a No. 200 sieve (0.075mm) until the wash water was clear. A sieve analysis was performed on the coarse fraction retained on the No. 200 sieve and a hydrometer analysis was performed on the fine particles that passed the No. 200 sieve. The hydrometer method is based on Stoke's law which governs the velocity at which the spherical particles settle out of a suspension. Multiple tests were not conducted due to the limited quantity of coal refuse sample and the time required to conduct the hydrometer test.

Test Results

The results of the measurements are shown in Figure 2-2. For both the KY and WV samples, the percent finer than No. 200 was higher than 80%. The WV sample had a finer average particle size and wider size range than the KY sample. Atterberg limits tests were also performed to determine the liquid and plastic limits, and the plasticity index of the coal refuse samples. The details of these test procedures are covered in Section 2.3.3. The tests showed that the coal refuse has low plasticity. Based on the measured particle size distribution and Atterberg

limits, both the KY and WV samples were classified as a low-plasticity silt (ML) using the Unified Soil Classification System.

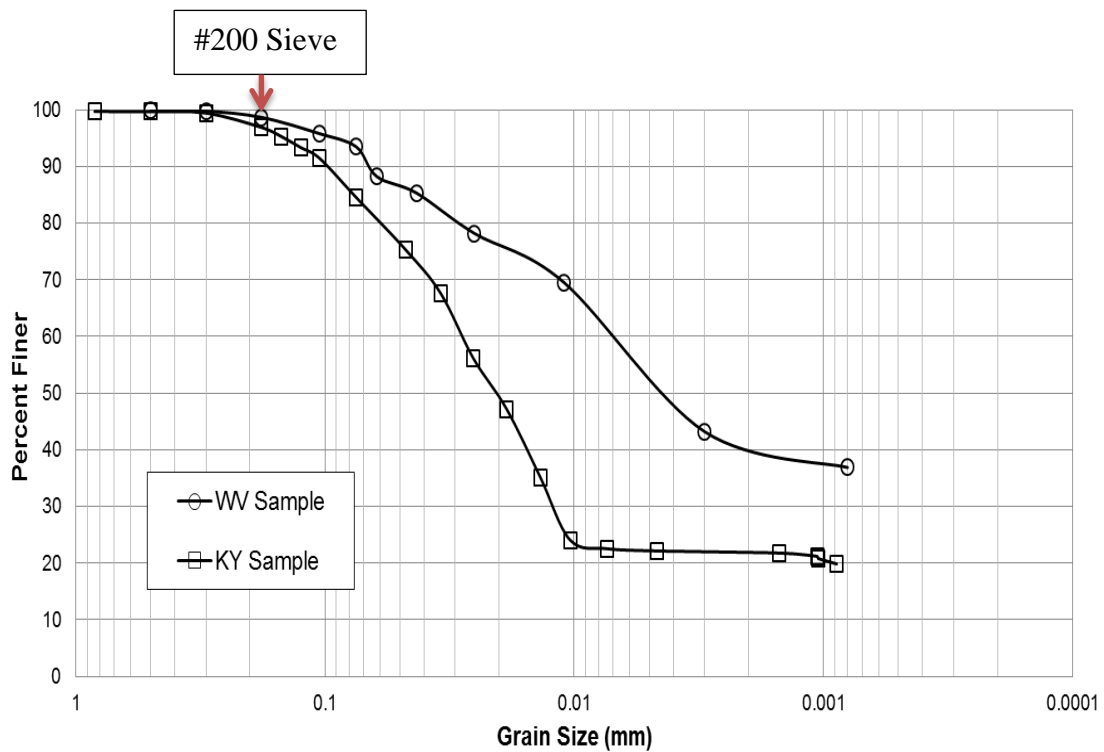


Figure 2-2 Particle size distribution curve for KY sample and WV sample

2.3.2 Specific Gravity

Introduction

The specific gravity (G_s) of a substance is defined as the density of the material divided by the density of distilled water at 20°C. Specific gravity is one of the most significant geotechnical parameters. A value of specific gravity can be used to compute the void ratio or dry density of a soil if the moisture content or wet density is known. The specific gravity is also useful for soil mineral classification.

Values of specific gravity for the coal refuse samples were determined in accordance with ASTM D854. This procedure involves determination of the weight of coal refuse particles

and the weight of an equivalent volume of water at a temperature of 20°C. A correction was applied, in accordance with the ASTM procedure to compensate for the actual water temperature of 23°C. This procedure was repeated three times for each coal refuse sample and the average was recorded.

Test Results

As shown in Table 2-2, the recorded average specific gravity was 2.03 for the KY sample and 2.14 for the WV sample. Typical values of specific gravity for soil forming minerals are on the order of 2.5-2.8. It should be noted that, due to the hydrocarbon content, the specific gravity of coal refuse is typically lower than those of inorganic soils. The relatively low specific gravity of this study's samples appears to agree with the findings of Busch et al. (1975) who performed laboratory tests on undisturbed Shelby tube samples of fine coal refuse samples with high coal content. The specific gravity of the samples was in the range of 1.25 to 1.70. Soils with low specific gravities tend to exhibit relatively low shear strengths.

Table 2-2 Summarized results of specific gravity test

Test Sample	KY	WV
Volume of flask at 20°C	500ml	500ml
Method of air removal	Vacuum	Vacuum
Temperature	23°C	23°C
Temperature correction coefficient $\alpha = \frac{\rho_t}{\rho_{20^\circ\text{C}}}$	0.9993	0.9993
Average Specific gravity $G_s = \alpha \frac{M_s}{M_w}$	2.03	2.14

2.3.3 Atterberg Limits Tests

Introduction

Atterberg limit tests were used to determine the liquid limit, plastic limit, and plasticity index of the coal refuse. The liquid limit and plastic limit are used by civil and geotechnical engineers for soil classification and for strength correlations (Bowles, 1992). The liquid limit w_L is conceptually defined as the moisture content at which the behavior of a fine grained soil changes from that of a plastic solid to that of a liquid. A soil sample with moisture content greater than the liquid limit will behave as a viscous fluid upon application of a small shearing force. The plastic limit is the water content above which a soil begins to exhibit plasticity. The plastic and liquid limits define the range of moisture contents over which a soil exhibits plastic behavior.

Testing Facilities and Procedures

The liquid limit is arbitrarily defined as the water content at which a paste of the soil sample placed in a brass cup, cut with a standard groove, and then dropped from a constant height of 10 mm, will undergo a groove closure of 12.7 mm when the cup of soil is dropped 25 times at the rate of 120 drops/minute. The liquid limit test using Casagrande's device (ASTM, D4318) is illustrated in Figure 2-3. The test is normally run at several moisture contents and the water content is plotted against the logarithm of the number of blows. The straight line that best fits the scattered points is drawn. The moisture content which requires 25 blows to close the groove defines the liquid limit.

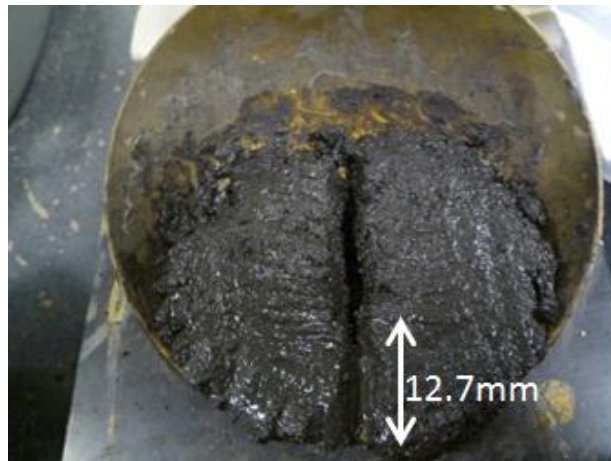


Figure 2-3 Liquid limit test on coal refuse sample (the groove has closed 12.7mm)

Test Results

The results of liquid limit tests for the two samples are shown in Figure 2-4 and 2-5. The liquid limits are 38.1 for the KY sample and 42.5 for the WV sample.

The plastic limit w_p is defined as the water content at which a soil thread crumbles when it is rolled down to a diameter of 3 mm. Figure 2-6 shows the measurement of plastic limit. The recorded plastic limits are 28.3 for the KY sample and 27.8 for the WV sample.

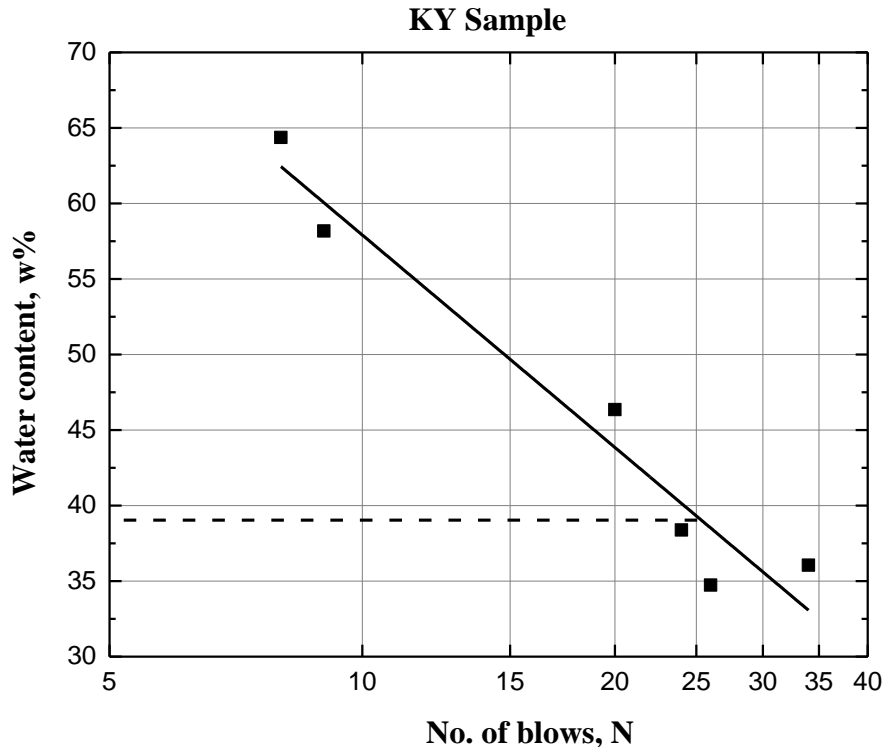


Figure 2-4 Relationship between water content and blow number N for KY sample

(Liquid Limit $w_L = 38.1$)

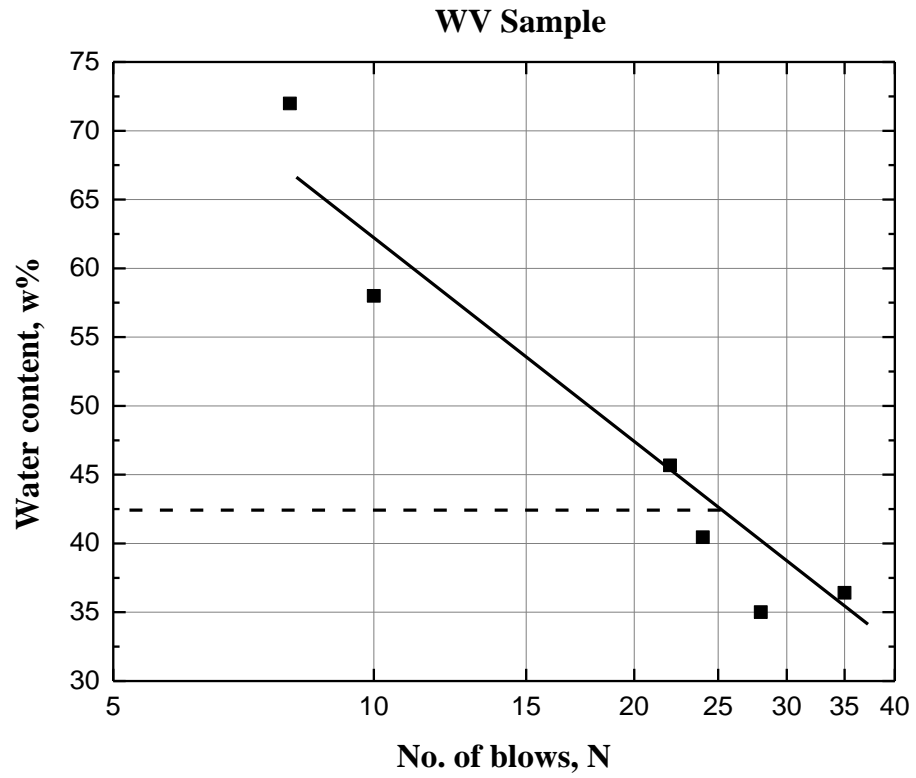


Figure 2-5 Relationship between water content and blow number N for WV sample
(Liquid Limit $w_L = 42.5$)



Figure 2-6 Plastic limit test on coal refuse sample

The plasticity index I_p is related to the range of moisture contents over which a soil remains in a plastic state while passing from a semisolid state to liquid state. The plasticity index can be obtained from the difference between the liquid limit and the plastic limit ($I_p = w_L - w_p$). The plasticity index was 9.8 and 14.7 for KY sample and WV sample, respectively. The values of plasticity index were grouped by Sower (1979) as:

- (0-3)- Nonplastic
- (3-15) - Slightly plastic
- (15-30) - Medium plastic
- >30 - Highly plastic

Both samples behaved in a slightly plastic manner which indicates that the sampled coal waste slurry should have a low response to changes in the water content. The summarized results of Atterberg limit tests are listed in Table 2-3. With the liquid limit and plasticity index known, the soil is classified as a low-plasticity silt (ML) using the Unified Soil Classification System (Figure 2-7).

Table 2-3 Summarized results of Atterberg limit tests

Property	KY Sample	WV Sample
Liquid Limit w_L	38.1	42.5
Plastic Limit w_p	28.3	27.8
Plasticity Index I_p	9.8	14.7

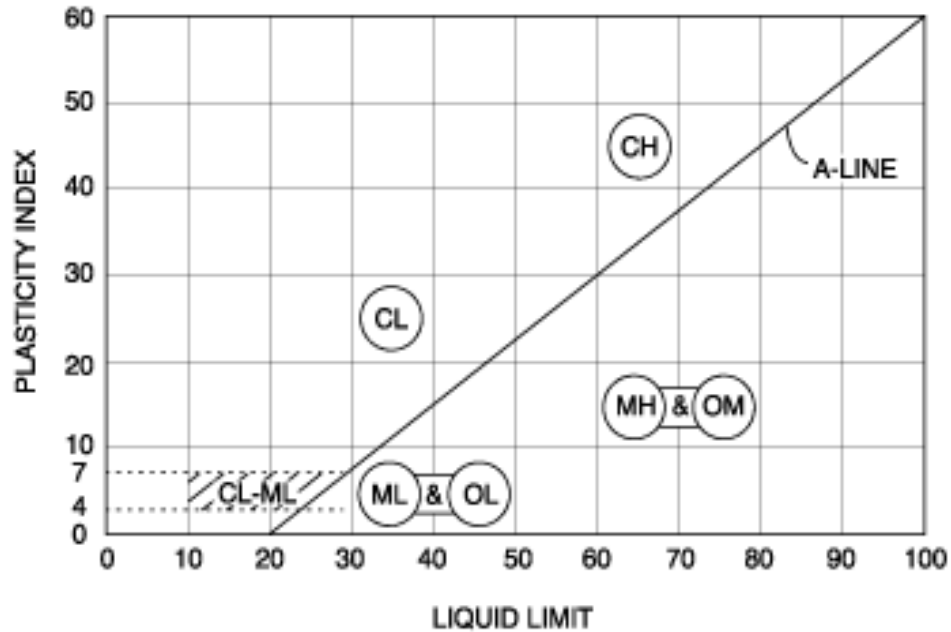


Figure 2-7 Plasticity chart to use for the Unified Soil Classification System

Conceptually, the flow of coal waste slurry should take place under static loading when the water content is above the liquid limit. Therefore, an important hypothesis in this research considers the liquid limit as the critical water content at which the flow of coal waste slurry will be triggered. Based on this hypothesis, samples were prepared with initial water contents higher than the liquid limit for the static loading tests. Another hypothesis is that excess pore water pressure will be generated in response to impact loading which will engender slurry flow even when the water content is below the liquid limit. Therefore, in tests involving impact loading some samples were prepared with water contents lower than the liquid limit.

2.3.4 Consolidation Tests

Introduction

Consolidation is the process by which the volume of soil decreases under external load. For a fully saturated soil sample, the reduction in volume results from the drainage of pore water.

As shown in Figure 2-8, the consolidation process for fully saturated soil can be interpreted by using an idealized system which comprises a spring in a water container with a valve in its top plate. Four stages in this analogy are as follows:

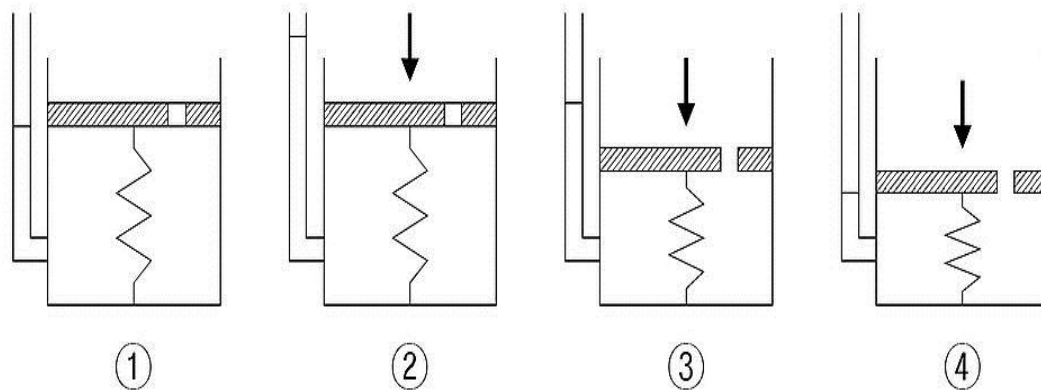


Figure 2-8 Consolidation spring analogy (Anonymous, 2007)

1. The water container is completely full of water with the valve on top plate closed.
2. A load is applied on the top plate with the valve still closed. At this time, only the water supports the load and excess pore water pressure is generated. (The spring keeps the same length as that in stage #1).
3. The drainage occurs as soon as the valve is opened. At this time, excess pore water pressure starts to dissipate and the spring gradually shortens.
4. When the water is completely drained, all excess pore water pressure engendered in stage #2 dissipates. The entire load is undertaken by the spring. The spring is most stable at its shortest length.

When soil is subjected to a load which is greater than its resistance to failure, the soil skeleton is broken and rearranged. This process of plastic deformation results in a reduction in

void ratio e . Although a small amount of elastic deformation may also take place, it can be neglected due to the magnitude of load and a large modulus of elasticity of the soil particles on the order of 20 MPa (Bowles, 1992).

The results of the consolidation test which include the coefficient of consolidation C_v , compression index C_c , and swelling index C_s allow us to address two important engineering issues:

- a. How much settlement of the fine refuse will take place under load in an impoundment?
- b. How fast will the process of consolidation take place?

Testing Procedures

The soil consolidation parameters can be obtained using a consolidometer (sometimes called oedometer). The detailed procedures and measurements are described in ASTM D 2435. As shown in Figure 2-9, a soil sample is placed in the consolidometer and subjected to a series of one-dimensional compressive loads with the load increment ratio $\Delta p / p = 1$. A dial gauge is used to take deformation readings at the specific elapsed times. Typically, the duration of each run is 24 hours or when the difference of deformation between two successive readings is sufficiently small. For each load increment, the results are graphically displayed as a semilog plot of consolidation dial readings versus log time so as to determine t_{50} , the time at which 50 percent consolidation is reached. The value of t_{50} is most commonly used in the Casagrande method to estimate the coefficient of consolidation C_v . Figure 2-10 exhibits the result of a trial test of a saturated soil sample under a specific load. The value of t_{50} is obtained by determining D_0 , D_{100} and D_{50} .

Alternative means of determining C_v have been proposed. For instance, Olson (1985) concluded that the only reliable way to estimate the C_v value is to base it upon the coefficient of volume compressibility and the coefficient of permeability. The coefficient of consolidation C_v (in m^2 / s) can be expressed as:

$$C_v = \frac{k}{m_v \gamma_w} \quad (2-1)$$

where

k = hydraulic conductivity (m/s)

m_v = coefficient of volume compressibility (m^2 / kN)

γ_w = unit weight of pore fluid (kN / m^3)

Alternative curve-fitting procedures based on Terzaghi's uncoupled consolidation theory have also been proposed for the determination of C_v (Taylor, 1948; Sridharan and Prakash, 1985; Olson, 1986; Sridharan and Prakash, 1995; Mesri et al., 1999; and Chan, 2003). Since many factors influence the value of C_v , the experimental behavior of soil in the one-dimensional consolidation test does not always support the theoretical relationship of consolidation as obtained by Olson's and Terzaghi's theories. Therefore C_v was determined by using Casangrade's method in this study.



Figure 2-9 Consolidometer used in consolidation test

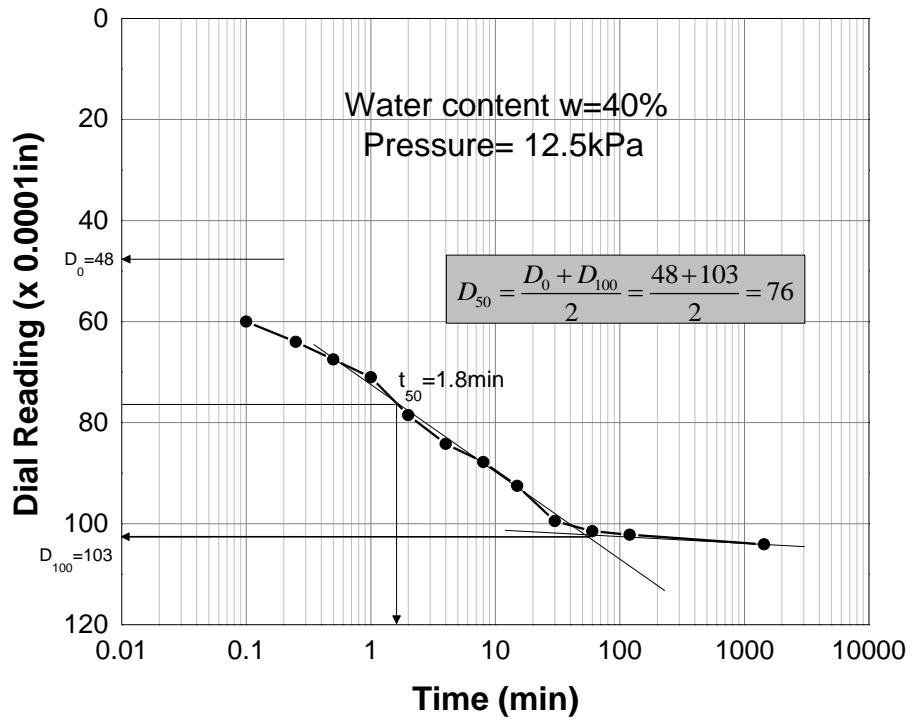


Figure 2-10 An example plot of dial reading vs. log time in minute

The void ratio at the end of primary consolidation for each load increment was also calculated. The results are plotted as void ratio versus log pressure. From the straight-line part of the curve, the compression index C_c is determined as:

$$C_c = (e_1 - e_2) / \log(p_2 / p_1) \quad (2-2)$$

where e_1 and e_2 are the void ratio of the fine refuse corresponding to the pressure (or load) of p_1 and p_2 , respectively. After the maximum load was reached, the load is gradually reduced at the decrement ratio $\Delta p / p = 1$ and the resulting void ratios are measured. From the recorded data on the unloading line, the swelling index of the sample C_s is determined as:

$$C_s = (e_1 - e_2) / \log(p_2 / p_1) \quad (2-3)$$

In this study, the fine coal refuse samples were prepared for consolidation tests at the initial water contents of 64%, 52% and 45%. A one-dimensional axial load were applied from the top of the sample in six increments (5, 20, 40, 80, 160, and 320 kPa). According to the recommendation in ASTM D2435, the duration of each load increment should be 24 hours. However, the results of trial tests indicated that this time period was not sufficient for the full primary consolidation of the coal refuse samples. That is, the difference of displacement between two successive readings was not in the negligible range after 24 hours. Therefore, the time span under each load increment was set as 72 hours in order to ensure the coal waste slurry sample reached the end of the primary consolidation. The unloading process entailed exactly the same as the loading process, only in reverse. The consolidation dial readings under each load increment were recorded at the elapsed time.

Test Results

As mentioned above, the coefficient of consolidation C_v under each load increment was determined by using Casangrade's method. The results of coefficient of consolidation C_v for the two coal waste slurry samples are summarized in Figure 2-11 and Figure 2-12. The coefficient of consolidation increased with load. Generally, a more significant increase was observed when the load exceeded 80 kPa. Both the KY and WV samples had larger coefficients of consolidation with lower initial water contents. The larger value of C_v indicates a faster consolidation rate under a given consolidation pressure.

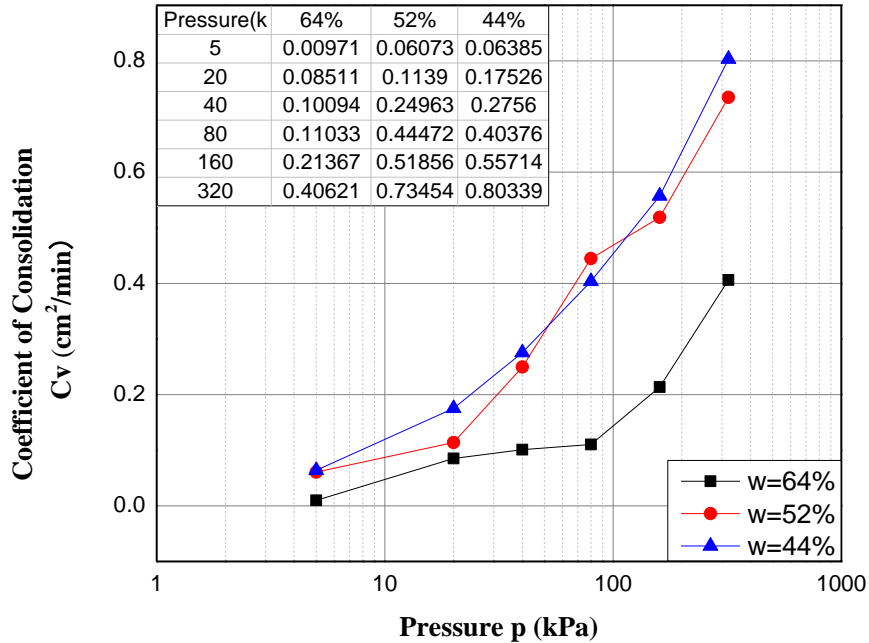


Figure 2-11 Summarized results of coefficients of consolidation C_v for KY sample

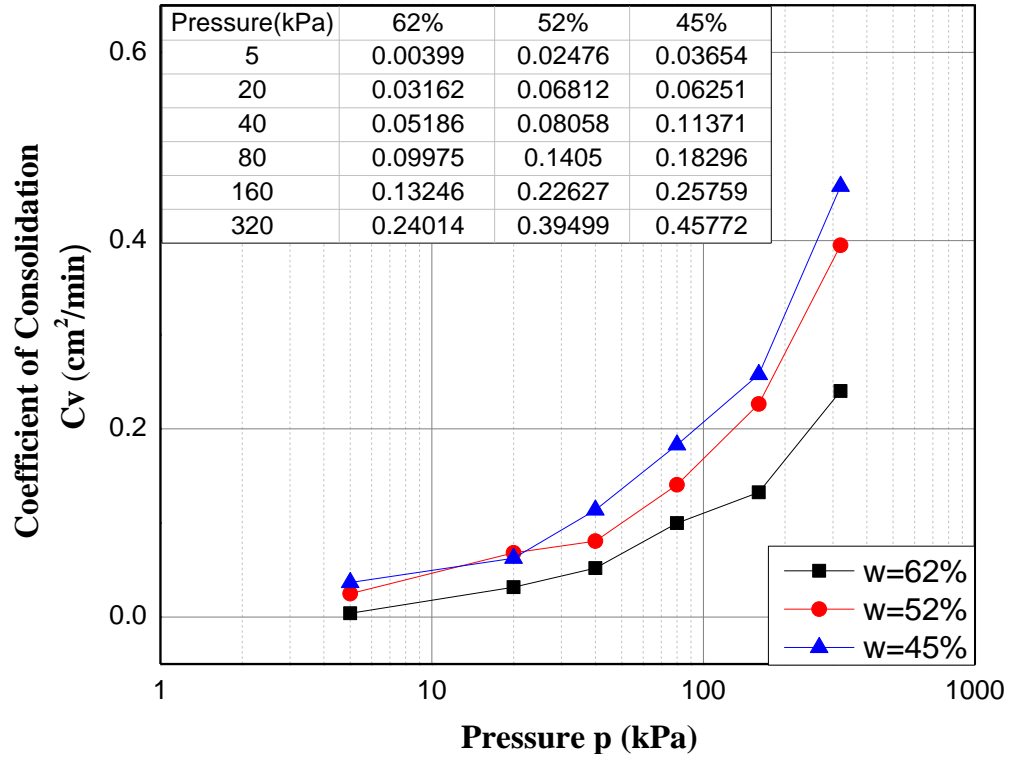


Figure 2-12 Summarized results of coefficients of consolidation C_v of WV Sample

Referring to Equation 2-1, Terzaghi and Peck (1967) found that both hydraulic conductivity k and coefficient of volume change m_v decrease rapidly when the effective vertical pressure increases. The ratio of k/m_v and therefore C_v should be fairly constant over a wide range of applied pressure. However, subsequent studies, including this one, have demonstrated that some materials undergo a significant change in C_v over the applied pressure range. This variation, particularly observed in clayey soils, needs further analysis. Recent investigations have found that the relationship between C_v and applied effective consolidation pressure is affected by clay mineralogy, soil type, and mechanical and physicochemical factors (Olson and Mesri, 1970; Sridharan and Rao, 1976; Robinson and Allam, 1998; and Sridharan and Nagaraf, 2004). Results of laboratory tests in several other studies showed that the coefficient of consolidation

increases with consolidation pressure for kaolinite, glacial silty clay, sandy clay, and Kawasaki Clay but decreases with consolidation pressure for residual clay and bentonite (Leonards and Ramiah, 1959; Samarasinghe et al., 1982; and Nagase et al., 1994). Robinson and Allam (1998) compared the compressibility of three clay minerals (kaolinite, illite, and montmorillonite) and found that the variation of coefficient of consolidation with applied pressure was dependent on whether the primary consolidation behavior was governed by mechanical properties of the grains or the lubricating effect of the pore fluid.

The void ratio versus applied consolidation pressure of the two samples with different initial water contents (or initial void ratios) is shown in Figures 2-13 and Figure 2-14 where the consolidation pressure is plotted on a logarithmic scale. The compressive index C_c is obtained from the slope of the steeper line showing the effect of increasing consolidation pressure. The swelling index C_s is acquired from the gentler slope of the line showing the effect of decreasing pressure. The results of the tests are summarized in Table 2-4. Typically fine grained soils have a relatively smaller capacity in bearing load than coarse grained soil. Consequently the former soil types have a higher degree of compressibility. The compressibility of different mine tailings were compared by Qiu and Sego (1998) and exhibited in the form of a semi-log plot between compressibility and void ratio ($\log \sigma' - e$). As shown in Figure 2-15, the coal waste slurry samples have much higher compressibility than other mine tailings. The values of compression index for different types of soil are listed in Table. 2-5. The compression index values of the coal waste slurry samples fall within the range of medium-soft clay.

Table 2-4 Comparison of Compression Index C_c and Swelling Index C_s

WV Sample	w=62 %	w=52 %	w=45 %
Compression Index C_c	0.278	0.205	0.176
Swelling Index C_s	0.056	0.034	0.015
KY Sample	w=64 %	w=52 %	w=44 %
Compression Index C_c	0.217	0.187	0.152
Swelling Index C_s	0.039	0.02	0.018

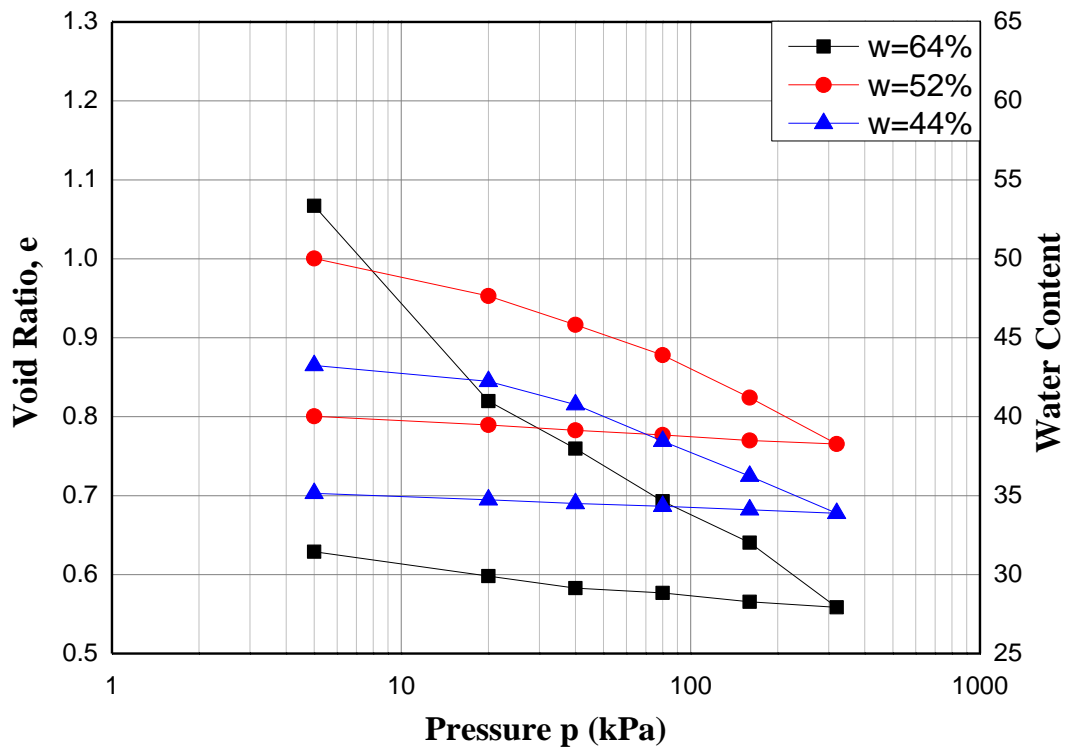


Figure 2-13 Void ratio vs. pressure for KY samples with different initial water content

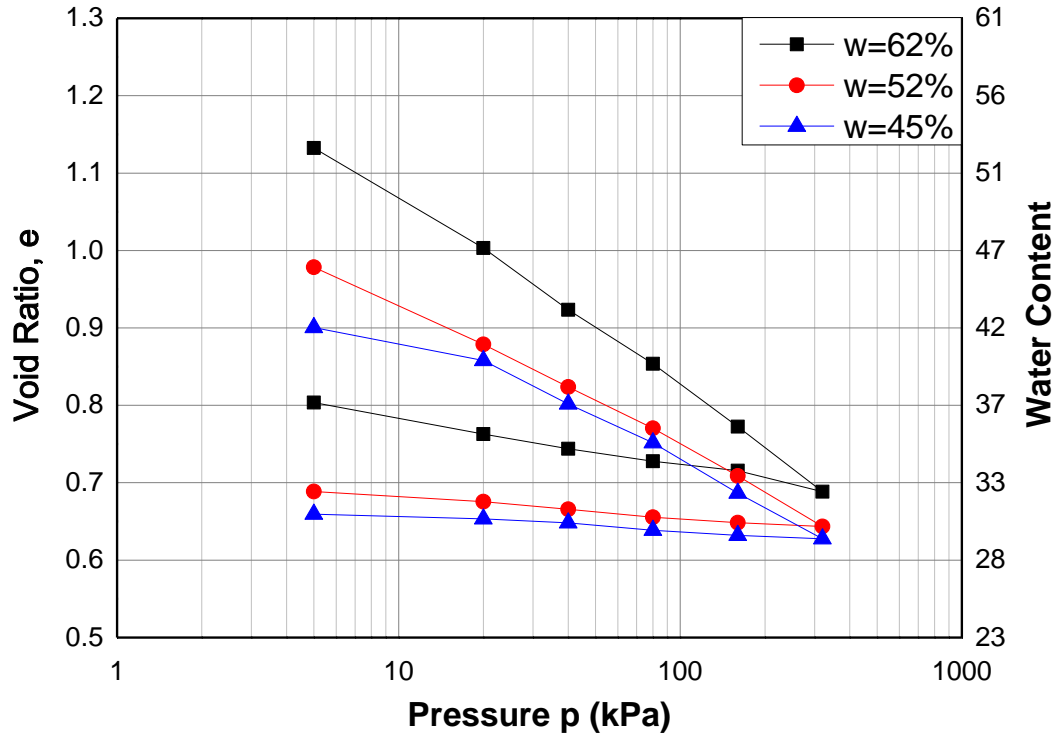


Figure 2-14 Void ratio vs. pressure for WV samples with different initial water content

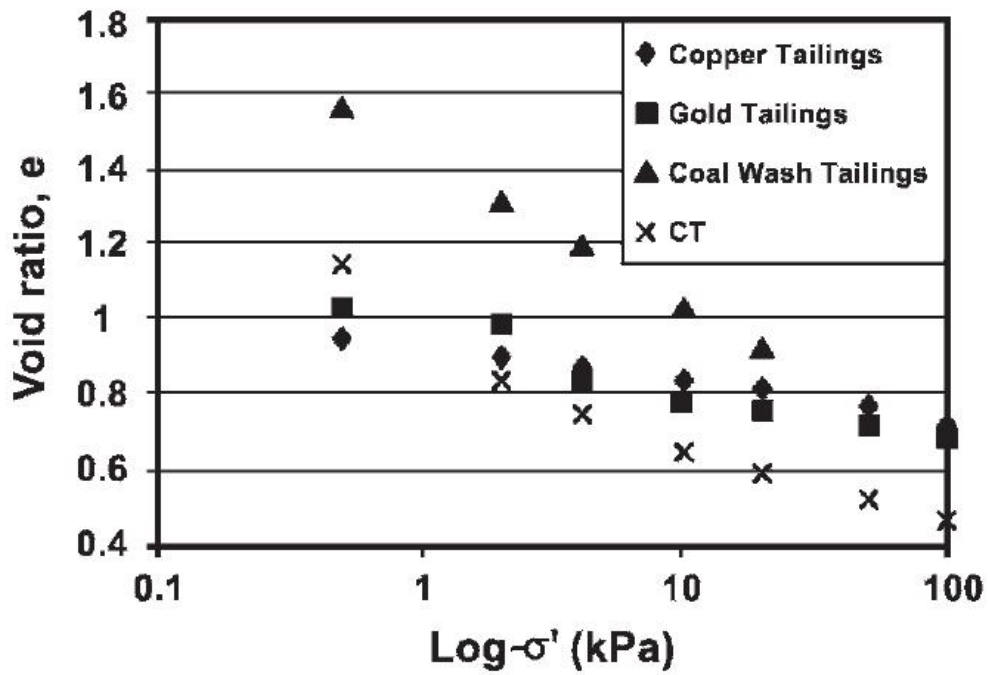


Figure 2-15 Compressibility of mine tailings as a function of void ratio (Qiu and Sego,

1998)

Table 2-5 Compression index C_c for different types of soils (Widodo and Ibrahim, 2012)

Type of Soil	Compression Index C_c
Dense Sand	0.0005 – 0.01
Loose Sand	0.025 – 0.05
Firm Clay	0.03 – 0.06
Stiff Clay	0.06 – 0.15
Medium – Soft Clay	0.15 – 1.0
Organic Soil	1.0 – 4.5
Rock	0

The relationship between compression index and other soil properties has been investigated by many researchers. Hough (1957) established the following relationship between compression index and void ratio and also water content for cohesive soil, silt, clay, silt clay and inorganic soil:

$$C_c = 0.4049(e_0 - 0.3216) \quad (2-4)$$

$$C_c = 0.0102(W_n - 9.15) \quad (2-5)$$

where e_0 is the initial void ratio and W_n the natural water content.

Terzaghi and Peck (1967) proposed the correlation between primary compression index and the liquid limit. The pertinent equation is:

$$C_c = 0.009(W_L - 10) \quad (2-6)$$

Koppula (1981) and Worth and Wood (1978) tried to relate the compression index to the plasticity index of remoulded clay as:

$$C_c = 1.325I_p \quad (2-7)$$

Several correlations have been developed between the primary compression index on the one hand and void ratio, water content, and Atterberg limits on the other (Skempton, 1944; Bowles, 1979; Rendon-Herrero, 1980; Sridharan and Nagaraj, 2000). Akayuli and Ofofu (2013) and Widodo and Ibrahim (2012) performed linear regression analyses using established empirical models to relate compression index and other index properties of different types of soils. They found that the liquid limit had the highest coefficient of determination with compression index and concluded that the former property may be used to estimate the compression index in engineering design.

As is shown in Figure 2-13 and Figure 2-14, the void ratio decreased with the increase of consolidation pressure. The volume of coal refuse sample swelled a little as the pressure was gradually reduced to zero. The results of both samples also indicated that the fine refuse samples had larger compression index and swelling index values with higher initial water contents (or void ratios). The larger the value of compression index of a soil, the greater is its compressibility. Accordingly, higher compressibility results in lower coefficients of consolidation C_v , and thus more strain is necessary for the buildup of the effective stress. This conclusion agrees with the results presented in Figures 2-11 and 2-12.

In engineering practice, the consolidation parameters are very important in the stability analysis of coal waste impoundment embankments and the flow behavior of coal waste slurry. The parameters determine the time required for the water content to drop below liquid limit; the material's density, and shear strength after consolidation; and its resistance to the static and dynamic loading. The influence of consolidation on the strength of fine refuse is covered in Section 2.3.6.

2.3.5 Permeability Tests

Introduction

The hydraulic conductivity (or coefficient of permeability) is defined as a constant of proportionality relating to the ease with which a fluid passes through a medium. Two general laboratory testing methods are available to determine the hydraulic conductivity of soils, i.e., constant-head method and falling-head method. The constant-head method is suitable for soils with higher permeability while falling-head method is for soils with relatively low permeability. Both methods are based on Darcy's law which is given as:

$$v = ki \quad (2-8)$$

The corresponding flow rate (or quantity per unit time) is

$$q = kiA \quad (2-9)$$

where

q = quantity of fluid flow in a unit time, m^3 / s

k = hydraulic conductivity, in velocity unit (m/s)

i = hydraulic gradient = h / L = head loss across a flow path of length L (dimensionless)

h = total head difference across the flow path of length L (m)

L = length of sample or flow path that produces the head difference h (m)

A = cross-sectional area of soil mass through which flow q takes place (m^2)

Constant-Head Method

The constant-head test is usually used for cohesionless soil with hydraulic conductivity $k > 10^{-4} cm / s$. A schematic diagram of the test is shown in Figure 2-16. Sufficient time is needed for the flow through the specimen to stabilize. After flow equilibrium has been established, the volume of outlet water that accumulates with time is measured. At least three

readings should be recorded to obtain an average value. The hydraulic conductivity can be determined by:

$$k = \frac{VL}{A\Delta Ht} \quad (2-10)$$

where

V = collected volume of water (m^3)

L = length of soil sample (m)

A = cross-sectional area of soil sample (m^2)

ΔH = head difference (m)

t = time required to get V volume (sec)

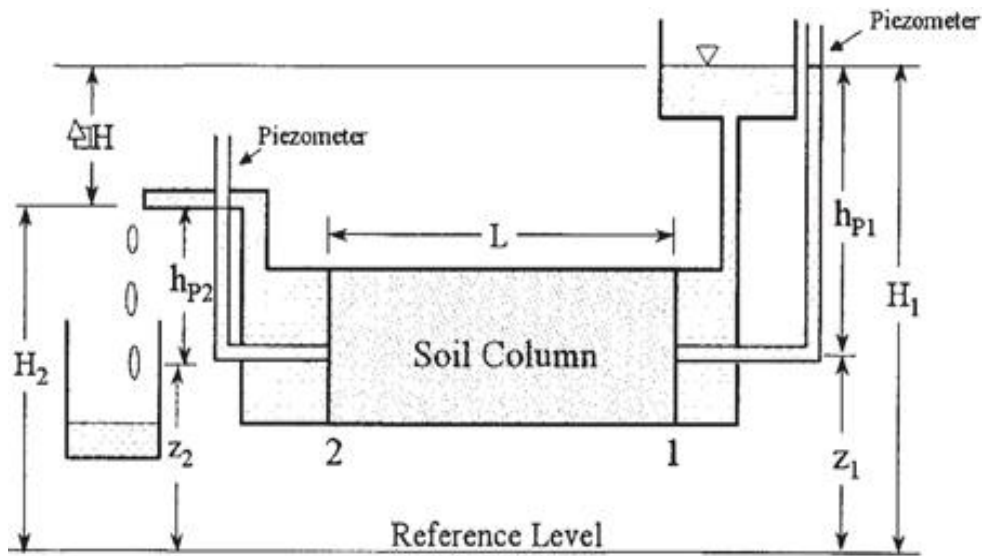


Figure 2-16 Schematic diagram of constant-head permeability test (after Hanson et al., 2013)

Falling-Head Method

The falling-head permeability test involves water flow through a cohesive soil sample with hydraulic conductivity $k < 10^{-4} cm/s$. A standpipe guides water into the sample and the

volume of water passing out of the sample is recorded against time. The test can be conducted in a falling-head permeability cell or in an odometer cell. A schematic diagram of the test is shown in Figure 2-17. Before starting the flow measurement, the soil sample is saturated and the standpipe is filled with water to a marked level. The test then begins by allowing the water to flow through the soil sample over a given time period or until the water level drops down to a given lower position. The process is repeated at least three times and the results are averaged. The hydraulic conductivity can be determined according to the following equation:

$$k = \frac{aL}{At} \ln \frac{h_1}{h_2} \quad (2-11)$$

where

a = cross-sectional area of standpipe

A = cross-sectional area of soil sample

h_1 = hydraulic head across soil sample at the begin of test ($t=0$)

h_2 = hydraulic head across soil sample at the end of test

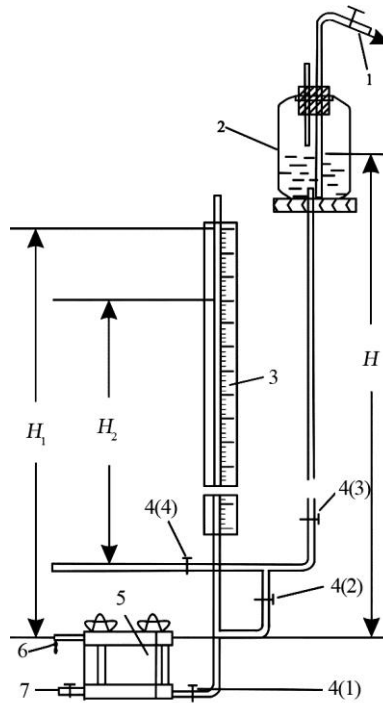


Figure 2-17 A schematic diagram of falling-head permeability test (after Chang et al., 2013)

Testing Facilities and Procedures

Considering the relatively low permeability of the fine refuse, a group of falling-head permeability tests was performed following the procedures provided in ASTM D2434 and ASTM D5084. Figure 2-18 is a photograph of the falling-head permeability test apparatus. The fully saturated coal waste slurry samples were pre-compressed in the permeability cell to reach different initial water contents or void ratios. The fluid used in the permeability tests was distilled water, which was de-aired prior to the tests. The hydraulic gradient was limited to within 10 in order to avoid the seepage-induced consolidation during the test process.

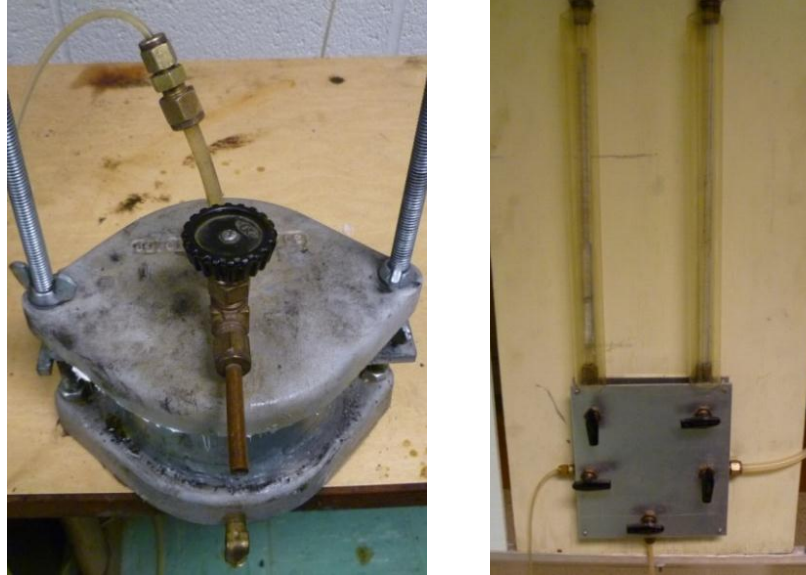


Figure 2-18 Falling-head permeability test apparatus

The hydraulic conductivity of a medium is affected by the viscosity and temperature of the fluid passing through it. The hydraulic conductivity is standardized at 20°C by using the following equation:

$$k_{20} = k_T (\eta_t / \eta_{20})$$

where k_{20} is the standard hydraulic conductivity, and η_t and η_{20} are viscosities of water at test temperature T and at 20°C, respectively. The test temperature was recorded as 23°C. Therefore $\eta_t / \eta_{20} = 0.9313$.

Test Results

A graphical representation of how hydraulic conductivities of the two fine refuse samples vary with void ratio or water content is presented in Figure 2-19. The hydraulic conductivity decreased with the reduction of void ratio. The standardized hydraulic conductivity k_{20} ranged from 10^{-4} to 10^{-8} cm/s for the KY sample and from 10^{-5} to 10^{-9} cm/s for the WV sample.

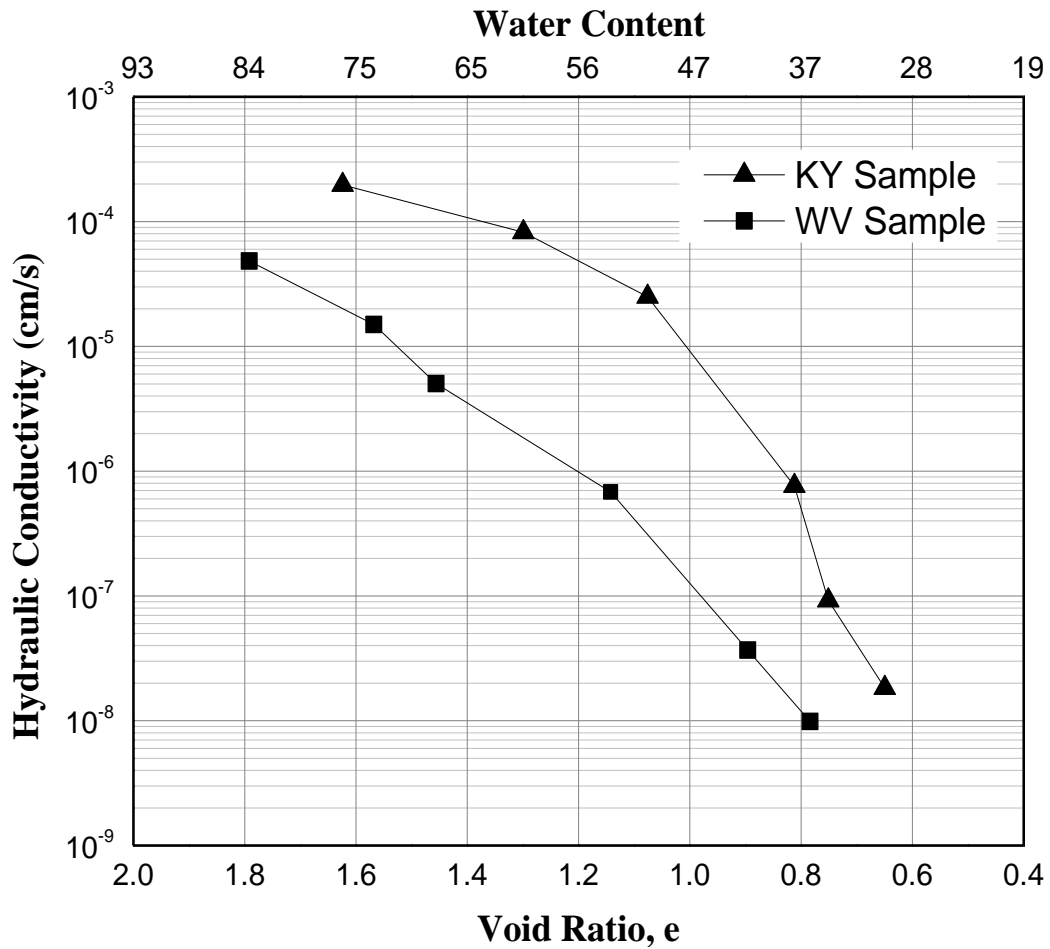


Figure 2-19 Comparison of permeability test results of two samples

The typical range of hydraulic conductivity for common soils is listed in Table 2-6 (Lewis, 1989; West, 1995). The fine coal refuse can be classified as low-plasticity silt in terms of the particle size distribution and index properties. For the most part, the measured hydraulic conductivities of both samples are consistent with the listed range of between 10^{-5} and 10^{-7} cm/sec for silty soils. The full range of the samples extends from low to zero permeability typical of fine sand and clay, respectively.

Table 2-6 Typical ranges of permeability for various soils

Soil	Hydraulic Conductivity, k (cm/sec)	Relative Permeability
Coarse gravel	Exceeds 10^{-1}	High
Sand	10^{-5} to 10^{-1}	Low - Medium
Silt	10^{-5} to 10^{-7}	Very low
Clay	Less than 10^{-7}	Impervious

As seen from the permeability test results, the hydraulic conductivity of the fine refuse samples was strongly dependent on the void ratio, decreasing from 10^{-4} cm/s to 10^{-9} cm/s as the void ratio was compressed from 1.8 to 0.65. It was also strongly affected by particle size gradation. A number of studies have been conducted attempting to establish empirical relationships between hydraulic conductivity and other physical properties. Chen et al. (1967) performed laboratory permeability tests on fine refuse samples and proposed several equations describing relationships between the permeability on the one hand and void ratio and grain size distribution on the other. They concluded that void ratio was the more important factor influencing the permeability of the material. Subsequent work resulted in proposals of other functions such as: $k = (1 + e)(A + Be)$ (Monte and Krizek, 1976); $k = Ce^D$ (Somogyi, 1979); and $k = Ee^F / (1 + e)$ (Carrier, Bromwell, and Somogyi, 1983), where e is the void ratio and A , B , C , D , E , and F are empirical constants (Krizek, 2004). However, the values determined by each of these empirical formulas significantly varied with changes in soil classification and other physical properties.

Permeability is considered as one of the most significant parameters affecting the flow behavior of impounded fine coal refuse and, consequently, both the stability of an impoundment

and the damaging effects of a breach or breakthrough. The property affects the time required for the consolidation and consequent strength buildup of impounded refuse slurry. The permeability of silt-like fine refuse is very low to impervious and the length of the drainage path from some parts of an impounding facility is very long. Consequently primary consolidation of the material can take many years to complete, especially as the void ratio is reduced during the process.

2.3.6 Triaxial Tests

Introduction

The triaxial test measures the shear strength of sampled soil material under drained or undrained conditions. The shear strength parameters, cohesion c and friction angle ϕ , effect the bearing capacity, slope stability, and flowability of a soil.

The shear strength of a soil can be characterized by the Mohr-Coulomb failure criterion which is represented as:

$$\tau_f = c + \sigma \tan \phi$$

where

τ_f = shear strength at failure

c = cohesion of the soil

σ = normal stress on the plane of shearing

ϕ = internal friction angle

The effective shear strength, as measured in a drained triaxial test, can be defined in terms of effective stress parameters, c' and ϕ' . The cohesion for pure sands and normally consolidated clay soils is equal to zero.

The shear strength parameters c and ϕ in either the undisturbed or remolded conditions are usually determined by the following two laboratory tests:

- a) Direct shear test
- b) Triaxial compression test

In the direct shear test, as shown in Figure 2-20, a soil sample is placed in the shear box and subjected to a specified normal load. The shearing force is applied in a direction perpendicular to the normal load. During the shear process, the normal load is held constant but the shearing force is applied to obtain a constant rate of strain. The normal pressure and the shear strength at failure of soil can be obtained by dividing the normal load and the maximum applied shear force by the cross-sectional area of the specimen at the shear plane. The Mohr-Coulomb failure criterion is determined from the results of at least three shear tests.

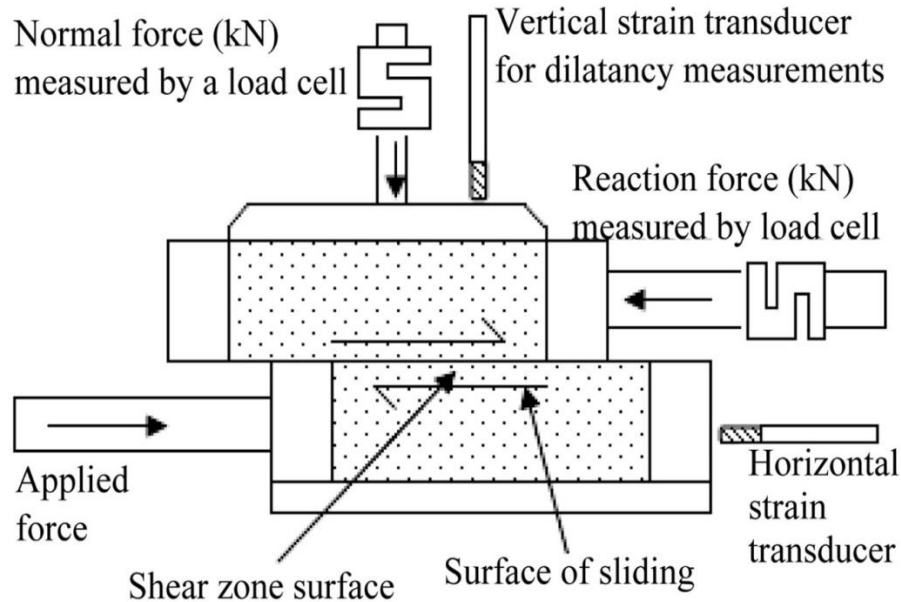


Figure 2-20 Direct shear apparatus

A schematic diagram of a triaxial test apparatus is shown in Figure 2-21. In the triaxial test, the cylindrical soil specimen is encased within a rubber membrane inside a pressure chamber. The lower and upper loading platens have porous disks connected to the drainage system for saturating and draining the soil specimen. The confining pressure σ_3 is applied before the axial compression. When the soil specimen is fully consolidated under the confining pressure, the axial stress σ_1 is applied to the soil until it fails. Although only compressive load is applied to the soil specimen, it fails by shear along an internal shear plane. Depending on whether the drainage is allowed during the consolidation phase and shearing phase, the triaxial tests can be categorized into three main types: Unconsolidated-Undrained (UU), Consolidated-Undrained (CU), and Consolidated-Drained (CD) test. Detailed information about these three tests can be found in Bardet (1997). The Mohr circle at failure can be drawn in terms of the applied confining pressure and the recorded axial load at failure. At least three triaxial tests are

required for one soil specimen under different confining pressures so that three Mohr circles can be obtained. The Mohr-Coulomb failure criterion can thereafter be defined as the tangent of the three Mohr circles. As shown in Figure 2-22, the slope of the tangent gives the angle of internal friction and the intercept on the ordinate gives the cohesion of soil specimen.

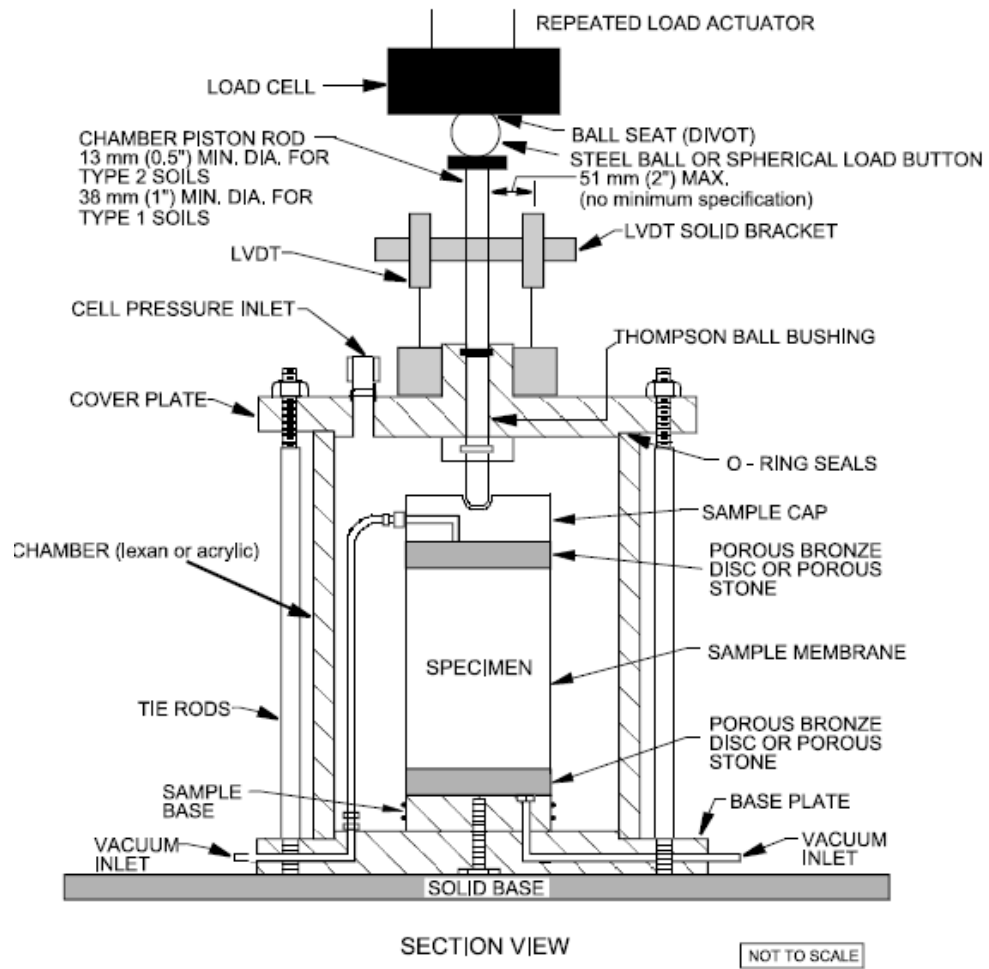


Figure 2-21 Triaxial chamber with external LVDT and load cell (FHWA, 2007)

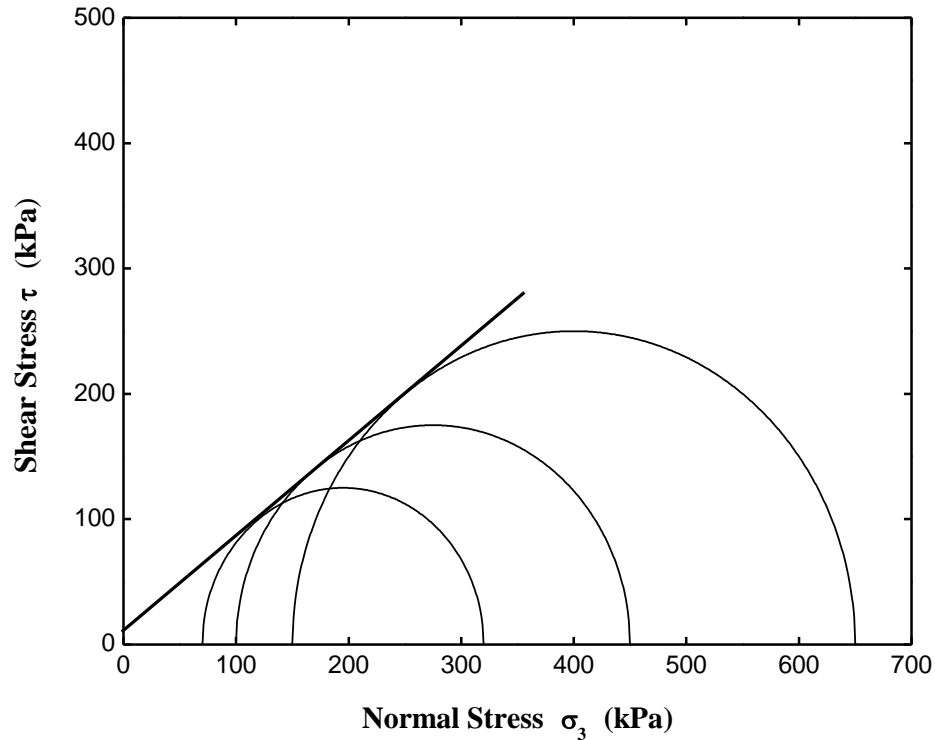


Figure 2-22 Mohr stress circles and developed strength envelope.

The direct shear and triaxial devices have been used for over 70 years to determine the shear strength parameters of soils (Saada and Townsend, 1981). The two testing methods result in pronounced differences in the stress condition developed in the soil specimen. Although some of previous laboratory tests achieved the same shear strength value of a soil sample when comparing the direct shear and triaxial methodologies (Skempton, 1964; Casagrande and Poulos, 1964; Moon, 1984; Thomson and Kjartanson, 1985; and Abdel-Ghaffar, 1990), the triaxial test is considered to be a more reliable and accurate method due to the uniform distribution of stress, accurate measurement of volume change, the known state of stress during all stages of the test, and realistic (as opposed to pre-determined) plane of failure (Murthy, 2002).

Testing Facilities and Procedures

In this study, a group of triaxial tests were conducted on the coal waste slurry samples with different initial void ratios under unconsolidated-undrained (UU) and consolidated-drained (CD) conditions in order to establish the relationship between the void ratio and shear strength. The preparation of samples and setup of the experimental apparatus are shown in Figure 2-23. Since the permeability of coal waste slurry is very low, a small amount of pressure was applied on the top of the buret to accelerate saturation process. However, the applied pressure was kept low enough to ensure that the uplift seepage force would not be excessive and induce liquefaction. The specimen was considered fully saturated based on the Skempton's pore pressure parameter $B = \frac{\Delta u}{\Delta \sigma_3} > 0.95$, where Δu is the change in pore water pressure due to any incremental increase in confining pressure $\Delta \sigma_3$. The confining pressure was applied at magnitudes of 70kPa, 100kPa, and 150kPa. The applied loading rate was set at 0.5 mm/min for UU tests and 0.015 mm/min for CD tests. During the test, failure of the specimens was defined at 20% of axial strain. The shear strength of each sample was developed by drawing the failure envelope based on the three Mohr stress circles at failure.



Figure 2-23 Prepared test sample and triaxial chamber for triaxial tests

Test Results

Unconsolidated-Undrained Tests

In the unconsolidated-undrained (UU) condition, drainage is not allowed throughout the experiment. For saturated fine refuse, the voids in the specimen are full of water (which is incompressible). The confining pressure was completely carried by the pore water instead of causing any increase of effective stress in the refuse. Therefore, the value of deviator stress $\bar{q} = \sigma_1 - \sigma_3$ is a constant, irrespective of the change of confining pressure. The result of one of the trial tests is exhibited in Figure 2-24 under confining pressures of 100 kPa, 150 kPa and 200 kPa. The procedure and data processing of the UU test can be found in ASTM D2850. The three Mohr's circles obtained under the different confining pressures had identical diameters ($\sigma_1 - \sigma_3$). The tangent to the three Mohr's circles was therefore a horizontal line with internal friction angle $\Phi=0$. The intercept on the ordinate is defined as the undrained shear strength c_u .

The undrained shear strength of the fine refuse slurry is a significant engineering parameter used in the design and stability analysis of coal waste impoundments and the flow behavior of the impounded slurry.

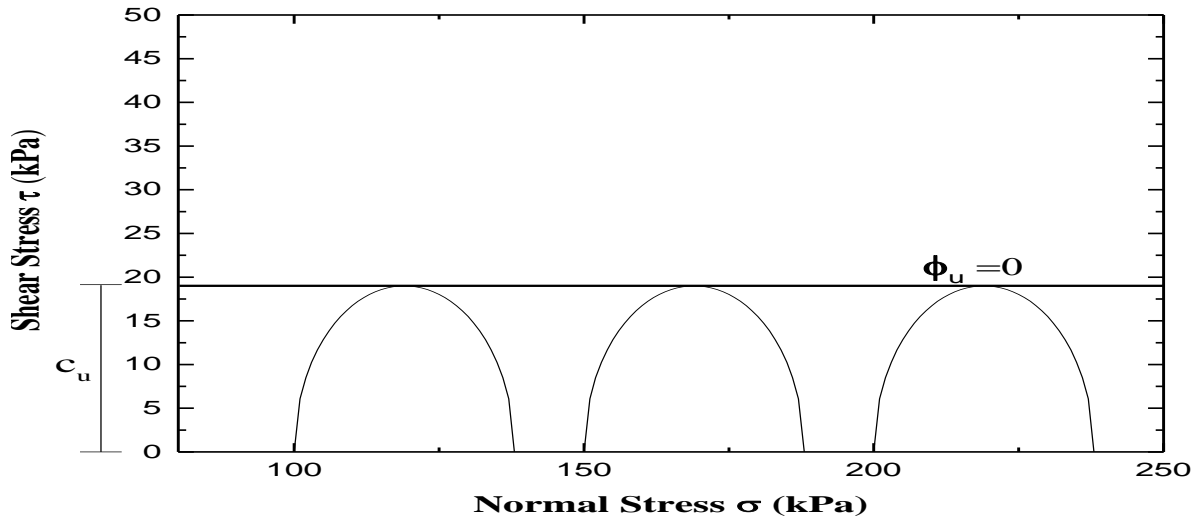


Figure 2-24 Example of Mohr stress circles for UU triaxial test

The variations of undrained shear strength c_u with water content or void ratio for KY sample and WV sample are shown in Figure 2-25. The measured undrained shear strengths of both samples exhibited consistent patterns and increased with the reduction of water content. Both of the two fine refuse samples had extremely low undrained shear strength of less than 10 kPa at water contents above the corresponding liquid limits (38.1% for KY sample and 42.5% for WV sample). As the water content decreased below the liquid limit, significant buildup of undrained shear strength was observed.

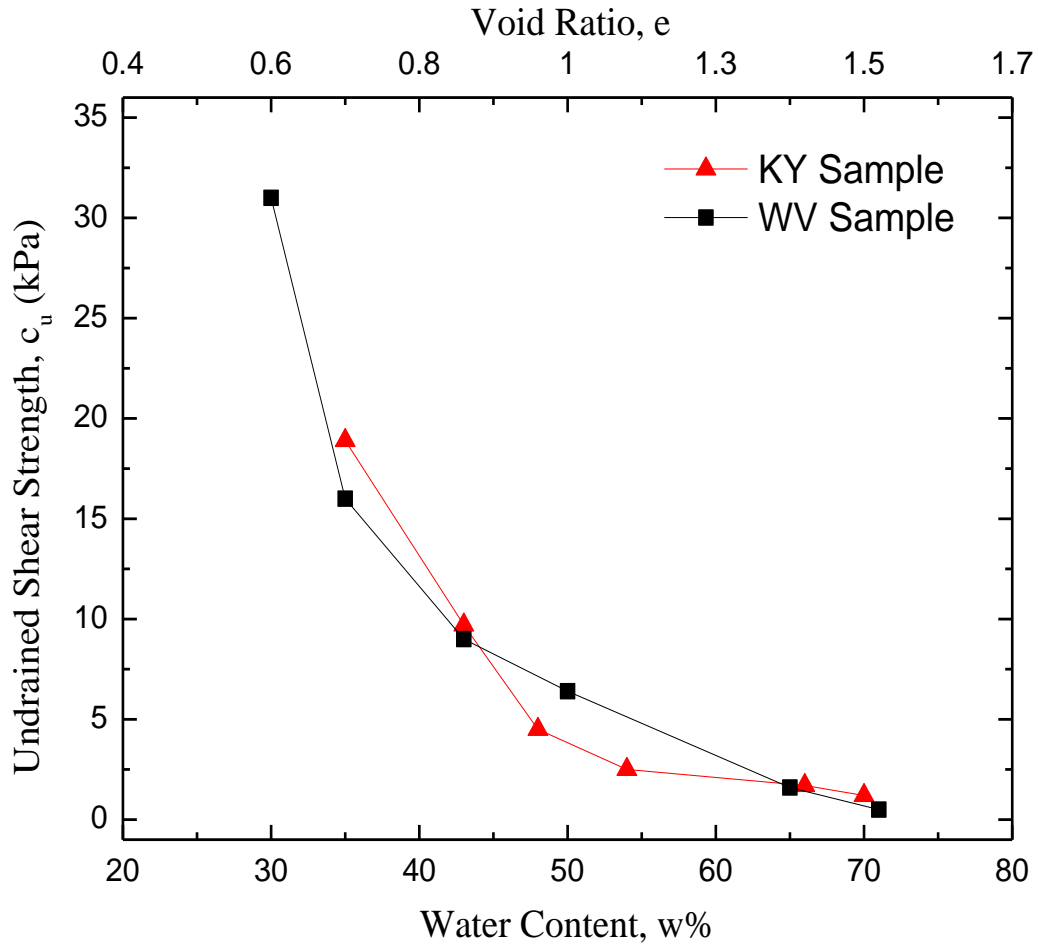


Figure 2-25 Variation of undrained shear strength with water content

Consolidated-Drained Tests

In the consolidated-drained (CD) tests, the saturated coal waste slurry sample was first consolidated to an initial effective stress under the applied confining pressure. Consolidation is an important step in testing frictional materials whose elastic properties and shear strength depend largely on effective stress (Bardet, 1997). The time required to complete consolidation was several days. After the completion of consolidation, the shearing stress was applied under the drained condition until the sample failed. In the CD test, the coal refuse sample was sheared at a much slower rate of 0.015 mm/min than the 0.5 mm/min rate in UU test in order to allow for

pore pressure equalization throughout the sample and to obtain an accurate effective strength value. Failure of the sample was defined as 20% of axial strain. The time required for failure to occur was several hours. Since drainage was allowed, excess pore water pressure remained equal to zero throughout the CD test. The measured total shear strength parameters were identical to the effective shear strength parameters (c' and ϕ').

The shear strength of impounded fine refuse, behaving similarly to silty soils, tends to be primarily influenced by the internal friction angle. When the fine coal refuse is subjected to an external load in the drained condition, the vast majority of the load is carried by the friction between internal particles rather than the cohesion. Previous work with CD tests has found fine coal refuse to have small cohesion values on the order of less than 30 kPa. The strength of the material was primarily based on the material's angle of internal friction (Zook et al., 1974; Sweigard et al., 1997; Zeng et al., 1998a and 1998b; Krizek, 2004; Hegazy et al., 2004; and Agarwal, 2009). However, the effective strength of fine refuse is very sensitive to water content. Reduction of effective internal friction angle with water content has been observed by Sweigard et al. (1997) and Burns et al. (2010).

In this study, both KY and WV fine refuse samples were prepared with different initial water contents ranging approximately from 30% to 80%. The developed $\sigma - \tau$ relationships with different water contents are displayed in Figure 2-26 for KY sample and Figure 2-27 for WV sample. The measured effective cohesion c' was in the extremely low range of 2 – 12 kPa for KY sample and of 0 – 26 kPa for WV sample.

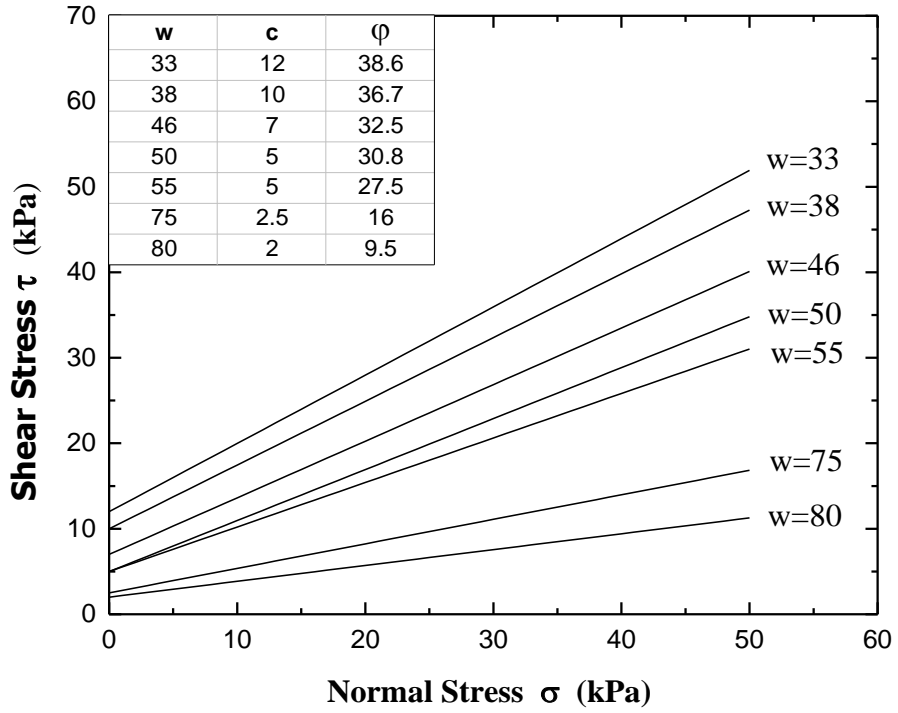


Figure 2-26 Results of consolidated-drained (CD) tests for KY sample

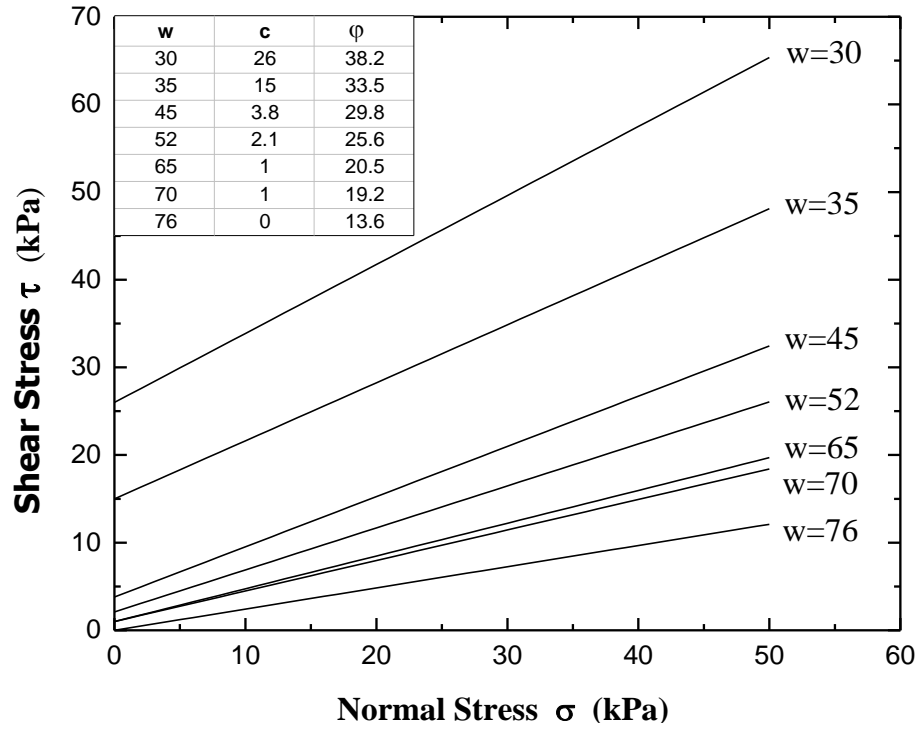


Figure 2-27 Results of consolidated-drained (CD) tests for WV sample

Lindeburg (2003) summarized the typical cohesion values for different soil groups. As shown in Table 2-7, the cohesion of fine grained silty soil is about 9 kPa which agrees with the measured results. The change of effective internal angle of friction with water content is shown in Figure 2-28. The linear variation ranges between more than 35° to less than 10° as the water content increased from 30%, which is below the liquid limit, to approximately 80%, which is above the liquid limit.

Table 2-7 Typical cohesion value for different soil groups (after Lindeburg, 2003)

USCS Soil Group	Cohesion (saturated) (kPa)
SM	20
SC	11
ML	9
ML-CL	22
CL	13
MH	20
CH	11

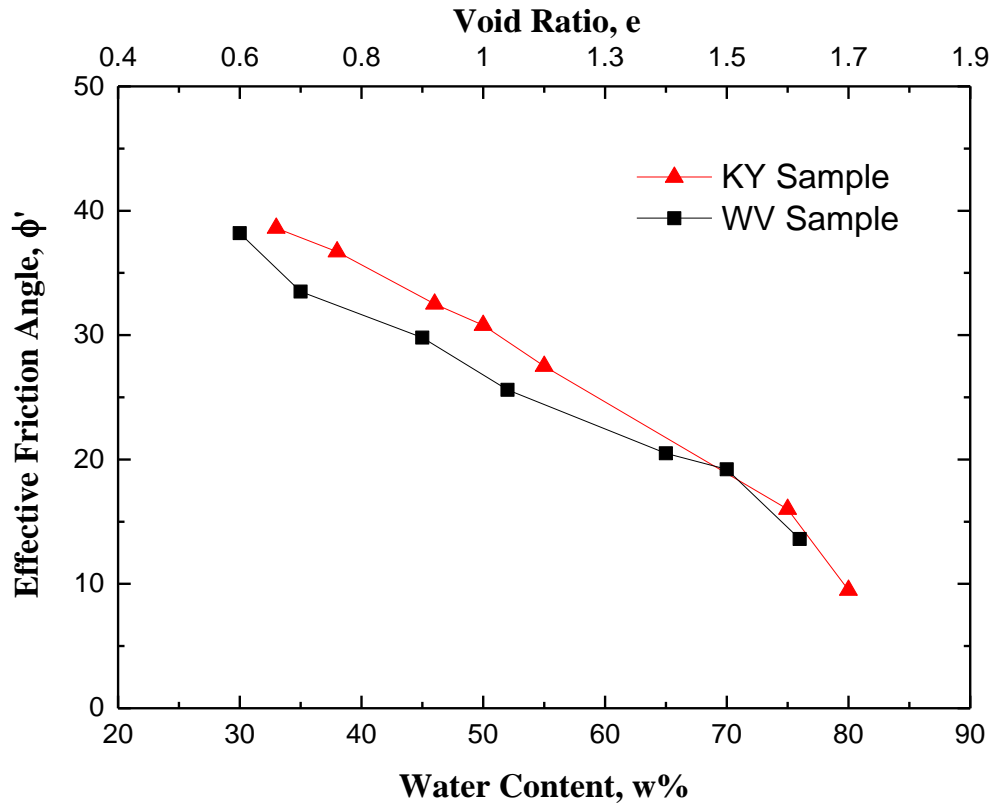


Figure 2-28 Variation of ϕ' with water content for two samples

Zook et al. (1974) stated that “the shear strength of coal refuse would be affected by its composition, moisture content, degree of compaction, amount and grain size of fines present”. According to the results in this study, the initial water content seemed to be the dominating factor controlling the material’s shear strength. Although the KY and WV slurry samples generally had somewhat different engineering properties there was little variation of shear strength. At high water content (above the liquid limit), the friction angle of the fine refuse was extremely small, making it vulnerable to static or dynamic disturbance. In the event of impact loading, excess pore water pressure in the material can rapidly increase and cause a further reduction in the shear strength or, in the worst case, a total loss of strength and consequent liquefaction. In the construction process, especially in the case of the upstream construction

method, it is necessary to provide enough time for the consolidation of fine refuse in order to develop sufficient shear strength.

In the construction of upstream and center line coal refuse impoundments, some of the coarse embankment material is placed on top of impounded fine refuse. An engineering concern relates to the effectiveness of consolidation on the shear strength of the slurry. In lab tests Huang et al. (1987), Suthaker and Scott (1994), Suthaker et al. (1997), Sweigard et al. (1997), and Jones and Uckert (2006) found that the internal angle of friction of impounded coal waste and oil-sand tailings slightly increased as the water content dipped below the liquid limit. However, the rate of consolidation was extremely slow due to the low permeability and long drainage paths in the material. A high void ratio was observed even after the full consolidation (Zeng et al, 1998b). Suthaker et al. (1997) conducted large scale consolidation tests on the oil-sand tailings and found no development of effective strength even after more than 14 years.

2.3.7 Viscosity Tests

Introduction

In a flowing fluid, particles and molecules move differentially and generate internal frictional forces that limit flow velocity. This shear resistance to flow is called viscosity. The Two-Plates-Model is often used to explain the mechanism of shear flow as well as define the fundamental concept of viscosity. As shown in Figure 2-29, two plates are placed on the top and bottom of a fluid. The distance between two plates is h . The upper plate with the shear area A starts to move under the drag force (shear force) F and the resulting flow velocity v (or “ U ” in Figure 2-29) on the surface is measured. The plate at the bottom is stationary with flow velocity

equal to zero. The fluid is sheared in the shear gap h . This model is only applicable to laminar flow and assumes that the fluid adheres to both plates without sliding or slipping.

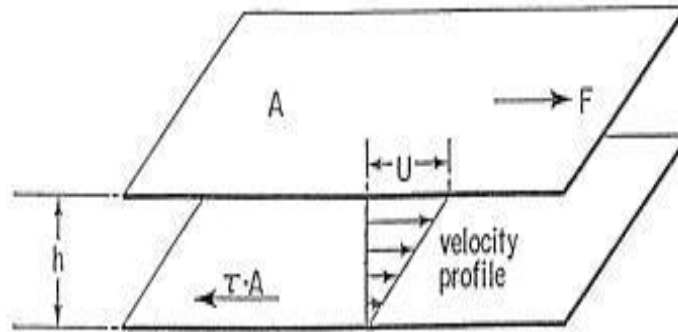


Figure 2-29 Shear flow by using Two-Plates-Model (after Vlachopoulos, 2003)

The shear stress τ , which is a constant, is represented as:

$$\tau = \frac{F}{A} \quad (2-12)$$

The shear rate $\dot{\gamma}$ is the rate at which a progressive shearing deformation is applied to a fluid. It is also called the shear gradient or velocity gradient. In terms of the Two-Plates-Model, the shear rate is defined as:

$$\dot{\gamma} = \frac{v}{h} \quad (2-13)$$

The viscosity of fluid η is defined as the ratio of the imposed shear stress and the shear rate:

$$\eta = \frac{\text{Shear Stress}}{\text{Shear Rate}} = \frac{\tau}{\dot{\gamma}} = \frac{F/A}{v/h}$$

The unit of viscosity is Pascal-seconds, otherwise called “Pas” or poise and designated as “P”. 1P = 100cP (centipoise). The typical values of viscosity for different materials are listed in Table 2-8.

Table 2-8 Typical viscosity values of various materials (after Mezger, 2002)

Material	Shear Viscosity η (cP)
Gas / Air	0.01 – 0.02 / 0.018
Water at 0°C / 20°C / 100°C	1.79 / 1.0 / 0.282
Mercury	1.55
Milk, Coffee cream	2 - 10
Glycerine	1480
Silicone polymers	$10^7 - 10^8$
Bitumen at 80°C / 20°C	$2 \times 10^5 / 5 \times 10^8$

The viscosity of a fluid can be measured by using a viscometer or rheometer. Strictly speaking, a viscometer is an instrument measuring viscosity under one flow condition while the rheometer can measure viscosity under varying flow conditions. Most of the time, however, a rheometer is also called a viscometer.

There are several different types of viscometers available to measure the viscosity of fluid. Some standard viscometers for liquids are introduced here:

U-Tube viscometer: This instrument is also known as Ostwald viscometer or glass capillary viscometer. As shown in Figure 2-30(a), A U-tube viscometer consists of a U-shaped glass tube held vertically in a controlled temperature bath (Anonymous, 2013). The liquid is placed into the upper bulb by suction, and then allowed to flow down through the tube into the lower bulb. Two marks, A and B, indicate the volume of the liquid. The time taken for the level

of the liquid to drop from A to B is proportional to the kinematic viscosity $\nu = \frac{\eta}{\rho}$. The kinematic viscosity is obtained by multiplying the time by a factor specific to the viscometer.

Falling sphere viscometer: The use of the falling sphere viscometer is based on the Stoke's law in which the fluid is stationary in a vertical glass tube. As shown in Figure 2-30(b), a sphere ball of known size and density is allowed to descend through the liquid. The time taken for the sphere to drop between two marks on the tube is called the terminal velocity. The viscosity can be calculated using Stokes' law (Lamb 1879):

$$\eta = \frac{2(\rho_p - \rho_f)}{9} \frac{gr^2}{v_s} \quad (2-14)$$

where

ρ_p = mass density of the sphere

ρ_f = mass density of the fluid

v_s = terminal velocity

g = gravitational acceleration

r = radius of the sphere

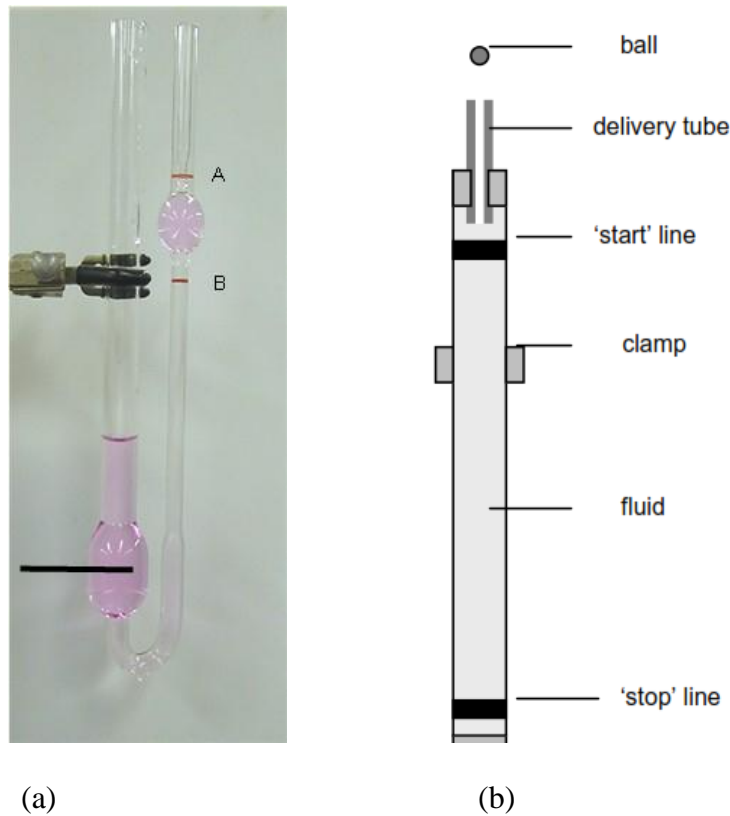


Figure 2-30 a) U-tube viscometer; b) Falling sphere viscosity

Rotational viscometer: The rotational viscometer is based on the idea that the torque required to turn an object in a fluid is a function of that fluid's viscosity. It collects viscosity data derived from the torque required to rotate a disk or bob at different speeds. As shown in Figure 2-31, a rotational viscometer typically consists of two parts: a head unit with a motor and a spindle that is driven by the motor.

The greatest advantage of rotational viscometer is that it can accurately measure viscosity for both Newtonian and non-Newtonian fluids. The viscosity of Newtonian fluids such as water, kerosene, mineral oils etc. does not change with increasing shear stress. By contrast, the viscosity of non-Newtonian fluids does change with increasing shear stress. Non-Newtonian fluids include paint, gels, inks, milk, ketchup etc. (Elcometer, 2006).

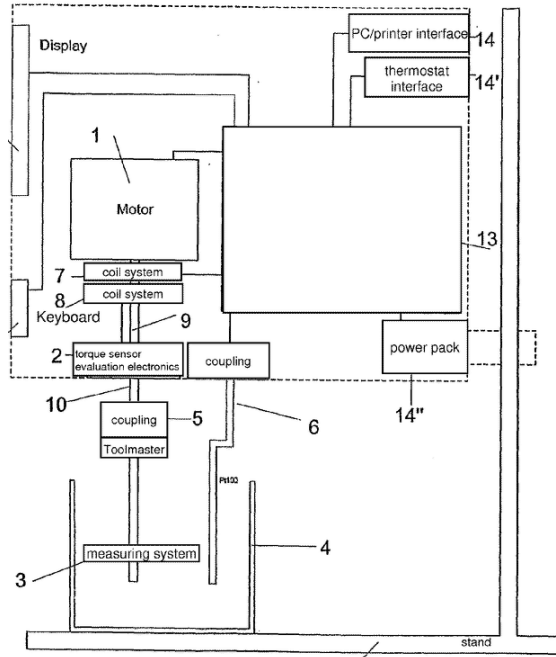


Figure 2-31 Schematic diagram of rotational viscometer (after Anonymous, 2012)

Other types of viscometers include the oscillating piston viscometer, vibrational viscometer, and stabinger viscometer. The different types of viscometers are based on different theories and principles; their applicability depends on the specific objectives and site conditions of an engineering design and construction project (Singh, 2012; and Anonymous, 2014).

Testing facilities and procedures

In this study, the viscosities of coal-waste slurry samples were measured by using an NDJ-8S digital rotary viscometer (Figure 2-32). This type of viscometer is applied to various liquids such as greases, paints, and adhesives. In comparison with other viscosity-measuring instruments, other advantages of the NDG-85 include high measuring accuracy, stability in the display, easy operation and read-out, and interference prevention.



Figure 2-32 Structure of NDJ-8S digital rotary viscometer: (1) Level indicator (2) Display Screen (3) Housing (4) Protection bracket (5) Base (6) Operation key (7) Rotor connector (8) Rotor (9) Level adjustment knob

The rotor of the NDJ-8S digital rotary viscometer is spun by a variable speed motor. During the rotation, the rotor is affected by a torque moment which is proportional to the viscosity of the liquid. The torque is detected by the sensors and the data is converted through a micro-computer to viscosity which is shown on the display. The rotary viscometer was designed with four different spindles shown in Figure 2-33 (1#, 2#, 3#, 4#) and 8 different velocities (0.3, 0.6, 1.5, 3, 6, 12, 30, 60 rpm), which enable it to measure viscosity within different ranges of

values. The measuring ranges of each spindle under different rotation speeds are listed in Table 2-9.



Figure 2-33 Four types of spindles of NDJ-8S digital rotary viscometer

Table 2-9 Table of maximum viscosity values (cp) for different spindles and velocities

Velocity (rpm)	1#	2#	3#	4#
0.3	2×10^4	10×10^4	40×10^4	200×10^4
0.6	1×10^4	5×10^4	20×10^4	100×10^4
1.5	4×10^3	2×10^4	8×10^4	40×10^4
3	2×10^3	10×10^3	4×10^4	20×10^4
6	1×10^3	5×10^3	2×10^4	10×10^4
12	500	2.5×10^3	1×10^4	5×10^4
30	200	1×10^3	4×10^3	2×10^4
60	100	500	2×10^3	1×10^4

Sample Preparation

Two groups of KY and WV coal waste slurry specimens were prepared with different initial water contents. The viscosity tests were conducted by referring to the manufacturer's instructions; and the ASTM D1084, D2556, D4402, and D5018 standards. The saturated coal waste slurry samples were prepared at 23 °C, and thoroughly stirred to obtain uniform mixtures before each measurement. In order to increase the accuracy of measurement, the spindle was located in the center of the specimen and immersed in the liquid for enough time to achieve the same temperature as the tested specimen. The viscometer was calibrated before each measurement by using the calibration fluids provided by CANNON Instrument Company.

The impounded coal waste slurry is typically considered to be a non-Newtonian fluid, especially at relatively low water content (Botsaris and Glazman, 1988; Deng et al., 1989; Boger et al., 2006; Chhabra, 2010; and Bilbao et al., 2011). The 4# spindle was selected in order to keep the recordings within an anticipated range of viscosity values, and the tests were conducted from slow to high rotational speeds. The viscosity of coal waste slurry specimen at various water contents and rotational speeds could be read directly from the LCD screen. Two rounds of tests were performed on each sample to check the repeatability of the results.

Test Results

A trial test was performed in order to study the variation of viscosity with time. As shown in Figure 2-34, the tested sample was subject to a constant shear rate for more than five minutes. The viscosity of coal waste slurry decreased with time and gradually converged to a constant. According to Chhabra (2010), the internal structure of the coal waste slurry is progressively broken under the constant shear rate. As the structural linkages are broken, the rate of reduction

of viscosity approaches zero. However, Aktas and Woodburn (2000) warned that the rate reduction might also be caused by the sinking of the finer fraction of the refuse particles. To avoid this second effect, the viscosity readings in the test were recorded as soon as they reached consistent level on the screen.

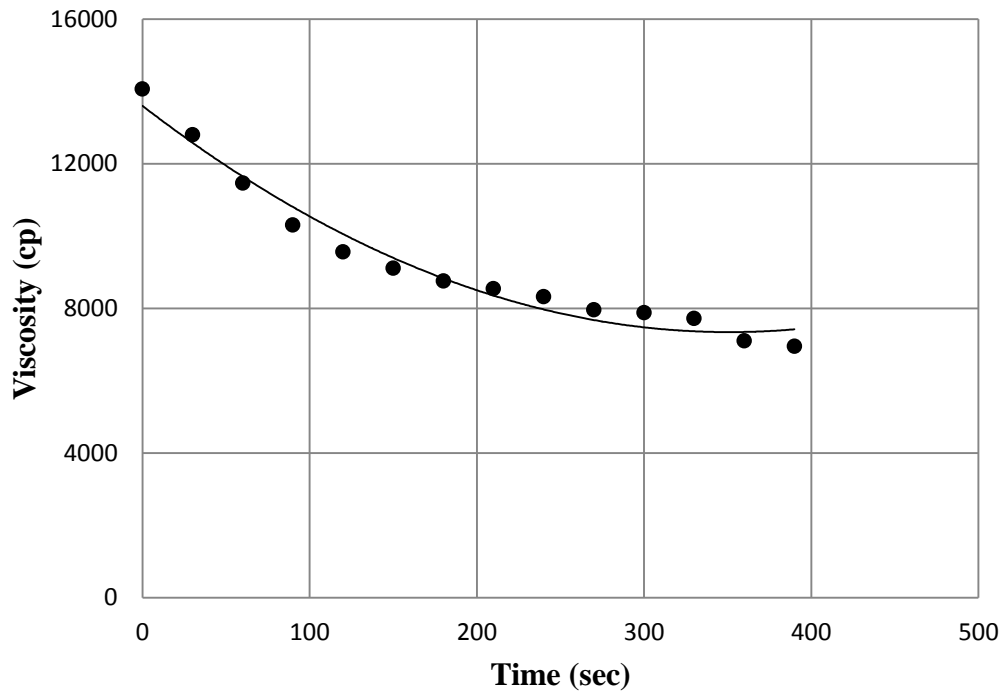


Figure 2-34 Example plot of viscosity vs. time (water content=40%, rotational speed=6rpm)

The relationship between water content and viscosity of the fine coal refuse at different rotational speeds are listed in Table 2-10 for the KY samples and Table 2-11 for the WV samples. The results are also presented graphically in Figures 2-35 and 2-36 for the KY and WV samples, respectively. For both sets of samples, the viscosity decreased with the water content at the same rotational speed. The decreasing of viscosity with rotational speed at the same water content resulted from the “shear-thinning” property of the fine refuse. Other shear thinning materials

include polymer solutions, paints, glues, and shampoos. During the shearing, the particles of such material are more likely to orient to the shear direction and disentangle to a certain extent, which lowers their flow resistance (Mezger, 2002). The recorded viscosities of the KY and WV samples were in the same order of magnitude. However, the WV sample was more viscous than KY sample since the WV sample had a higher clay content (Figure 2-2).

A number of researchers (Round and Hessari, 1985; Kaji et al., 1986; Woskoboenko et al., 1989; Leong and Boger, 1990; Kawatra et al., 1995; Aktas and Woodburn, 2000; and Atesok et al., 2002) have studied the effects of properties of suspended solids on the viscosity of slurry. It was found that the viscosity of the slurry was related to several factors such as particle size distribution, microstructure, temperature, pH, presence of electrolytes and chemical additives. However, the percent of solid particles was considered to be the most significant factor. Kawatra and Bakshi (1995) performed viscosity tests on slurry and observed non-Newtonian flow behavior when the solid content was greater than 20 percent.

Table 2-10 Recorded viscosities of KY (cp) samples with different water contents

Rotate Speed (rpm)	w=38%	w=43%	w=50%	w=64%	w=70%	w=80%
0.6	248000	98500	38250	15000	12500	5760
1.5	97600	36200	16200	8000	4200	2080
3	44400	17800	8800	3000	2235	1050
6	25400	9700	4450	1700	1270	560
12	14650	5325	2300	1100	771	346
30	8140	2940	1285	880	415	258
60	4280	2080	790	570	267	175

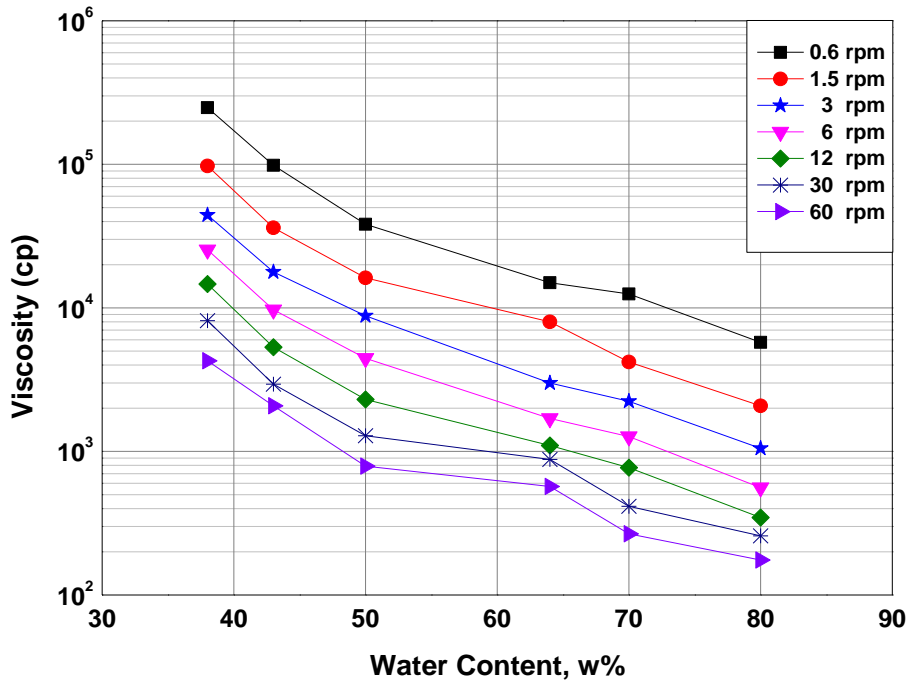


Figure 2-35 Water content vs. viscosity of KY sample under different rotational speeds

Table 2-11 Recorded viscosities of WV samples with different water content (unit: cp)

Rotate Speed (rpm)	42%	50%	56%	64%	71%	75%	80%
0.6	128960	42300	26100	14235	11310	8188	6500
1.5	54210	20856	12280	5970	4728	3605	3120
3	28335	13744	6700	3240	2473	1978	1540
6	15323	6430	3910	1800	1350	1050	976
12	7980	3050	2500	1135	936	715	688
30	3298	1986	1584	846	680	540	420
60	2960	1140	977	668	525	438	340

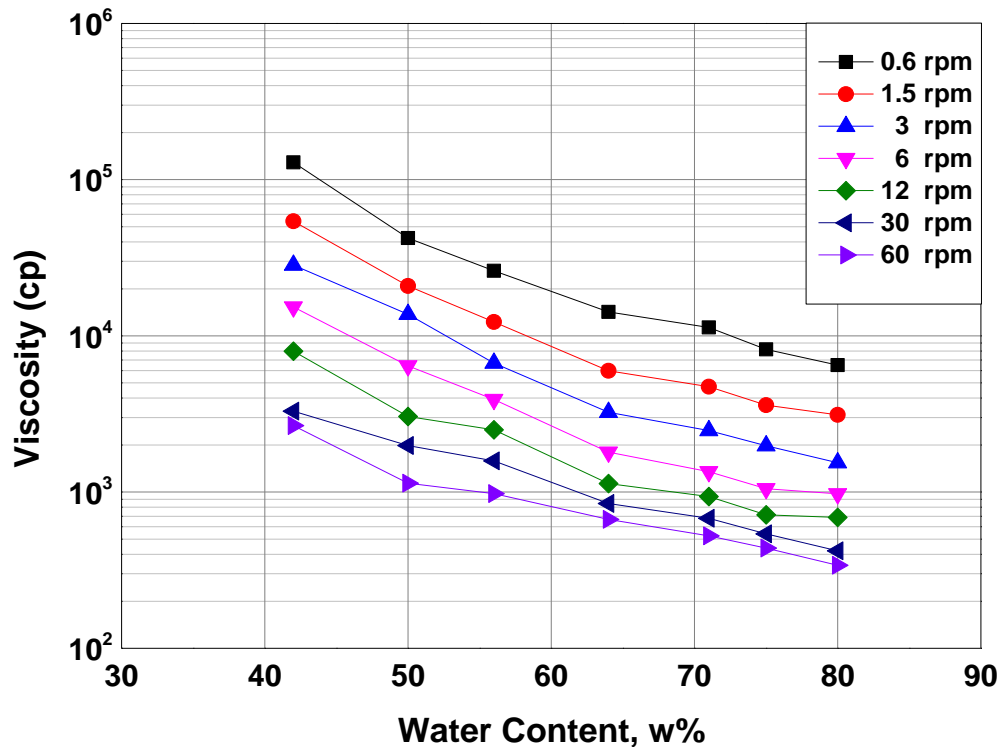


Figure 2-36 Water content vs. viscosity of WV sample under different rotational speeds

Viscosity is considered as one of the most significant factors governing the flow behavior of coal waste slurry. Once a flow starts, the speed of flow and distance that the flow will go is dependent on the viscosity of the material. Therefore, the measurement of viscosity of the slurry can, to a great extent, be a predictive tool for evaluating the potential damages caused by a hypothetical failure of a coal waste impoundment. The influence of viscosity on the flow behavior of coal waste slurry will be assessed in Chapters 3 and 4.

2.4 Conclusions

Geotechnical laboratory tests have been conducted on the coal waste slurry samples obtained from two impoundments in Kentucky and West Virginia. The measurements of geotechnical properties of impounded coal waste slurry included particle size distribution, specific gravity, soil index properties, consolidation coefficient, compression index, hydraulic

conductivity, shear strength, and viscosity. The relationships between some of the geotechnical properties and water content and initial water content were established. The following conclusions can therefore be drawn:

1) For both the KY and WV samples, more than 80% of fine particles pass the No. 200 (0.075mm) sieve. The particle size distribution of the WV sample is finer than that of the KY sample.

2) Based on particle size distribution and soil index properties (specifically liquid limit and plasticity index), the impounded fine refuse is classified as a silt with low plasticity (ML).

3) The specific gravity values of fine refuse are 2.03 for the KY sample and 2.14 for the WV sample, which are lower than typical soils. The values result in a lower level of effective stress and shear strength. The loose granular structure of the material after full consolidation should be more susceptible to disturbance by dynamic loading.

4) The liquid limit of the KY and WV coal waste slurry samples is 38.1% and 42.5%, respectively.

5) The coefficient of consolidation C_v increases with compressive pressure and decreases with water content. The value of C_v may help to determine the time required for the water content to drop low enough to prevent flow failure. However, C_v is affected by many factors in addition to water content such as clay mineralogy, soil type and other mechanical and physicochemical parameters. Impounded coal waste slurry should therefore be tested site-specifically.

6) Both the compression index C_c and swelling index C_s increase with initial water content. Coal waste slurry has a higher degree of compressibility in comparison with other soils and mine tailings.

7) The hydraulic conductivity k of the fine refuse decreases with the reduction of the initial void ratio and is in the range of 10^{-9} to 10^{-4} cm/sec. The hydraulic conductivity affects the ability of the pore water to exit an impounding facility and consequently the time needed for coal refuse slurry consolidation. The rate of consolidation, in turn, influences the geotechnical strength of the fine refuse and stability of the impoundment.

8) Since the permeability of slurried fine refuse is classified as very low to impervious and the length of the drainage path from some areas of the impoundment basin is long, the rate of primary consolidation is considerably slow. In general, coal waste slurry freshly deposited in an impoundment requires up to many years to complete primary consolidation.

9) A variation of undrained shear strength c_u with initial water content was observed when conducting unconsolidated-undrained (UU) tests. The undrained shear strength increased with the reduction of the water content. A significant buildup of strength is observed when the water content dropped below the liquid limit.

10) The relationship between effective shear strength of the fine refuse and initial water content was developed based on the results of consolidated-drained (CD) tests. Decreasing water content resulted in a linear increase in the effective internal angle of friction.

11) As the initial water content changed from 80% to 30%, the effective cohesion c' of the refuse increased from 0 to 26 kPa and the effective internal angle of friction increased from 10° to nearly 40° . The impounded coal waste slurry exhibited low shear strength even when the water content was below the liquid limit. Consequently, an improperly designed coal waste

impoundment embankment could have great failure potential if subjected to either static or dynamic disturbance even after some degree of consolidation.

12) The viscosity of coal refuse was measured using a rotational viscometer. The coal waste slurry is considered a “shear-thinning” non-Newtonian fluid whose viscosity decreases with the rotational speed.

13) The percent of solid coal waste particles, the inverse of water content, is considered the most significant factor influencing the viscosity of the coal waste slurry samples.

14) At a given rotational speed, the viscosity of coal slurry is found to decrease with water content.

15) The geotechnical properties of coal waste slurry are important factors affecting its flow behavior. Their measurement provides data potentially useful in predicting the extent and energy of flow following an impoundment embankment breach or basin breakthrough, and consequent impacts on human safety, property, and the environment.

ANALYSIS OF FLOW BEHAVIOR OF COAL SLURRY BY SMALL SCALE MODEL TESTS

3.1 Introduction

Flow failure of coal slurry impoundment can cause significant property and environmental damages. In the past few decades, a number of tailings impoundments have failed releasing huge quantities of slurried waste. A typical example of such flow failure was the failure of the EL Cobre Dam in Chile in 1965 when 2 million tons of copper tailings traveled 12 km in minutes and killed more than 200 people (Jeyapalan et al, 1983). For regions where the underground mine workings are adjacent to or beneath an impoundment, the impounded coal waste slurry may break through into the underground mine works and endanger the lives of mine workers and quality of groundwater resources (Michael et al. 2010).

In order to evaluate the hazards associated with flow failure of coal waste impoundments and the failure potential of impoundments under static and impact loading, it is important to identify the flow characteristics of slurried coal waste under a variety of conditions. Only a limited number of investigations on the flow failure of coal waste slurry impoundments have been documented. The flow behavior of coal waste slurry under static and impact loading and its relationship to the material's geotechnical properties have not been well studied.

A literature review of past studies on the flow properties of coal waste slurry and other viscous fluids has identified a number of different approaches to predicting flow characteristics. Jeyapalan et al. (1983) performed a series of laboratory flume flow tests on the coal waste slurry and similar materials. The measured results were compared with existing theories and models built into the computer program TFLOW. Laboratory flume tests were also conducted by Kwak et al. (2005) in order to investigate the effect of water content on the flow behavior and

depositional geometry of tailings and kaolinite pastes. Brisson et al. (2002) proposed an instantaneous profile method to estimate unsaturated flow characteristics in the nickel mine tailings based on the measurements of volumetric water content and matric suction. Sawyer et al. (2012) triggered mudflow using the dam-break method in order to explore how the difference between shear stress and shear strength controls the dynamics of mudflow and the morphology of the deposit. The results indicated that a flow with high flow factor F_f (defined as the ratio of the shear stress to the yield strength) would produce a rapid and extensive release of the impounded material (approximately 70% of the total impounded volume) post embankment failure with an accelerating, long-distance run-out flow of only 10 seconds from flow initiation.

3.1.1 Review of Rheological Models

Under a static or impact disturbance, saturated and loosely deposited coal waste slurry may flow as a viscous fluid. In order to describe the flow characteristics associated with the measured results from laboratory flume test, it is helpful to refer to an applicable rheological model.

In Equation 2-15, the term $\frac{v}{h}$ is the velocity gradient and can be expressed in the differential form of $\frac{dv}{dh}$. Equation 2-16 can therefore be rewritten as:

$$\tau = \eta \frac{dv}{dh} \quad (3-1)$$

This equation is known as Newton's law of viscosity. It has long been known that different fluids exhibit different behaviors under stress. A fluid is either Newtonian or non-Newtonian depending on whether its flow behavior complies with Newton's law.

Newtonian fluids obey Newton’s law and have a constant value of viscosity η which does not depend on the stress state and velocity of the flow (Anonymous, 2014). As shown in Figure 3-1, the viscous stress arising from flow is linearly proportional to the shear rate. The Newtonian fluid is considered to be the simplest mathematical model of fluid pertaining to viscosity. However, it is hard to find an ideal Newtonian fluid in reality. Some common fluids such as water and air are assumed to be Newtonian under ordinary conditions.

In contrast, the non-Newtonian fluids do not obey Newton’s law and the value of viscosity is not constant but varies with shear rate or shear rate history. In a non-Newtonian fluid, the relationship between the shear stress and the shear rate changes and can even vary with time (a phenomenon called “time - dependent” viscosity). Based on the nature of the relationship between shear stress and shear rate, non-Newtonian fluids are divided into several categories designated as Pseudoplastic, Pseudoplastic with yield, Bingham Plastic, and Dilatant fluids. The $\tau - \dot{\gamma}$ relationships are graphically shown in Figure 3-1.

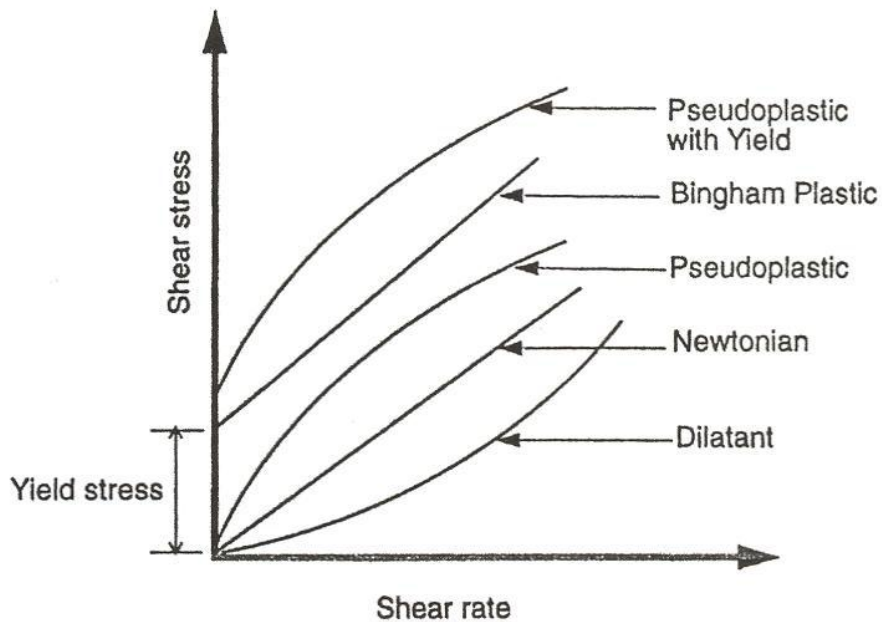


Figure 3-1 Basic models of rheological behavior (after Kawatra et al., 1995)

In general, shear stress increases with shear rate. The differences among the rheological models are associated with the nature of the increase. When the rate of shear stress increase decreases with the shear rate (e.g. in a Pseudoplastic material), the fluid is called “shear-thinning”. The opposite case (in a Dilutant fluid) is called “shear-thickening”. In reality, shear-thinning behavior is more common than shear-thickening. Brief descriptions of the physical properties of the rheological models follow:

- ***Pseudoplastic Fluid:*** A Pseudoplastic fluid is a shear-thinning fluid. No minimum shear stress (yield stress) is necessary to initiate the flow. Examples of a Peudoplastic fluid include milk and cement. The mathematical representation is:

$$\tau = m(\dot{\gamma})^n = m(\dot{\gamma})^{n-1} \dot{\gamma} \quad (3-2)$$

where $\dot{\gamma}$ is the shear rate and m and n are coefficients affecting the shape of the curve shown in Figure 3-1. Pseudoplastic behavior occurs where $n < 1$.

- ***Pseudoplastic with Yield Fluid:*** This is another type of shear thinning fluid. However, the shear stress must reach a certain minimum value, or yield stress, before flow commences. The mathematical representation of a pseudoplastic with yield fluid is:

$$\tau = \tau_y + m(\dot{\gamma})^n = \tau_y + m(\dot{\gamma})^{n-1} \dot{\gamma} \quad (3-3)$$

As with pseudoplastic fluids, $n < 1$.

- ***Bingham Plastic Fluid:*** Similar to the pseudoplastic with yield fluids, Bingham Pastic fluids must achieve a yield stress before they begin to flow. The ideal Bingham plastic fluid

behaves as an elastic solid below the yield stress but as a Newtonian fluid once the yield stress is exceeded. That is, the shear rate is zero when the applied shear stress is less than Bingham yield stress but above the yield stress there is a linear relationship between shear stress and the shear rate. Examples of Bingham plastic fluids include clay suspensions, sewage sludge, drilling mud, toothpaste, mayonnaise, chocolate, and mustard (Anonymous, 2014). The mathematical representation of the Bingham plastic fluid is:

$$\tau = \tau_y + \eta_p \dot{\gamma} \quad (3-4)$$

where the yield stress τ_y is also called Bingham yield stress and η_p is called the plastic viscosity.

- ***Dilatant Fluid:*** A Dilatant fluid is shear-thickening. As shown in Figure 3-1, the rate of shear stress increase increases with shear rate and the yield stress is negligible. The most common dilatant fluid is corn starch dissolved in water. The mathematical representation of dilatant fluid is the same as that of pseudoplastic fluid which is:

$$\tau = m(\dot{\gamma})^n = m(\dot{\gamma})^{n-1} \dot{\gamma} \quad (3-5)$$

However, dilatant behavior occurs where the coefficient $n > 1$.

3.1.2 Determine Rheological Parameters of Bingham Plastic Flow

The flow characteristics of coal waste slurry have not been extensively documented due to limited field and lab data. The nature of viscous flow is influenced by the interrelationship among a number of factors. Based on a few studies, the Bingham Plastic model is considered most applicable to the coal waste slurry (Jeyapalan, 1980; Krizek, 2004; and Michael et al.,

2010). The two primary parameters of Bingham Plastic fluid, the plastic viscosity η_p and yield stress τ_y , can be easily determined and utilized in a flow analysis. Using the Bingham plastic model, Blight (1969), Bishop (1973), Whitney et al. (1977), Castillo and Williams (1979), Deysarkar and Turner (1980), and Jeyapalan, (1980) performed laboratory tests on mine tailings and other natural debris materials and predicted the flow behavior with reasonable accuracy.

In order to represent the coal waste slurry by using Bingham Plastic model, it is necessary to determine the two governing parameters: plastic viscosity η_p and yield stress τ_y . However, the actual flow of coal waste slurry might behave more like a Pseudo-Bingham Plastic fluid (or Herschel–Bulkley fluid). As shown in Figure 3-2, the slope of the tangent to a curve of empirical data stands for the viscosity of a Pseudo-Bingham Plastic fluid. The “apparent” viscosity initially decreases but gradually becomes constant with increasing shear rate. The mathematical expression of the flow behavior represented by the curve itself is hard to work with in a flow analysis. In order to simplify the Bingham plastic model analysis, Krizek (2004) recommended that “the plastic viscosity is taken as the slope of the more-or-less linear portion of the curve for high strain rates; and the yield stress is taken as the point where the projection of this linear portion of the curve intersects the shear stress axis”. The application of his approach to viscosity data collected in this study is discussed in Section 3.3.1.

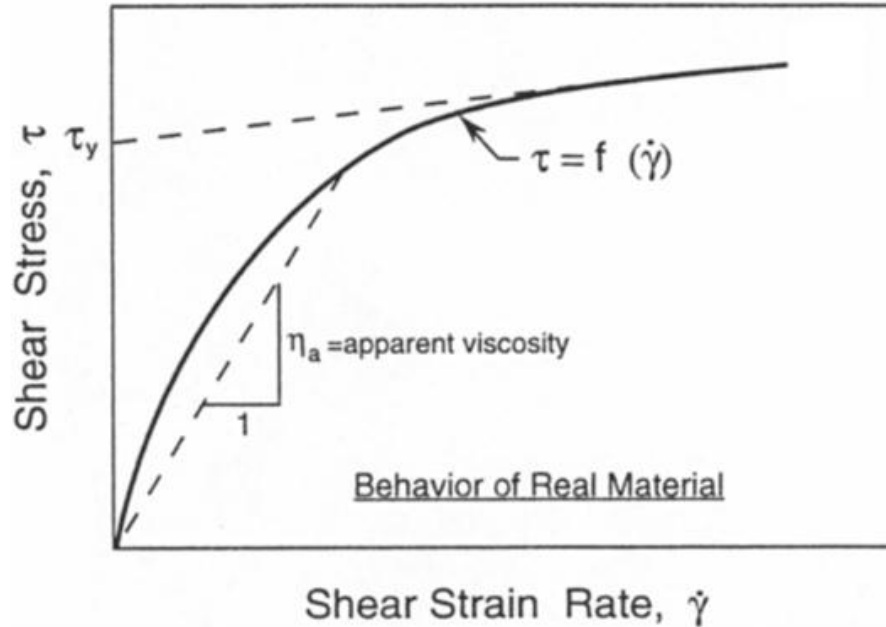


Figure 3-2 Pseudo-Bingham Plastic Model (after Krizek, 2004)

3.2 Model Preparations and Test Procedures

In order to evaluate the influence of important parameters on the flowability of impounded coal waste slurry and to provide physical data for the rheological analysis, a group of small-scale flume tests were conducted under both static and impact loading. The measured data was compared with the results obtained from centrifuge tests which are covered in Chapter 4.

3.2.1 Flume Tests under Static Loading

The test setup for flow failure under static loading is shown in Figure 3-3. A pond with internal dimension of 30cm (length) \times 30cm (width) \times 60cm (height) is at the top of a slope 2 meters tall. The flume is 5 m long and 35 cm wide, and has red lines on the surface of the slope marking the distance traveled by a slurry sample from the top. The distance between two successive mark lines is 30 cm.

For each test, 12 gallons of coal waste slurry sample were placed in the pond. The slurry was prepared with different water contents and thoroughly agitated before pouring it into the pond. Before starting each test, the viscosity and shear strength of the sample was measured in the laboratory.

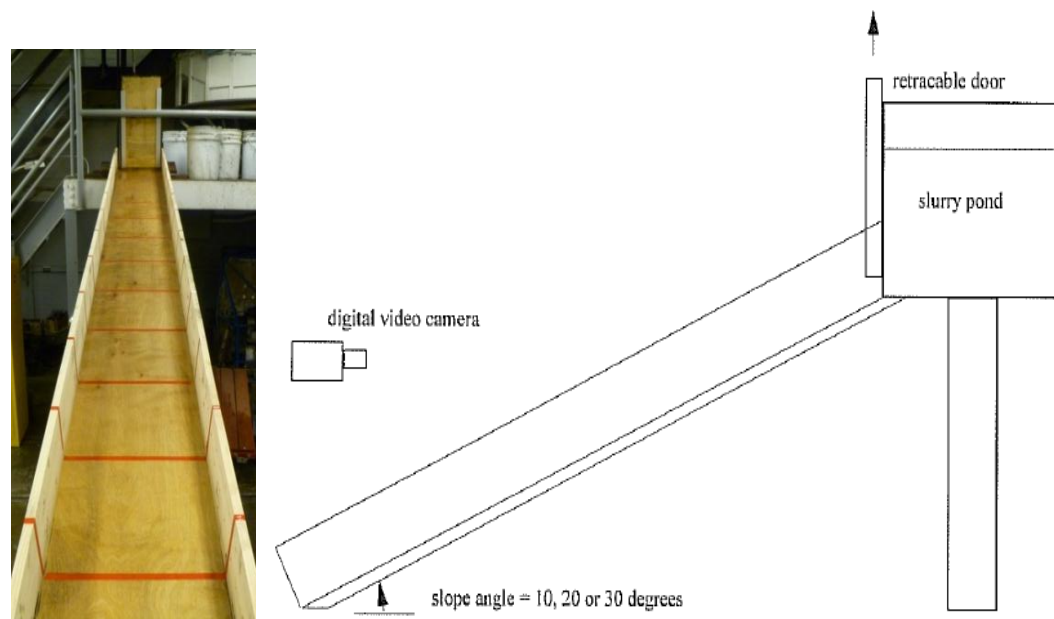


Figure 3-3 Small-scale model for flow study under static loading

The flume tests were conducted at three slope angles of 10° , 20° , and 30° in order to subject the material to different shear stresses. Impoundment failure was simulated by rapidly pulling the gate upwards. A high-speed digital video camera was placed in front of the slope to record the movements of the slurry so that the free surface velocity and travel distance could be measured. The time interval between two successive frames recorded by the video camera was $1/25$ second. The flow velocity along the entire flow path was determined by averaging the velocities between the marked intervals of 30 cm. The water content of the slurry samples started at approximately 80% and was reduced during subsequent tests until flow no longer occurred.

3.2.2 Flume Test under Impact Loading

Tests under impact loading were conducted in order to study whether a blasting disturbance in the field could trigger liquefaction and flow of impounded coal waste slurry at water contents lower than the threshold for flow under static conditions.

The configuration of the impact model test is shown in Figure 3-4. A solid mass was dropped from a pre-selected height on to the surface of the pond. This generated a P wave that propagated through the coal waste slurry sample, similar to that of the monotonic effect of a blasting event in the coal mining field. The retractable door was opened right after the impact of the solid mass.

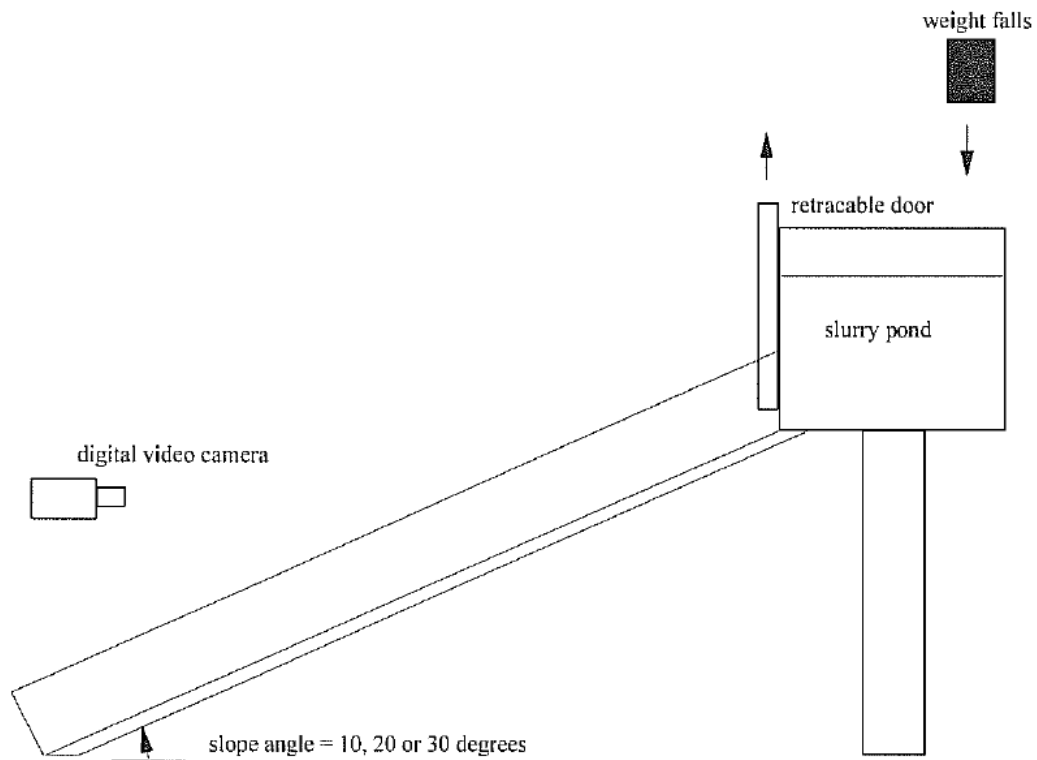


Figure 3-4 Small-scale model test for flow study under impact loading

There are different approaches available to simulate dynamic impact loading. A comprehensive literature review was performed by Charlie (1988) on published laboratory and field tests investigating the effects of impact loading (see Table 3-1). In this study, the “dropping weight” method was chosen because the dynamic load it generates is similar to that of a monotonic wave from a blast event. Although use of a small explosive might have been more representative of a blast event, that procedure would have required very costly safety precautions.

Table 3-1 Reference summary of published researches on the impact loading (after Charlie, 1988)

Author of Article	Loading Type	Soil Type and Density	Degree of Saturation	Comments
Kok (1977)	Hammer on cylinder	Loose sand	100%	Compaction decreases with increase in number of impacts
Van Der Kogel et al. (1980)	Falling weight	Sand Dr=8-93%	85-97%	Transient negative pwp* some liquefaction observed
Vesic et al. (1967)	Impact weight	Dense Sand Dr=80%	100%	Positive pwp only if soil densifies
Florin & Ivanov (1961)	Surface impact	Loose Sand	100%	Liquefaction observed
Tanimoto (1967)	Pendulum	Loose fine sand	100%	Settlement is the result of the impact and the dissipation of pwp

(*pwp: pore water pressure)

Previous testing on saturated soils indicated that liquefaction takes place under single compressive strains greater than 0.01% for soils with low effective stresses and low relative densities and 1% for soils with high effective stresses and high relative densities (Charlie et al. 1982; Veyera 1985). In this study, solid objects of varying weight were dropped from the height of 80cm in order to induce the compressive strain of 0.1%, 1%, and 5%. As with the static tests, flows were analyzed from flow data recorded by the high-speed video camera.

3.3 Test Results and Analysis under Static Loading

In this group of tests, the flow of coal refuse slurry was driven by its own weight. The KY and WV samples were prepared at different water contents and directed down the slope set at gradients of 30, 20, and 10 degrees. The movement of the slurry was recorded by high-speed video camera and thereafter analyzed frame by frame using film processing software in order to determine the velocity and travel distance of flow.

An example of the variation of flow velocity of a KY sample with a water content of 80% is exhibited in Figure 3-5. The flow at first accelerated and then stabilized at a constant velocity (at “midstream”). The slurry flow under the maximum initial shear stress (at the maximum slope angle of 30°) had the fastest velocity and took the least time to reach peak velocity. Samples with lower water contents decelerated more quickly.

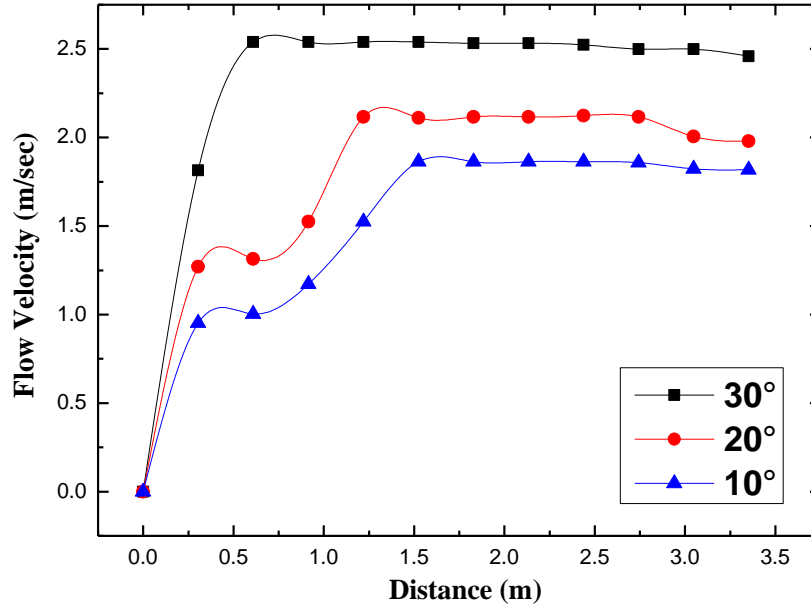


Figure 3-5 Example of the variation of flow velocity with distance for KY sample at initial water content of 80%

To simplify the analysis and obtain conservative results the maximum velocity on the surface and in the center of the slurry stream was recorded as the flow velocity. The recorded flow velocities of the KY and WV coal waste slurry samples at different water contents and slope angles are summarized in Table 3-2 and Table 3-3, respectively. The travel distance of the slurry and the depth of flow normal to the slope in the midstream were also recorded. The flow depth was measured by using several thin nails placed in the centerline of the slope. The depth was determined from the height of the dye on the nails. The results are listed in Tables 3-4 and 3-5 and photographs of the experimental results are provided in Figures 3-6 and 3-7.

Table 3-2 Variation of flow velocities of KY sample with water content and slope angle

(Unit: m/sec)

Water Content	30°	20°	10°
80	2.541	2.116	1.863
75	2.177	1.715	1.347
70	1.465	0.896	0.635
63	1.385	0.747	0.544
57	0.692	0.381	0
51	0.401	0.265	0
48	0	0	0

Table 3-3 Variation of flow velocities of WV sample with water content and slope angle

(Unit: m/sec)

Water Content	30°	20°	10°
82	2.291	1.742	1.525
76	1.824	1.329	1.114
72	1.389	0.847	0.701
65	0.862	0.635	0.423
55	0.398	0.227	0
52	0	0	0

Table 3-4 Recorded travel distance and flow depth in the midstream of KY sample

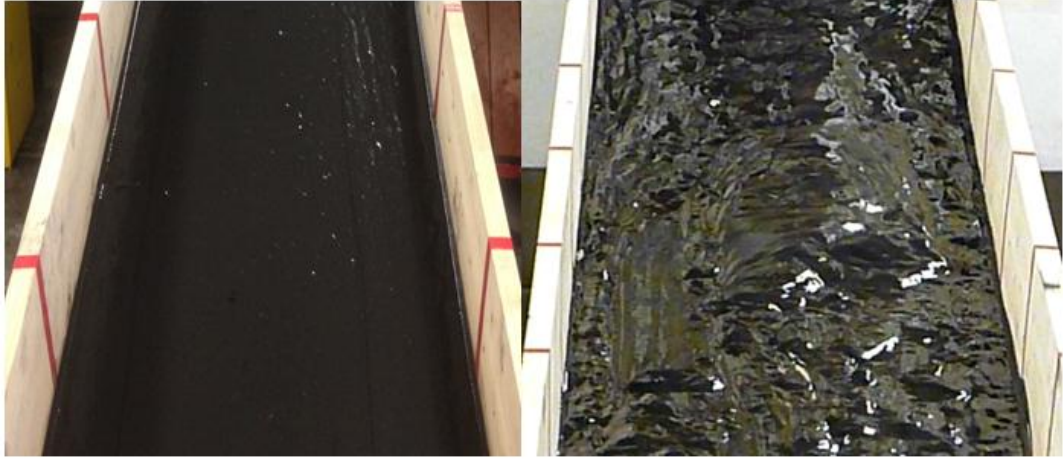
	30°		20°		10°	
Water content (%)	L (m)	D (cm)	L (m)	D (cm)	L (m)	D (cm)
80	>5	2	>5	3	>5	3.4
75	>5	3	2.5	5	1.4	7.8
70	>5	3.6	1.6	5.8	0.6	10
63	2.7	6	1.2	9	0.4	17
57	1.2	7.6	0.8	9.2	N/A	N/A
51	0.5	13	0.3	15	N/A	N/A

(L: extent of the flow; D: depth of the flow in the midstream)

Table 3-5 Recorded travel distance and flow depth in the midstream of WV sample

	30°		20°		10°	
Water content (%)	L (m)	D (cm)	L (m)	D (cm)	L (m)	D (cm)
82	>5	2	>5	2.8	>5	3.5
76	>5	2.5	3.4	3	2.6	4.5
72	>5	3.8	1.4	5	0.7	12
65	1.1	8	0.8	11	0.5	19
55	0.6	10	0.5	13	N/A	N/A

(L: extent of the flow; D: depth of the flow in the midstream)



$w=80 \quad \alpha=30^\circ$

$w=80 \quad \alpha=10^\circ$



$w=57 \quad \alpha=30^\circ$

$w=51 \quad \alpha=30^\circ$

Figure 3-6 The flows of KY sample at different water content (w) and slope angle (α)



$w=82 \quad \alpha=30^\circ$



$w=82 \quad \alpha=10^\circ$



$w=65 \quad \alpha=30^\circ$



$w=55 \quad \alpha=30^\circ$

Figure 3-7 The flows of WV sample at different water content (w) and slope angle (α)

Similar results were obtained from the flume tests between the KY and WV samples. The flow velocity of the slurry was approximately 2.55 m/sec at the water content of about 80%. The velocity and travel distance of flow decreased as the water content and applied shear stress (or slope angle) were reduced. At the water contents of 51% and 55%, the flow was very slow and traveled less than 1 m. The coal waste slurry changed from smooth to very viscous flow with the

reduction in water content. Slurry samples with lower water contents developed thicker overriding crusts of zero shear strain during the flow.

The flow of the KY and WV samples were compared. As previously discussed, the percent of fine particles is one of the most significant factors influencing the viscosity of coal waste slurry (Kawatra and Bakshi, 1995). As shown in Figure 3-8, the WV slurry samples exhibited more viscous behavior than KY samples at the same water content. Correspondingly, the KY coal waste slurry samples flowed slightly faster than the WV samples, as shown in Figure 3-9.

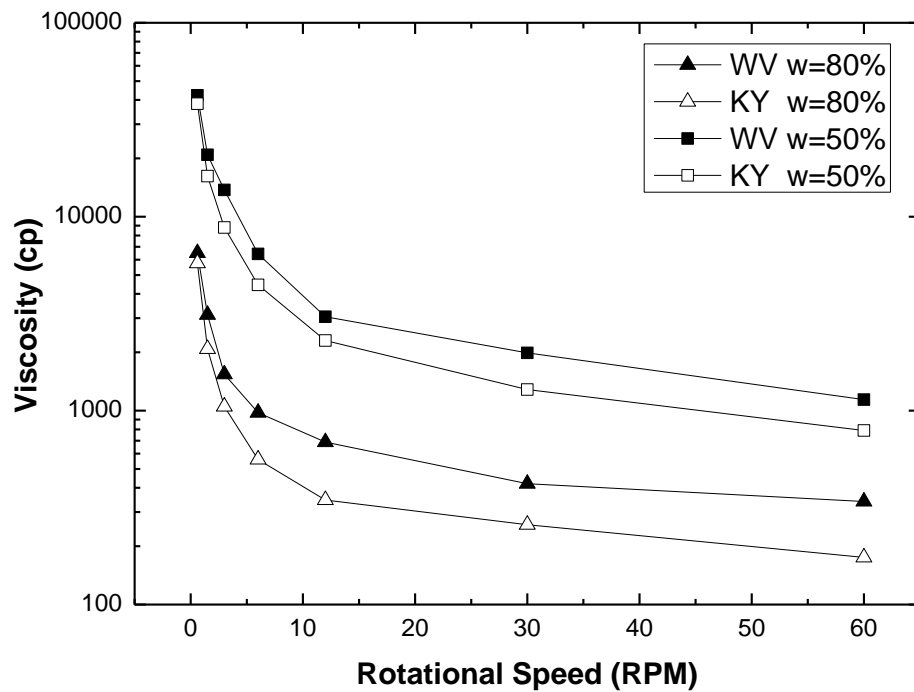


Figure 3-8 Comparison of variations of viscosities with rotational speed at 50% and 80% example water content

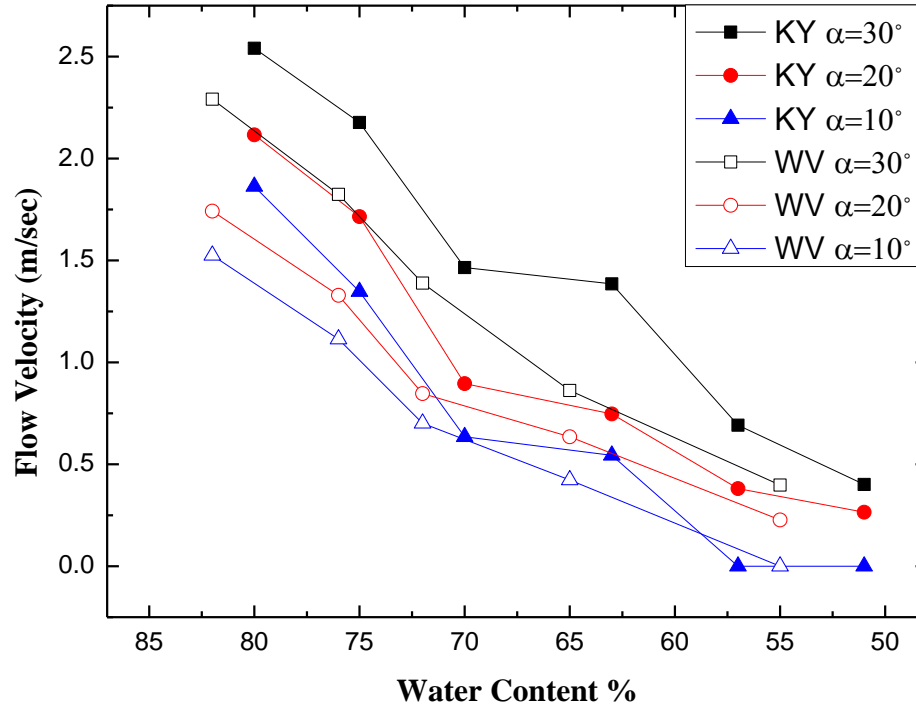


Figure 3-9 Comparison of flow velocity of two coal refuse samples varying with initial water content and slope angle

The liquid limits w_L of the two samples were measured in the laboratory tests as 38.1 and 42.5 for the KY and WV samples, respectively (see Table 2-3). As shown in Tables 3-2 and 3-3, the flows of samples at 30° slope angle ceased at the water contents of 48% and 52%, which is about 10 percentage points higher than the samples' liquid limits. A value for critical water content may serve as a workable dividing line between flowability and non-flowability of impounded coal waste slurry. Using the liquid limit of the slurry as the critical water content would be a conservative approach in the design and construction of impoundments.

3.3.1 Representation of Coal Waste Slurry by Bingham Plastic Model

The behavior of a Bingham plastic fluid is governed by plastic viscosity η_p and yield stress τ_y . A method of graphically determining these two significant parameters in terms of the

relationship between shear stress and shear rate has been demonstrated in Section 3.1.2. Some of the advanced digital viscometers can directly measure the value of shear rate based on the internal processing and converting. However, the use of the NDJ-8S digital rotary viscometer (Figure 3-10) results in data that can only be used to develop a relationship between the measured apparent viscosity and rotational speed. In this case the shear rate is calculated by treating it as a function of rotational speed (Brookfield, 2009).

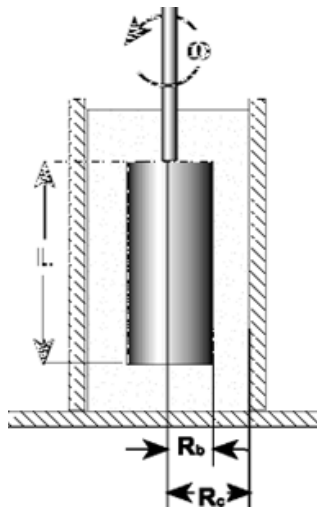


Figure 3-10 Sketch of cylindrical spindle rotating in the tested fluid

For cylindrical spindles with diameter of R and length of L , the contact area between the spindle and the fluid can be determined as $\pi R^2 L$. Torque is computed as the force acting on the outer surface of the spindle times the radius (“lever arm”). Therefore, the following relationship is derived:

$$\dot{\gamma} = \frac{2\omega R_c^2 R_b^2}{x^2 (R_c^2 - R_b^2)} \quad (3-6)$$

where

$\dot{\gamma}$ = shear rate (sec^{-1})

ω = angular velocity of spindle (rad/sec)

R_c = radius of container (cm)

R_b = radius of spindle (cm)

x = radius at which shear rate is being measured from the center of the spindle

As mentioned in the Section 2.3.7, #4 spindle was used in the viscosity test (Figure 2-33).

The parameters can thereby be determined as:

$$R_b = 1.683 \text{ mm}$$

$$R_c = 42.437 \text{ mm}$$

$$x = R_b = 1.683 \text{ mm}$$

Accordingly, the shear rate is obtained in terms of the corresponding rotational speed which is expressed in the following equation and listed in Table 3-6:

$$\dot{\gamma} = \frac{2\omega R_c^2 R_b^2}{x^2 (R_c^2 - R_b^2)} = 2.0032 \times \omega \quad (3-7)$$

Table 3-6 Determination of shear rate from rotational speed

rpm	Rad/sec	Shear rate
0.6	0.0628	0.1258
1.5	0.1571	0.3147
3	0.3142	0.6294
6	0.6283	1.2586
12	1.2566	2.5172
30	3.1416	6.2933
60	6.2832	12.5865

A small amount of slurry was collected from the middle depth of the pond before each flume test. The viscosities of these samples were measured at different rotational speeds by using NDJ-8S digital rotary viscometer. The initial water content was considered the same as that in the small-scale model test. Based on the equation and coefficients by Brookfield (2009) and Brookfield Engineering Laboratories (2005), the variations of viscosity with the shear rate and water content were established. The results are shown in Tables 3-7 and 3-8 for the KY and WV samples, respectively.

Table 3-7 Recorded viscosities of KY sample at different water contents and shear rates

Rotational Speed (rpm)	Shear Rate $\dot{\gamma}$ (sec^{-1})	Viscosity η (cp)					
		w=80%	w=75%	w=70%	w=63%	w=57%	w=51%
0.6	0.1258	5360	8700	12500	15000	25000	38250
1.5	0.3147	2180	3380	4700	6400	10500	16200
3.0	0.6294	1050	1700	2350	3100	5600	8800
6.0	1.2586	530	850	1270	1700	2700	4450
12	2.5172	346	470	680	1100	1700	2300
30	6.2933	258	310	375	880	1020	1285
60	12.5865	175	206	267	570	680	790

Table 3-8 Recorded viscosities of WV samples at different water contents and shear rates

Rotational Speed (rpm)	Shear Rate $\dot{\gamma}$ (sec ⁻¹)	Viscosity η (cp)						
		w=80 %	w=75 %	w=71 %	w=64 %	w=56 %	w=50 %	w=42 %
0.6	0.1258	6500	8188	11310	14235	26100	42300	128960
1.5	0.3147	3120	3605	4728	5970	12280	20856	54210
3.0	0.6294	1540	1978	2473	3240	6700	13744	28335
6.0	1.2586	976	1050	1350	1800	3910	6430	15323
12	2.5172	688	715	936	1135	2500	3050	7980
30	6.2933	420	540	680	846	1584	1986	3298
60	12.5865	340	438	525	668	977	1140	2960

The variations of recorded viscosity with shear rate are also graphically exhibited in Figure 3-11 and Figure 3-12. The viscosity of coal waste slurry decreased with the shear rate. Dramatic reduction in viscosity took place over shear rates of 0 and 2 sec⁻¹. Only a slight change of viscosity was observed for shear rates greater than 6 sec⁻¹. The relationship between shear stress ($\tau = \eta \dot{\gamma}^2$) and shear rate can be developed with the known viscosity. The Bingham plastic viscosity and yield stress can therefore be determined based on the simplified method described in Section 3.1.2 and exemplified in Figure 3-13. The Bingham plastic viscosity was determined from the slope of the linear portion of the curve at high shear rate, and the yield stress was taken as the intersection of the slope and the shear stress axis.

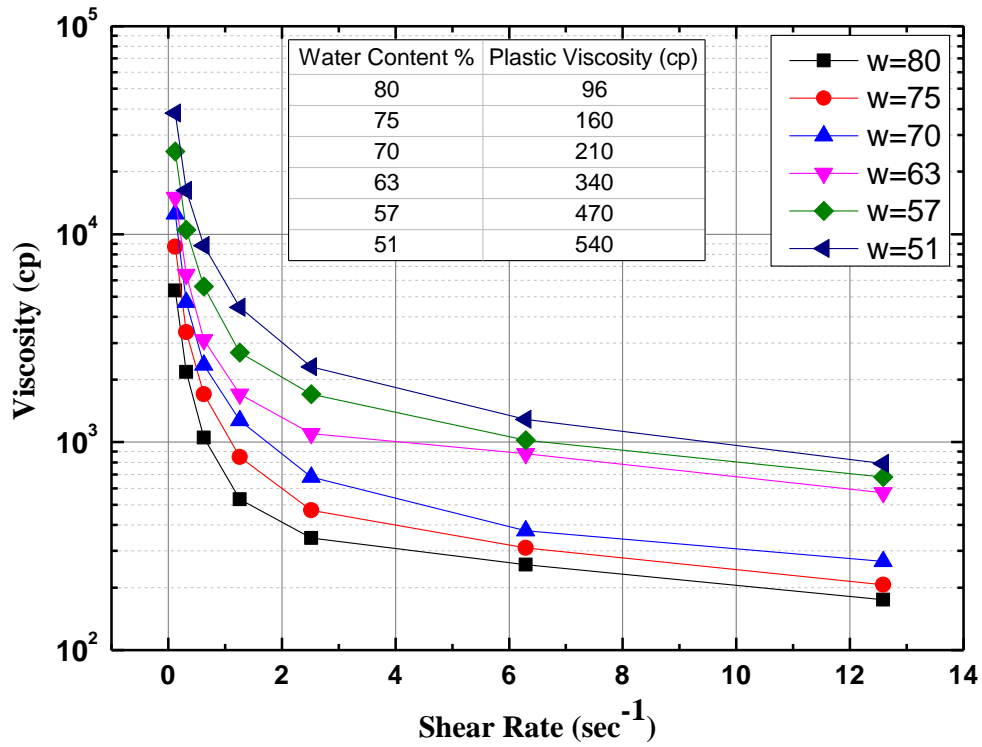


Figure 3-11 Variation of viscosity with shear rate for KY coal refuse sample (23°C)

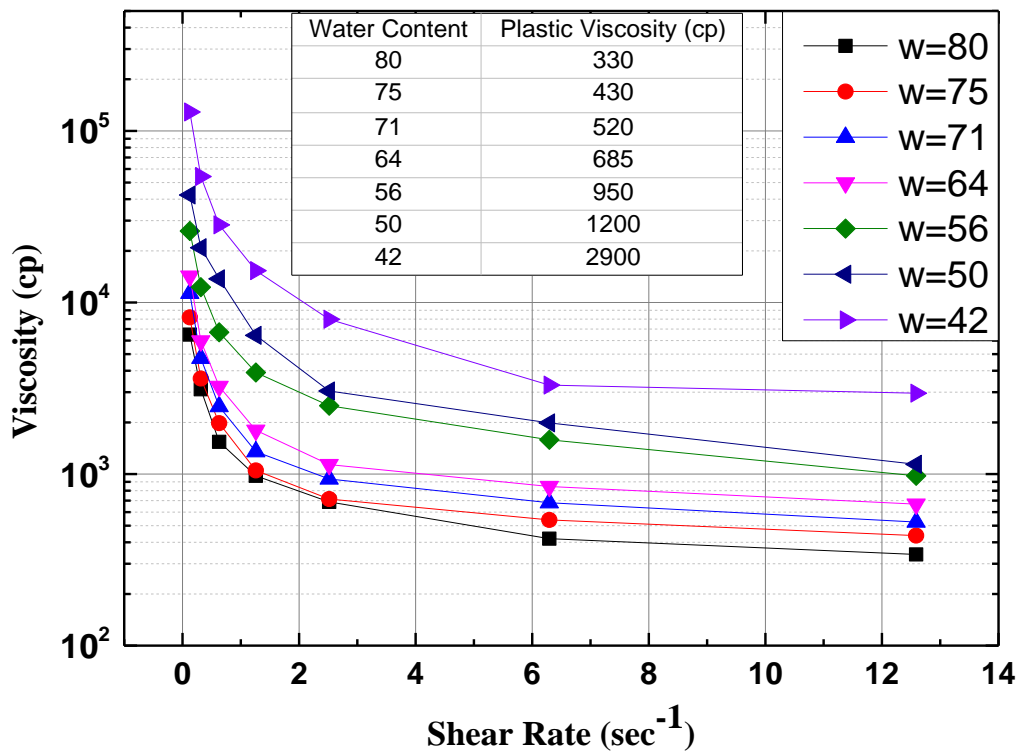


Figure 3-12 Variation of viscosity with shear rate for WV coal refuse sample (23°C)

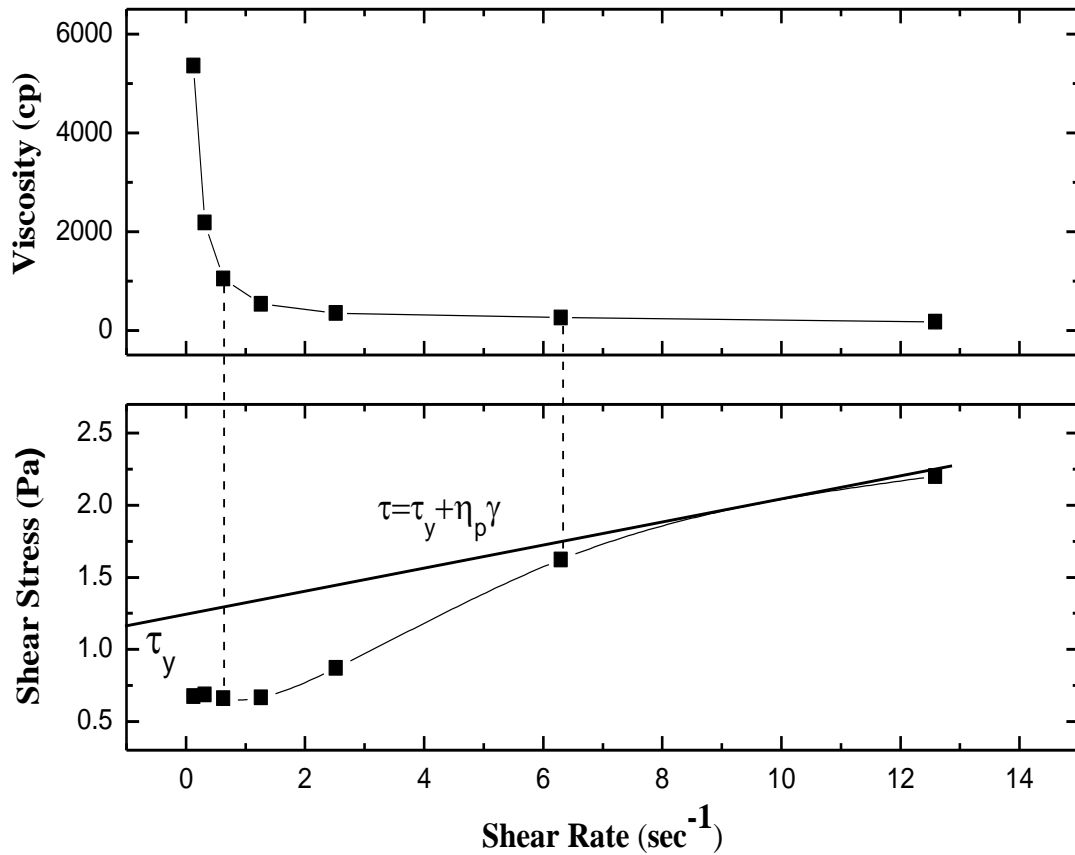


Figure 3-13 Determination of flow parameters of Bingham Plastic model (KY coal refuse sample, w=80%)

The developed Bingham Plastic models at different water contents are graphically presented in Figures 3-14 and 3-15. The yield stress increased with the reduction of water content. The yield stress at higher water content (60 or 70 percent and above) was extremely low. Similar results were also obtained by Krizek (2004). The coal waste slurry can be considered as Newtonian at those levels. This approximation was also adopted by Logos and Nguyen (1996), Boylu et al. (2004), and Sawyer et al. (2012). The negligible yield stress at high water contents would render impounded slurry to be very susceptible to flow failure with minimal disturbance.

The plastic viscosity also increased as the initial water content was reduced. A marked increase of yield stress and plastic viscosity was observed at water contents lower than 60%.

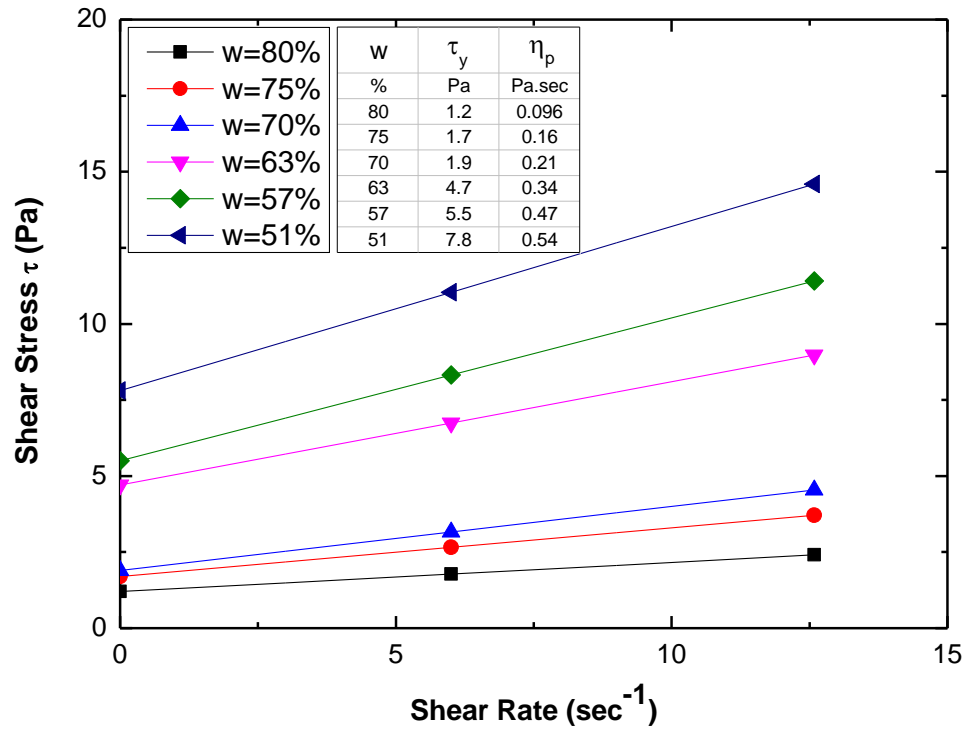


Figure 3-14 Bingham Plastic model for KY samples at different water content

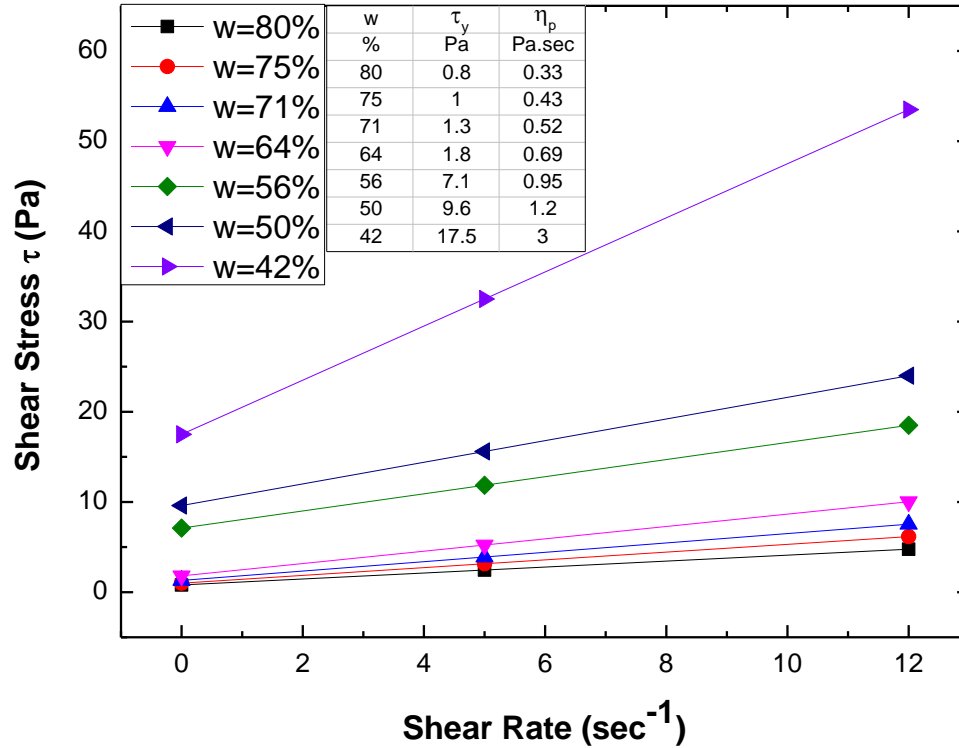


Figure 3-15 Bingham Plastic model for WV samples at different water content

It is notable that some researchers have indicated that the yield stress might not be accurately defined due to the break-down of particle structures under the applied shear rate (Terzaghi, 1931; Ter-Stepanian, 1963; and Phillips and Davis, 1991). Palmer and Krizek (1987), and Vallejo and Scovazzo (2003) studied the properties of mudflow under the assumption that the yield stress of a fluid equaled its undrained shear strength c_u . However, the yield stress and undrained shear strength measured in this study are clearly different, which is probably a result of the thorough agitation of each sample (in the procedure) and consequent particle breakdown that occurred prior to the viscosity measurements.

3.3.2 Estimation of Flow Regime

It is known that the characteristics of flow are greatly influenced by the flow velocity. Two types of flow have been well identified and studied with respect to velocity, i.e., laminar flow and turbulent flow. Laminar flow occurs when flow velocity is below a certain critical value known as the Reynolds number, while turbulent flow occurs above that value. The flow regime of a fluid at a certain velocity is typically estimated by comparing the actual Reynolds number (which is a measure of the ratio of inertial forces to viscous forces) to the critical Reynolds number, Re_c . In the case of open channel flow, the Reynolds number for Newtonian fluids is defined as:

$$Re = \frac{\rho v R}{\eta} \quad (3-8)$$

where

Re = Reynolds number

ρ = density of the fluid

v = mean flow velocity

R= hydraulic radius in the open channel

η = the viscosity of fluid

The Reynolds number for non-Newtonian fluids has not been precisely defined even though much research on the subject has been performed by Chhabra and Richardson (2008) and Haldenwang et al. (2010). In this study calculation of Reynolds numbers is derived from the equation applicable to Newtonian fluids.

For Bingham Plastic fluids Hanks and Pratt (1967) and Swamee and Aggarwal (2011) expressed the critical Reynolds number as a function of the Hedstrom number:

$$He = \frac{\rho R^2 \tau_y}{\eta^2} \quad (3-9)$$

where R is the hydraulic radius in the open channel which equals to the cross-sectional area of the flow divided by the wetted perimeter ($R = \frac{A}{X} = \frac{BD}{B+2D}$, where B and D are the width and depth of the channel respectively).

The critical Reynolds number is defined as:

$$Re_c = 2100 \left(1 + \frac{He}{3600}\right)^{0.35} \quad \text{for } 1 \leq He \leq 10^8 \quad (3-10)$$

$$Re_c = 161 He^{0.334} \quad \text{for } 10^8 \leq He \leq 10^{12} \quad (3-11)$$

Based on the dimension of flume channel and measured flow parameters shown in Tables 3-2 and 3-5, the Hedstrom number and critical Reynolds number are listed in Tables 3-9 and 3-10 for the two coal waste slurry samples.

Table 3-9 Determination of critical Reynolds number for KY sample

Water Content	ρ	B	D	R	η_p	τ_y	He	Re_c
%	kg/m ³	m	m	m	Pa·sec	Pa		
80	1393	0.3	0.02	0.02	0.10	1.2	56	2111
75	1408	0.3	0.03	0.03	0.16	1.7	58	2112
70	1425	0.3	0.04	0.03	0.21	1.9	52	2111
63	1452	0.3	0.06	0.04	0.34	4.7	108	2122
57	1477	0.3	0.08	0.05	0.47	5.5	94	2119
51	1506	0.3	0.13	0.07	0.54	7.8	195	2139

Table 3-10 Determination of critical Reynolds number for WV sample

Water Content	ρ	B	D	R	η_p	τ_y	He	Re_c
%	kg/m ³	m	m	m	Pa·sec	Pa		
82	1413	0.3	0.02	0.02	0.33	0.8	3	2100
76	1434	0.3	0.03	0.02	0.43	1.0	4	2100
72	1448	0.3	0.04	0.03	0.52	1.3	6	2101
65	1476	0.3	0.08	0.05	0.69	1.8	15	2103
55	1523	0.3	0.1	0.06	0.95	7.1	43	2109

Since the velocity of the coal waste slurry increased with the slope angle, the flow regime analysis was only performed on velocities measure at the largest slope angle of 30°. The flow regimes of the two slurry samples are summarized in Tables 3-11 and 3-12. The actual Reynolds numbers for all water contents were much lower than the corresponding critical Reynolds numbers. Therefore the flow of coal waste slurry can be considered as a steady, uniform laminar flow in the open channel of the flume. The laminar regime of coal waste slurry was also observed in experiments by Schaflinger et al. (1990), Coussot (1994), Cooke (2002), Spelay (2007), and Xia et al. (2009). There is no flow-regime data in the literature from flow failure events at coal waste impoundments.

Table 3-11 Determination of flow regime for KY sample

Water Content	ρ	v	R	η	Re	Re_c	Regime
%	kg/m³	m/sec	m	Pa·sec			
80	1393	2.541	0.02	0.10	650	2111	Laminar
75	1408	2.177	0.03	0.16	479	2112	Laminar
70	1425	1.465	0.03	0.21	289	2111	Laminar
63	1452	1.385	0.04	0.34	253	2122	Laminar
57	1477	0.692	0.05	0.47	110	2119	Laminar
51	1506	0.401	0.07	0.54	78	2139	Laminar

Table 3-12 Determination of flow regime for WV sample

Water Content	ρ	ν	R	η	Re	Re_c	Regime
%	kg/m³	m/sec	m	Pa·sec			
82	1413	2.29	0.02	0.33	173	2100	Laminar
76	1434	1.82	0.02	0.43	130	2100	Laminar
72	1448	1.39	0.03	0.52	117	2101	Laminar
65	1476	0.86	0.05	0.69	97	2103	Laminar
55	1523	0.4	0.06	0.95	38	2108	Laminar

3.3.3 Velocity Profile

Having established a laminar flow regime for the slurry samples, the velocity profile of the observed flow behavior can be evaluated. An ideal Bingham Plastic fluid flow down an inclined plane is illustrated in Figure 3-16. The yield stress τ_y effects a plug-like section of the profile extending downward from the free surface of flow ($X \leq X_0$). There the applied shear stress is below the yield stress and consequently the solid plug moves with the flow without a velocity gradient. When the driving shear stress is larger than the yield stress at $X > X_0$, the fluid exhibits a parabolic distribution of flow velocity. Shear stresses develop from the differential movement of the fluid.

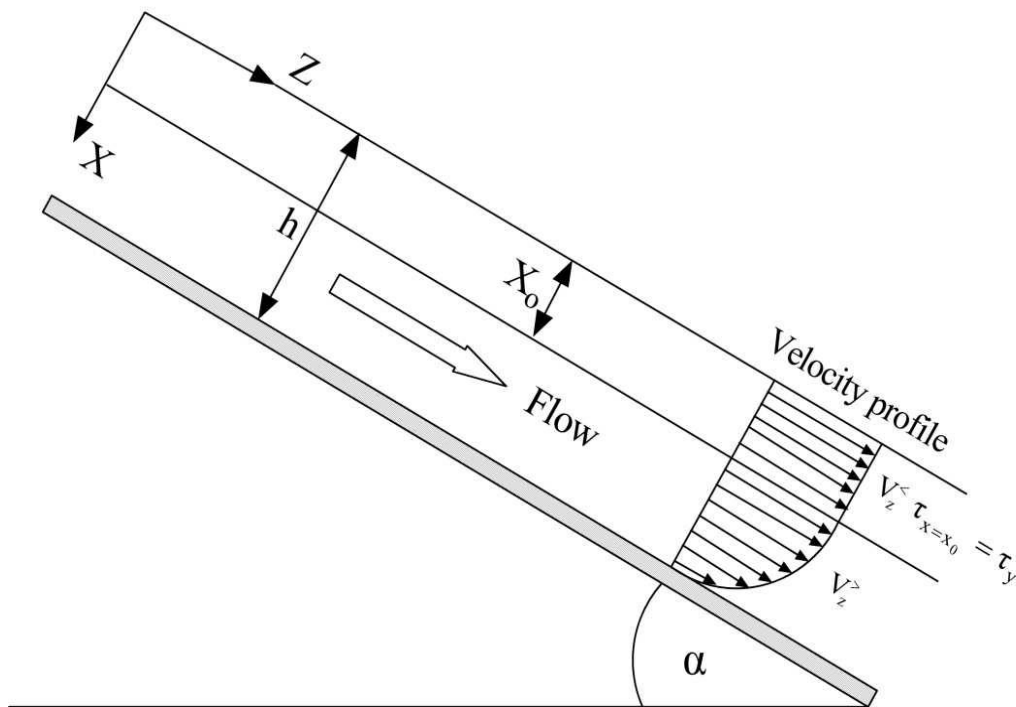


Figure 3-16 Schematic of flow configuration (De Kee et al., 1990)

To fully evaluate the velocity profiles of coal waste slurry flow, the thickness of the solid plug needs to be determined for different water contents. As mentioned before, slurry flow at high water content can be considered Newtonian due to the negligible yield stress; and in fact a plug-like region in the flow was not apparent in samples with water contents of 80 and 82 percent for the KY and WV samples, respectively (see Figures 3-6 and 3-7). As demonstrated in Figure 3-17, a solid plug formed and appeared to thicken at the water content was decreased. Unfortunately, the relationship between plug thickness and water content could not be quantitatively confirmed because a reliable method to locate the boundary or yield surface between the plug and underlying region of shear was not available.



w=65 $\alpha = 30^\circ$



w=55 $\alpha = 30^\circ$

Figure 3-17 Comparison of flow profile at different water content (WV sample)

Identification of yield surface in a flow is one of the most complicated problems associated with the Bingham Plastic Fluid (Liu, 2003). In the past few decades, many studies have been conducted on the velocity distribution of non-Newtonian fluids. Analytical and numerical models have been developed by Oldroyd (1947), De Kee et al. (1990), Abdali et al. (1992), Mitsoulis et al. (1993), Wilson and Taylor (1996) and Balmforth et al. (2002). The flow

behavior was also studied based on the experimental observation (Kozicki and Tiu 1986; Chhabra and Richardson 2008; Haldenwang et al. 2010). Haldenwang et al. (2012) and Kotze (2007) presented experimental results on the velocity profiles of non-Newtonian fluids by using an Ultrasonic Velocity Profiling technique. However, the findings varied significantly.

3.3.4 Relationship between Flow Velocity and Viscosity

As mentioned in the previous sections, the viscosity of coal waste slurry largely influences its flow velocity. In this study the representative velocity was selected from the maximum velocity obtained from the free surface during the midstream of the flow. At low water content, the flow was very slow and extended over short travel distance. It was not possible in that case to clearly identify the acceleration, duration, and deceleration stages of slurry flow. The mean velocity was thereby used as the flow velocity.

In general, the flow failure of coal waste slurry impoundments occurs at an extremely high shear rate. Therefore viscosities approaching constant values at higher shear rates (see Figure 3-11 and Figure 3-12) were compared to flow velocity. The representative viscosities are the plastic viscosities in the Bingham Plastic model.

The relationships between flow velocity and viscosity of the two coal waste slurry samples are shown in Figure 3-18 and Figure 3-19. The flow velocity decreased with viscosity and varied from approximately 2.5 m/sec to less than 0.5 m/sec at the slope angle of 30°. The WV sample exhibited a more linear relationship between flow velocity and viscosity whereas the KY sample experienced a dramatic drop in velocity as its viscosity approached 200 cp. Provided there is sufficient flow test data, an empirical relationship can be established between flow velocity and viscosity so that the length of travel and consequent degree of damage caused from flow failure of an impoundment can be estimated.

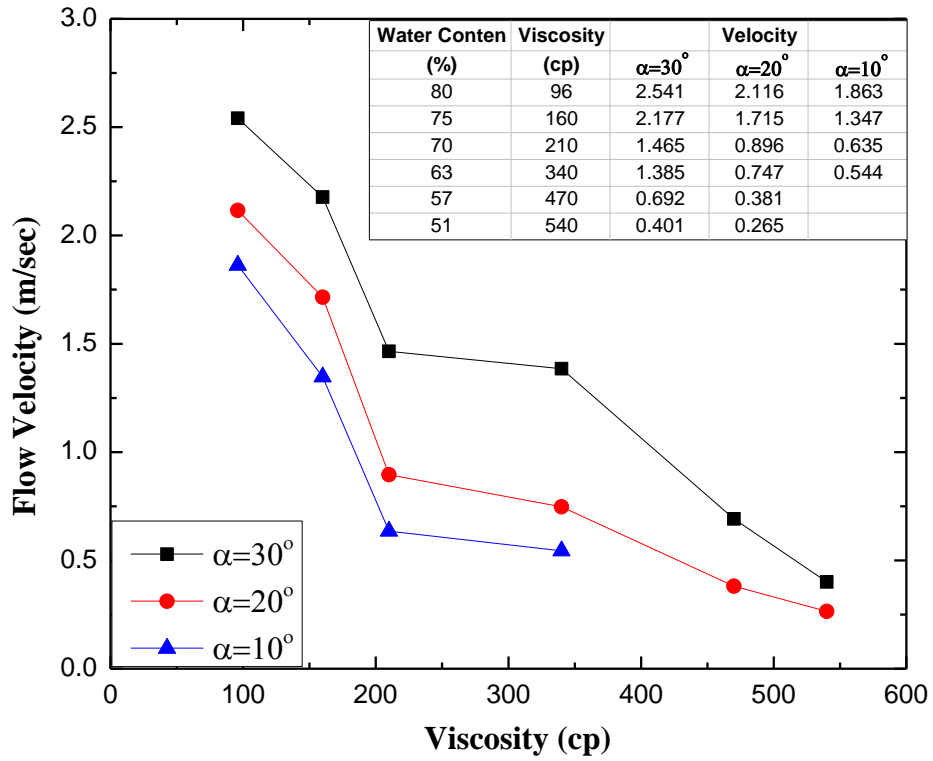


Figure 3-18 The relationship between flow velocity and viscosity of KY sample

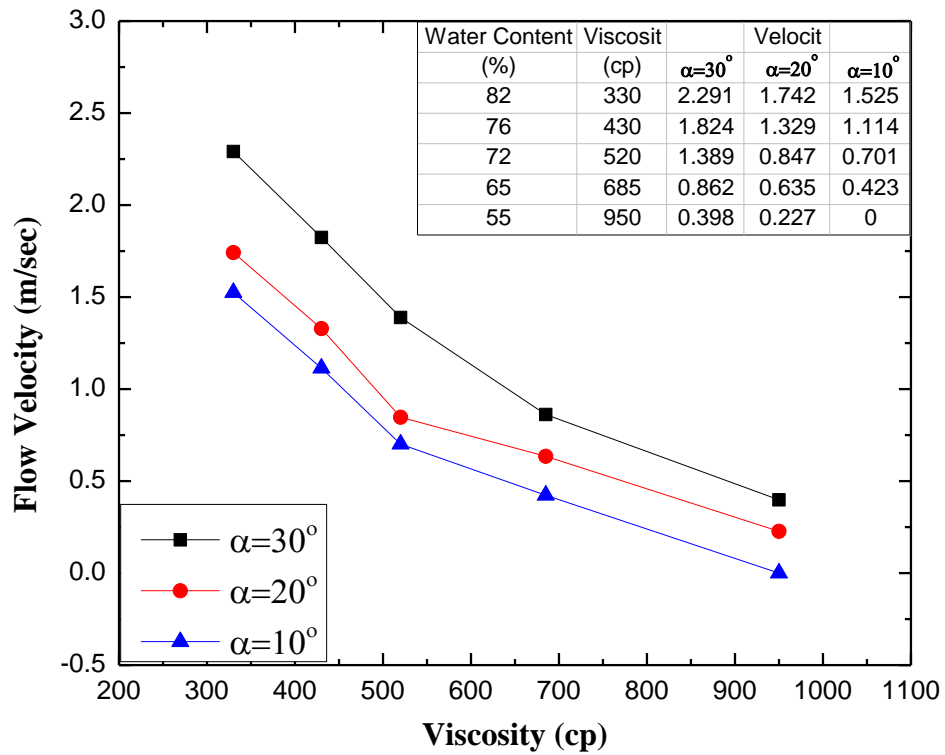


Figure 3-19 The relationship between flow velocity and viscosity of WV sample

In addition to the properties of coal waste slurry itself, many other factors also impact flow velocity. The volume (or weight) of overlying impounded refuse is one such factor. The peak flow velocity was found to increase with the gravitational stress by Kailey et al. (2011). The peak velocity did not increase indefinitely and eventually became a constant as the weight of the overlying slurry continued to increase. Nevertheless, the effect of increased volume of impounded coal waste slurry was far less significant than that of increased water content (Kailey et al., 2011). Jeyapalan et al. (1983) pointed out that flow velocity varies when the fluid flows across the planes and prismatic valleys with different cross sections. Shape factors were defined in open channel investigations by Straub et al. (1958) and Kozicki and Tiu (1967). The velocity profile of laminar Bingham Plastic fluids was also found to be affected by the roughness of the channel surface (Tani, 1969; Mekle et al., 1974; and Engin et al., 2004). Due to the limited quantity of coal waste slurry samples, the effects of these other factors on flow velocity were not tested in this study.

3.4 Test Results and Analysis under Impact Loading

Impact loading such as from mine blasts has a potentially negative effect on the stability of coal waste impoundments that are improperly designed or constructed. A single blast generates high-frequency and high-intensity compressive stress waves over a short duration. In the event of an impact loading, excess pore water pressure in the fine refuse can quickly build up and cause a severe reduction in the strength of the material. In practice, the duration and magnitude of blast loading is considered as a function of the charge size, embedded depth of charge, and the distance from the charge to the site of interest (Lyakhov, 1961; Melzer, 1978; and Fragaszy et al., 1983). The effects of blast loading on the surrounding soil also depends on

the soil properties such as degree of saturation, particle size and shape, compressibility, permeability, and initial effective stress (Florin and Ivanov, 1961; Kurzeme, 1971; Studer and Prater, 1977; Damitio, 1977; Rischbieter, 1977; Studer and Kok, 1980; Ivanov et al., 1981; and Hubert, 1986). Liquefaction of the fine coal refuse can change normally non-flowable material into a heavy viscous fluid that in turn can significantly increase pressure against an embankment or mine barrier.

A second group of small-scale model tests were performed in order to investigate the influence of impact loading on the flow behavior of coal waste slurry. The configuration of model test is shown in Figure 3-4 and the test procedures are discussed in detail in Section 3.2.2. The test started at the lower water contents at which the flow of the slurry samples ceased under static loading (water contents of 51 and 55 percent for the KY and WV samples, respectively); and the flow was only measured at the slope angle of 30°. Since the sensitivity of the pore pressure transducer was not adequate for the 1-g test, liquefaction was considered to have occurred when compressive strain exceeded 0.01% for soils with low effective stresses and low relative densities and 1% for soils with high effective stresses and high relative densities (Charlie et al., 1982; Veyera, 1985). In this study, the samples were also tested at 5% compressive strain in order to observe more evident flow behavior under impact loading. The solid was dropped onto a thin plate placed on top of the pond to generate a uniformly distributed stress wave. A series of trial tests were conducted by dropping solids of varying weight from a height of 80 cm in order to achieve the designed compressive strains.

The results were summarized in Table 3-13 and Table 3-14 and graphically exhibited in Figure 3-20 and Figure 3-21. For the KY sample, the flow under static loading ceased at the water content of 48% which was 10 percentage points higher than the liquid limit of 38.1. Under

impact loading, no flow was observed at 0.1% compressive strain. Although a small amount of water seeped from the slurry the material still behaved as a plastic solid. As shown in Figure 3-20, the flow was triggered when the compressive strain reached 1%. The solid fine refuse changed into very thick and viscous liquid but travelled a very short distance of less than 0.3 m. At 5% compressive strain, the effect of more significant liquefaction was observed. The flow was much thinner and smoother than at 1% compressive strain and travelled a greater distance. The effect of impact loading was insignificant at the water content of 38% as no flow was observed. There was flow at the water content of 43% but only in response to 5% compressive strain.

Table 3-13 The summarized test results of KY sample under impact loading ($\alpha = 30^\circ$)

Compressive Strains ε	0.1%	1%	5%
Weight	0.3kg	0.8kg	1.5kg
Height	80cm	80cm	80cm
	Water Content w=48%		
Extent of Flow	0	0.2m	0.34m
Flow Velocity	0	0.007m/s	0.026m/s
	Water Content w=43%		
Extent of Flow	0	0	0.15m
Flow Velocity	0	0	0.005m/s
	Water Content w=38%		
Extent of Flow	0	0	0
Flow Velocity	0	0	0

Table 3-14 The summarized test results of WV sample under impact loading ($\alpha = 30^\circ$)

Compressive Strains ε	0.1%	1%	5%
Weight	0.3kg	0.8kg	1.5kg
Height	80cm	80cm	80cm
Water Content w=52%			
Extent of Flow	0	0.15m	0.45m
Flow Velocity	0	0.005m/s	0.048m/s
Water Content w=45%			
Extent of Flow	0	0	0.1m
Flow Velocity	0	0	≈ 0
Water Content w=40%			
Extent of Flow	0	0	0
Flow Velocity	0	0	0

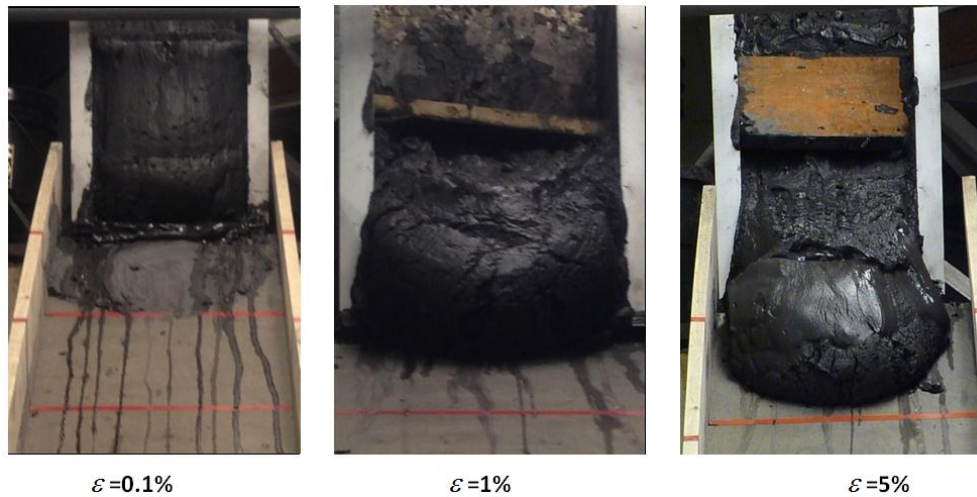


Figure 3-20 Results of impact loading tests on KY sample under different compressive strains ($\alpha = 30^\circ$, w=48%)

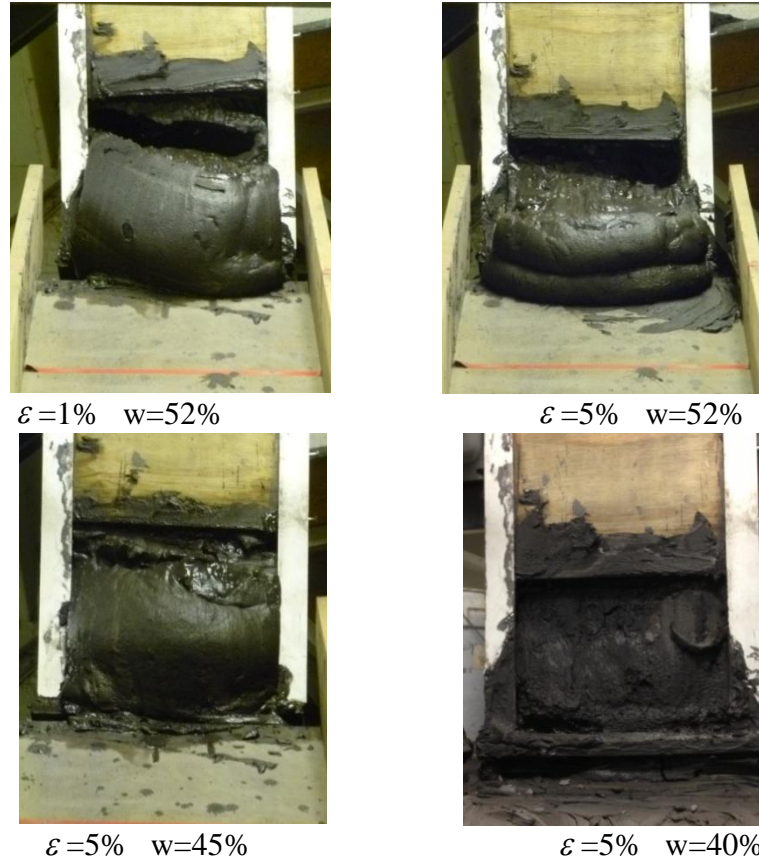


Figure 3-21 Results of impact loading tests on WV sample under different compressive strains ($\alpha = 30^\circ$)

Flow of the WV slurry under static loading ceased at 52% water content which was also approximately 10 percentage points higher than its liquid limit of 42.5. Similar to the KY sample, no flow took place under 0.1% compressive strain. The sample was very stiff under 1% compressive strain as a thick solid plug slowly snapped from the rest of the sample before slowly sliding 0.15m down the flume. As shown in Figure 3-21, greater flowability was observed at 5% compressive strain. The flow was limited to a slight plastic deformation at the same strain when the water content was reduced to 45%.

The small scale model tests under impact loading on the two coal waste slurry samples exhibited consistent results. More evident liquefaction and flow of the slurry was observed at the

highest compressive strain of 5%. However, it was difficult to estimate whether the saturated samples truly liquefied at 1% or 5% compressive strain without the use of a sufficiently sensitive pore pressure transducer. However, these results were verified by comparing the results of the small scale model impact tests with those of the centrifuge model tests presented in Chapter 4. Both samples exhibited sufficient resistance to impact loading at water contents approximately 5% higher than the corresponding liquid limits. It is recommended that fine coal refuse contained in an upstream-constructed impoundment be dewatered to a water content lower than the liquid limit prior to expansion of the embankment. The practice will help to ensure stability of the facility against blast loading and other types of dynamic loading such as earthquakes.

3.5 Conclusions

In this study, a group of small-scale model tests have been performed on coal waste slurry samples from two impoundments. The flow behavior of the slurry samples were studied under both static and impact loading. Based on the recorded results, the following conclusions can be drawn:

- 1) Similar results were obtained from the tests on the two slurry samples.
- 2) Flow of coal waste slurry generally followed the characteristics of non-Newtonian fluids. Among the different non-Newtonian rheological models, the Bingham Plastic model was confirmed to be most applicable to the flow of the impounded fine coal refuse samples.
- 3) The behavior of Bingham Plastic Flow is primarily governed by yield stress τ_y and plastic viscosity η_p . In terms of the shear stress vs. shear rate curve, plastic viscosity is taken as the slope of the linear portion of the curve at high shear

rates while the yield stress is taken as the point where the projection of the straight line intersects the shear stress axis.

4) At higher water content, the yield stress of the samples was extremely small. Therefore, the flow of coal refuse slurry at high water content can be considered to be Newtonian with flow properties largely dependent on a constant value of viscosity.

5) Coal waste slurry flow under the maximum initial shear stress (i.e. at the maximum slope angle) had the fastest velocity.

6) Under the static loading, the flow velocities and travel distance of coal waste slurry gradually decreased as the water content and slope angle of the flume was reduced. The flow of the two coal waste slurry samples ceased at water contents approximately 10 percentage point higher than the samples' liquid limits.

7) By studying the flow regime, it was determined that the slurry flow (as measured midstream where the flow velocity stabilized at a constant value) can be considered as a uniform, steady, laminar flow.

8) The velocity profile of coal waste slurry flow includes a solid plug near the free surface of the flow, underlain by a viscous fluid with a parabolic distribution of velocity. As the water content was reduced the solid plug appeared to thicken.

9) Viscosity, the frictional force within a fluid resisting its flow, greatly influences flow velocity. At lower water content, the slurry samples exhibited higher viscosity and flowed at lower velocity.

10) Blast loading was simulated by dropping a solid of several specific weights from a standard height onto the small scale model slurry pond. The

experiment was only applied to samples with low water content at which no flow occurred under static loading. The onset of liquefaction was identified based on the compressive strain generated by the impact of the falling solid.

11) Slurry flow was triggered by impact loading when the compressive strain exceeded 1%. The slurry changed from a solid mass to a highly viscous fluid.

12) The coal waste impoundment with water content below liquid limit should have sufficient resistance to both static and impact loading. The water content/liquid comparison is worthy of consideration as a conservative criterion used to prevent flow failure during the construction of a slurry impoundment.

ANALYSIS OF FLOW BEHAVIOR OF COAL WASTE SLURRY BY CENTRIFUGE MODEL TESTS

4.1 Introduction

As flow failure from impoundments takes place, millions of tons of impounded coal waste slurry may flow into surface water ways or break through into the nearby underground mines. The viscous flow under a high stress field can travel several kilometers in just a few minutes and result in significant loss of lives, property damages, and environmental impacts.

A number of laboratory tests related to the rheological properties of coal waste slurry and other non-Newtonian fluids have been performed in the past few decades (Zhang and Ren, 1982; Jeyapalan, 1983; Shook and Roco, 1991; Coussot, 1994; Haldenwang, 2003; Henriquez et al., 2009). However, test results significantly vary and may not adequately reflect the flow characteristics of slurry contained within an impoundment because of the limited quantity of the samples evaluated and low stress fields applied. Although there have been many flow failures since the instability of impounded mine waste was first documented by Casagrande (1950), documented data on the flow behavior of the impounded waste slurry remains insufficient.

The geotechnical centrifuge provides an effective way to scale model large-scale problems for which gravity is a primary driving force. The centrifuge enables samples in a small model to be subjected to the same effective stress as a full scale prototype. This makes it possible to obtain real-world data useful for solving complex problems such as seismic-induced liquefaction; strength, stiffness, and bearing capacity of foundations and other geo-infrastructures; and the rheological characteristics of different types of fluids under various site conditions.

In this project, a group of centrifuge model tests were performed on the two coal waste slurry samples collected from coal preparation plants in Kentucky and West Virginia in order to study their flow properties under prototype stress fields. The test was also used to verify an engineering countermeasure to the potential of flow failure, i.e. the storage of fine refuse in slurry cells instead of large, MSHA-class impoundments. A special container was designed to conduct flow tests under static loading and dynamic impact loading. The results were compared with those of the small-scale model tests to identify whether and how much the prototype stress field (i.e. from the load imposed by the impoundment pool) should influence the flow behavior of released coal waste slurry.

4.1.1 Review of Geotechnical Centrifuge Test

Centrifuge modeling provides a useful and powerful experimental tool for the study of complex geotechnical problems. The original idea of performing geotechnical centrifuge tests, proposed in 1869 by Phillips in Paris, France, was to increase the self-weight of the material tested in a small scale model (Craig, 1995). Phillips derived the similitude relationship between a prototype and a small scale model by using equilibrium differential equations for elastic solids. He suggested using inertial forces, particularly the centrifugal force, in cases where gravity is a major factor in the response of the solids (Taylor, 1995). Centrifuge modeling was not widely utilized until Bucky (1931) applied the methodology while studying the effects of rock structure on mine roof stability. Pokrovsky and Davidenkov (Ng, 2014) employed centrifuge modeling to investigate embankment instability in 1933. Between the 1940s and 1960s, a number of geotechnical centrifuges were developed in the Union of Soviet Socialist Republics and applied to geotechnical problems and stress analysis in both soils and rocks. Schofield developed the first

geotechnical centrifuge in the United Kingdom in 1966 and thereafter played a key role in the modernization of the technology (Schofield, 1980). Other technical papers related to the centrifuge modelling were authored by Avgherinos and Schofield (1969), Mikasa et al. (1973) and Ter-Stepanian and Goldstein (1969). Four international conferences specific to centrifuge modeling (Centrifuge 88, 91, 94, 98) and eight international conferences on physical modeling (including centrifuge modeling) were organized by the International Committee on Physical Modelling in Geotechnical Engineering. The conferences have resulted in useful reference sources on state-of-the-art developments in the technology.

Presently, advantages of centrifuge modeling are widely recognized and the technique is used in many countries. There are now over 50 geotechnical centrifuges in operation around the world. Recent developments in the modeling technique and the results of its application were reported by Craig (1984), Corte (1988), Ko and McLean (1991), Leung et al. (1994), Taylor (1995), Kimura et al. (1998), and Phillips et al. (2002). Data from centrifuge tests can be used to study the mechanism of complex problems in geotechnical engineering, to validate numerical procedures when field data is lacking, and verify new design concepts when existing standard design procedures are inadequate.

4.1.2 Scaling Law

The centrifuge applies gravitational acceleration to a physical model in order to simulate self-weight stress in a prototype impoundment. In other words, the centrifuge sample of coal waste slurry should experience stresses and material strengths equal to those that would occur within a full scale impounding structure. This objective can be mathematically stated as:

$$\sigma^* = \frac{\sigma_{\text{model}}}{\sigma_{\text{prototype}}} = 1 \quad (4-1)$$

where the asterisk on a quantity denotes a scaling factor for that quantity, i.e. the ratio of the quantity in the model to the quantity in the full scale prototype.

In soil mechanics, the total vertical stress at depth H in a uniform soil layer can be calculated by:

$$\sigma_t = \rho g H \quad (4-2)$$

where

σ_t = total vertical stress at depth H

ρ = mass density of the layer

g = gravity acceleration

In the conventional form of centrifuge modeling (Garnier et al., 2007), the same materials are prepared at the same mass density $\rho^* = 1$ so as to ensure similar behavior in the model and prototype.

The equivalence relationship illustrated in Figure 4-1 can thereafter be established based on Equation 4-1 and Equation 4-2:

$$\rho g H_p = \rho g N H_m \quad (4-3)$$

where

H_p = corresponding height in the prototype

H_m = corresponding height in the model

N = scaling factor

By cancelling the identical items in Equation 4-3, the scaling factor for linear dimension can be expressed as:

$$L^* = \frac{H_m}{H_p} = \frac{1}{N} \quad (4-4)$$

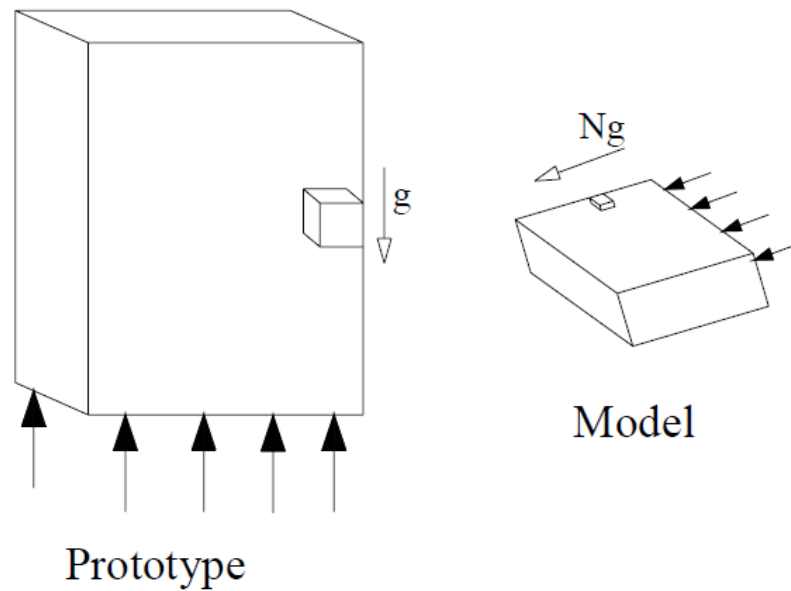


Figure 4-1 Gravity effects in prototype and model (after Schofield, 1980)

Commonly-used scaling factors for centrifuge testing are summarized in Table 4-1 (Kutter, 1992).

There is an increase in complexity related to the scaling factors of time from the effects of dynamic loading and consolidation. The equation in the dynamic case is:

$$L = \frac{1}{2}at^2 \quad (4-5)$$

where

L = distance an accelerating mass moves with time

a = acceleration

t = time

Therefore, the scaling factor of time in the dynamic situation is:

$$t^* = \sqrt{\frac{L^*}{a^*}} = \sqrt{\frac{1/N}{N}} = \frac{1}{N} \quad (4-6)$$

The duration of the dynamic event in the model is N times less than that in the full scale prototype.

In the case of consolidation, the time factor is given as:

$$T_v = \frac{C_v t}{H_{dr}^2} \quad (4-7)$$

where

T_v = time factor

C_v = coefficient of consolidation

H_{dr} = maximum drainage path

The scaling factor of time can be obtained by:

$$t^* = \frac{T_v^* H^{*2}}{C_v^*} = \frac{H^{*2}}{C_v^*} \quad (4-8)$$

If the specimen and pore fluids used in the model tests are the same as those in the prototype, the coefficient of consolidation equals one. The scaling factor for time becomes:

$$t^* = H^{*2} = \frac{1}{N^2} \quad (4-9)$$

The duration of the consolidation in the model is N^2 times less than that in the full scale prototype, which conflicts with the scaling factor of time in the dynamic situation. Both the dynamic effect and consolidation (including the dissipation of generated excess pore water pressure under dynamic loading) play significant roles in determining soil behavior. In some cases, the build-up of pore water pressure may not be observed due to its rapid diffusion.

Table 4-1 Scaling relationship for centrifuge test (N: scaling factor)

Quantity	Prototype	Model
Length	N	1
Area	N^2	1
Volume	N^3	1
Velocity	1	1
Acceleration	1	N
Mass	N^3	1
Force	N^2	1
Stress	1	1
Strain	1	1
Mass Density	1	1
Time (Dynamic)	N	1
Time (Diffusion)	N^2	1
Frequency	1	N

It is impossible to separate the dynamic effect and diffusion effect in one dynamic centrifuge modeling test. The most common solution is to slow down the rate of diffusion by reducing coefficient of consolidation C_v by N times. Recalling the expression of $C_v = \frac{k}{m_v \gamma_w}$ in Equation 2-1, the value of coefficient of consolidation is proportional to the hydraulic conductivity of soils. According to the equation given by Taylor D.W.:

$$k = D_s^2 \frac{\gamma_w}{\eta} \frac{e^3}{1+e} \frac{c_s}{36} \quad (4-10)$$

where

D_s = effective grain diameter

η = viscosity of pore fluid

e = void ratio of soil

c_s = shape factor

Provided that soil used in the centrifuge test is the same as in the prototype, the reduction of coefficient of consolidation could be realized by increasing the viscosity of pore fluid by N times.

Liu (2009) provided a comprehensive literature review of viscous pore fluids used as alternatives to water in centrifuge modeling tests. Commonly used viscous fluids include silicone oil, Glycerin-water mixture and Methycellulose. The advantages and limitations of those specific pore fluids have been discussed by Kutter (1995), Zeng et al. (1998) and Ko and Dewoolkar (1998). Silicone oil was first used at Cambridge University twenty years ago (Steedman and Zeng, 1990; and Madabhushi, 1994). At present silicone oil is not widely used because it is potentially deleterious to the user, and difficult to remove when cleaning the centrifuge apparatus

and to dispose. Glycerin-water mixtures have been used by Whitman and Lambe (1988), Whitman and Ting (1993), and Liu and Dobry (1994). However, Zeng et al. (1998) found that the fluid tends to clog within high-density soils. In addition, the density of Glycerin-water mixture is significantly different from the pure water, which makes the hydraulic conductivity in Equation 4-10 dependent on more than just viscosity. The Methylcellulose water mixture is one of the most popular viscous fluids used in centrifuge tests (Kimura, 1993; Ko et al., 1998; and Stewart et al., 1998). Its suitability is largely attributed to its easy preparation and cleaning, identical density as pure water, and ready availability.

In this study, pure water was used in the centrifuge modeling test under the impact loading. The flow behavior of impounded slurry as it exists in the field would not have been accurately determined if the pores of the sampled fine refuse was filled with a more viscous fluid. In addition, the development and dissipation of pore pressure under dynamic impact loading can be more readily observed in the centrifuge tests with pure water. The centrifuge modeling tests were conducted at 50 g centrifugal acceleration. If a fluid with viscosity 50 times of pure water was employed, the duration of pore pressure dissipation would have been prolonged 50 times. The existing data acquisition system used in the centrifuge would not have been able to observe and analyze the whole process of excess pore pressure buildup, maintenance, and dissipation.

4.2 Facilities and Instrumentation

4.2.1 Centrifuge

The centrifuge modeling tests were conducted with the geotechnical centrifuge at Case Western Reserve University (CWRU) which is shown in Figure 4-2. The centrifuge has been used in various projects associated with earthquake analysis, environmental hazard mitigation,

and advanced infrastructure geo-technology. As shown in Figure 4-3, the CWRU centrifuge has dual platforms with a radius of 1.37 m. The payload capacity is 20g-ton with a maximum acceleration of 200g for static tests and 100g for dynamic tests. The centrifuge arm is balanced by adjusting the counterbalance weights on the opposite swing platform. The centrifuge has a 16-channel data acquisition system. The laboratory is equipped with transducers such as Linear Variable Differential Transducers (LVDTs), accelerometers, and pore pressure transducers. The rigid modeling container (see Figure 4-4) has been commonly used in many centrifuge tests with the inside dimensions of 53.3 cm (length) \times 24.1 cm (width) \times 17.7 cm (height).



Figure 4-2 CWRU geotechnical centrifuge

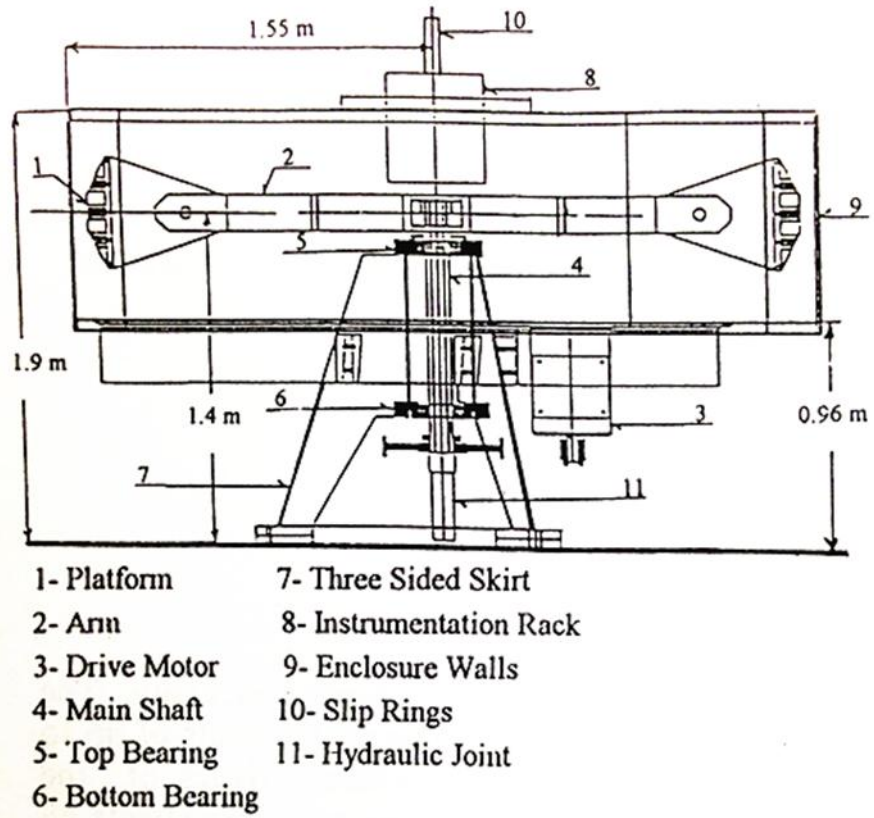


Figure 4-3 Cross-sectional view of CWRU centrifuge (after Figueroa et al., 1998)



Figure 4-4 Rigid box on the CWRU geotechnical centrifuge

4.2.2 Pore Pressure Transducers

Druck model PDCR81 pore pressure transducers were used in CWRU centrifuge modeling test. They are cylindrical with a diameter of 5.8mm and a length of 11.4mm. The transduction is performed by a silicon diaphragm with a strain gauge bridge diffused on the surface. Pore pressure reaches the diaphragm through a porous stone with a 2 micron filter grade. The specifications of the transducers are listed as Table 4-2.

Table 4-2 Pore Pressure Transducer PDCR81 (Source: GE Sensing)

Model No.	PDCR81
Mechanical Shock	1000g for 1 ms
Resolution	Infinitely small
Sensitivity	0.16 mV/V/psi
Temperature Range	-20°C - 120°C
Weight	2g
Size (Length×Diameter)	11.4×5.8 mm

4.2.3 Flow Container for Centrifuge Test

As shown in Figures 4-5 and 4-6, a special model container was designed for the centrifuge flow tests with the dimensions of 44 cm (length) × 15 cm (width) × 44 cm (height) so that the container could be put inside of the rigid box shown in Figure 4-4. About one gallon of coal waste slurry sample was contained in the upper right part of the container. The slope and the camera mount could be adjusted at three different angles.

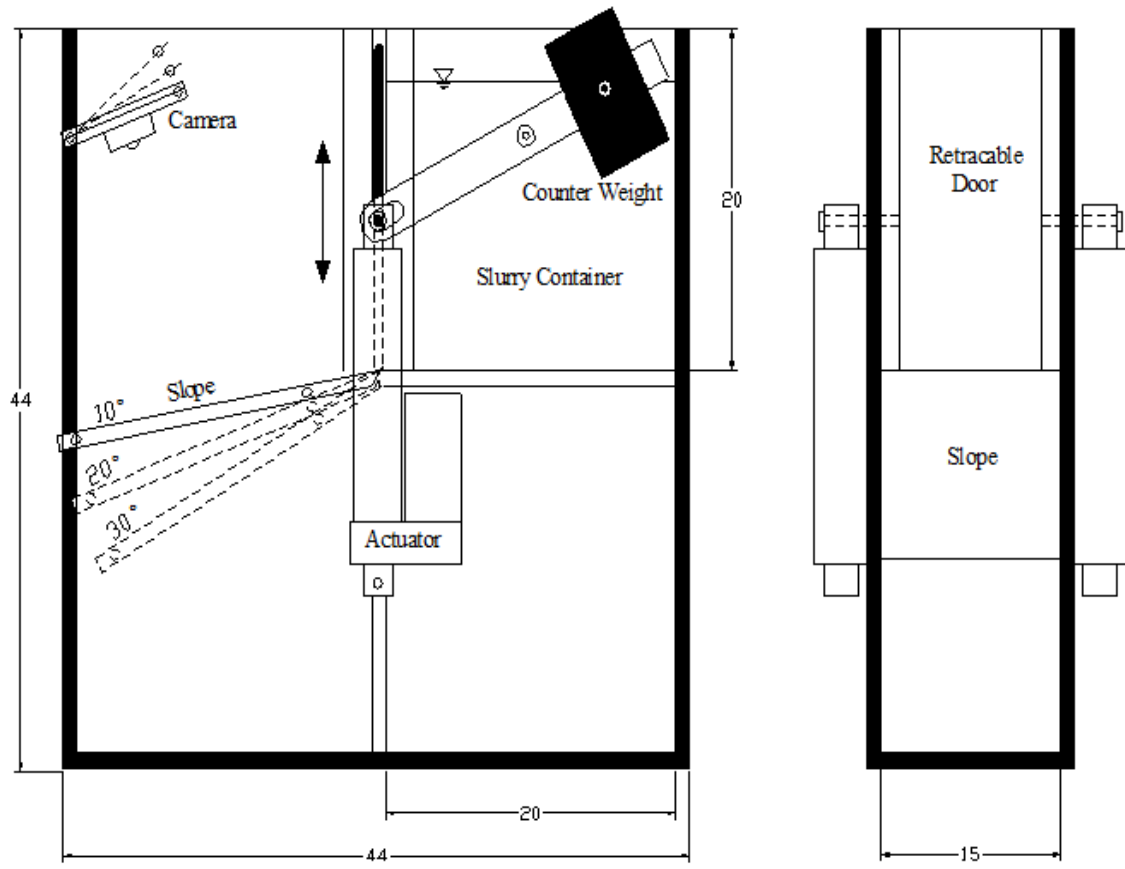


Figure 4-5 The design drawing of model container for centrifuge test (unit: cm)

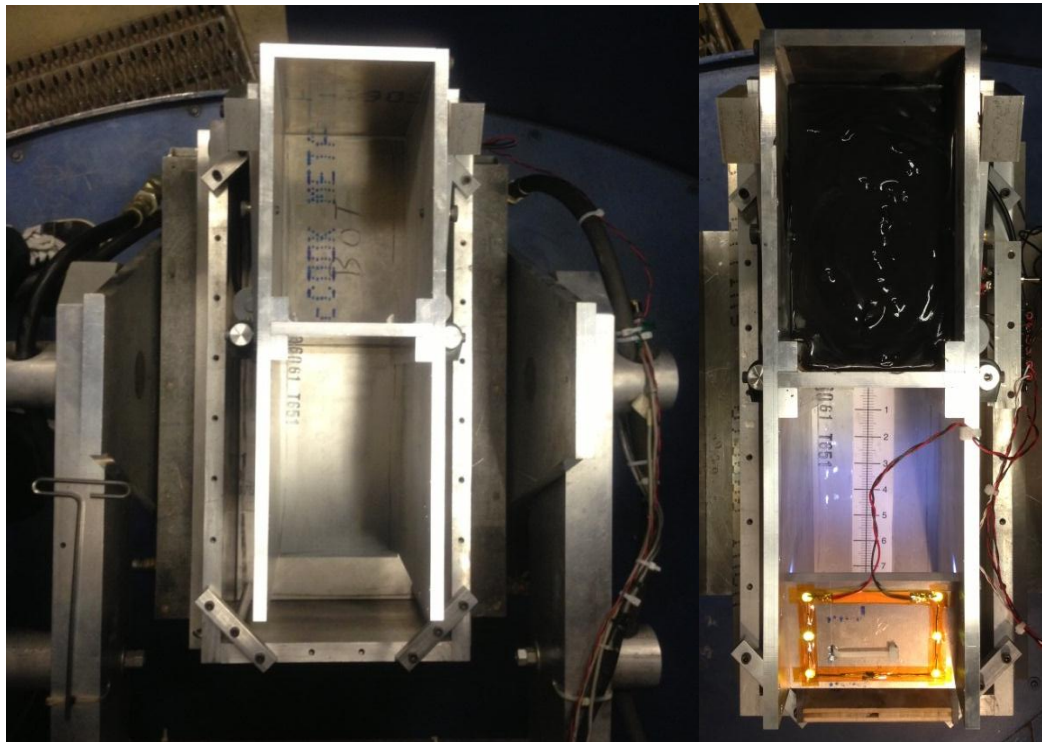
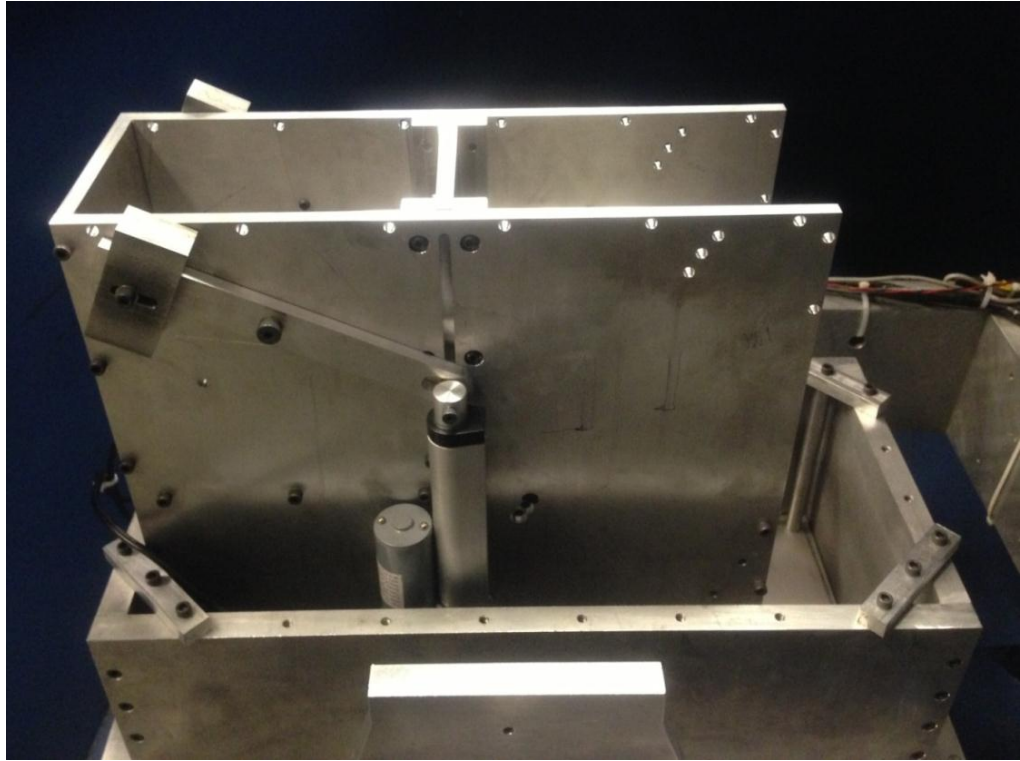


Figure 4-6 The flow container in the centrifuge test

The procedure of the centrifuge tests were the same as that of the small scale tests. Since the centrifuge tests were carried out at 50 times gravitational acceleration, some detailed designs were developed to address potential problems under such a high stress field. Specifically, three challenges were: (1) how to open and close the door under the generated high stress field; (2) how to prevent leakage of slurry from the container during the spin at 50g; and (3) how to generate impact loading.

Based on a rough estimation of static pressure exerted behind the door and the induced friction during the opening process, two actuators (FA-150-S-12-4) produced by Firgelli Automations were selected to lift the door. As shown in Figure 4-7, each actuator has a 4 inch stroke length and can withstand 150 lbs of push/pull force. The speed of stroke can reach 0.5 in/sec under 12V DC. The actuators are mounted on the two sides of the container and work simultaneously. To ensure that the door opens at 50g, a solid mass is added on each side of the container to counter the weight of the door and part of the friction force. The details are graphically shown in Figure 4-5.

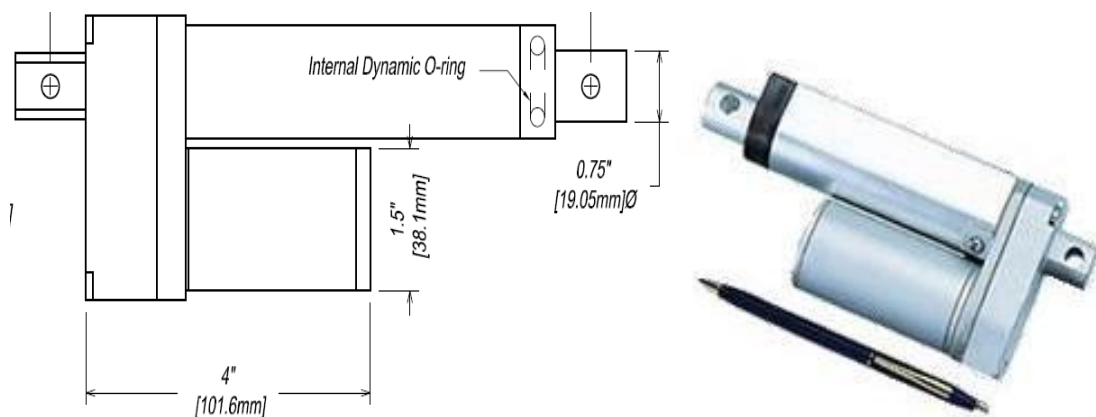


Figure 4-7 Actuator used in the centrifuge test

In order to prevent the leakage of water from the container under the high stress field, the connections and joints were all coated with silicone rubber adhesive sealant when assembling the model container. A thick layer of grease was also applied on the sides and bottom of the door before filling it with slurry. A couple of trial tests were successfully conducted without any leakage under 50g. The door could be opened smoothly and then closed as the flow ceased.

One of the greatest challenges in designing the centrifuge apparatus was developing a method of generating impact loading. A significant challenge in the model container design was how to hold the weight in place before dropping it onto the slurry sample; how to release the weight; and how to let the falling weight strike the desired location. After comparing various options, the electromagnet method was selected due to its safety and effectiveness. When the centrifuge reached the designed gravitational acceleration, the mass was released by shutting down the electromagnetic force. The electromagnet was 2 inches in diameter and 1 5/8 inches in height. The electromagnetic power could hold the maximum weight of 180 lbs. The magnet was equipped with a spring-loaded pin that quickly released the object when the power was turned off. As shown in Figure 4-8, the electromagnet was placed on top of a tube which mounted right above the slurry sample so that the mass could fall down from the designed heights. The weight and drop height of the mass was calibrated to the desired strain induced on the sample by conducting several trial runs of the testing procedure.

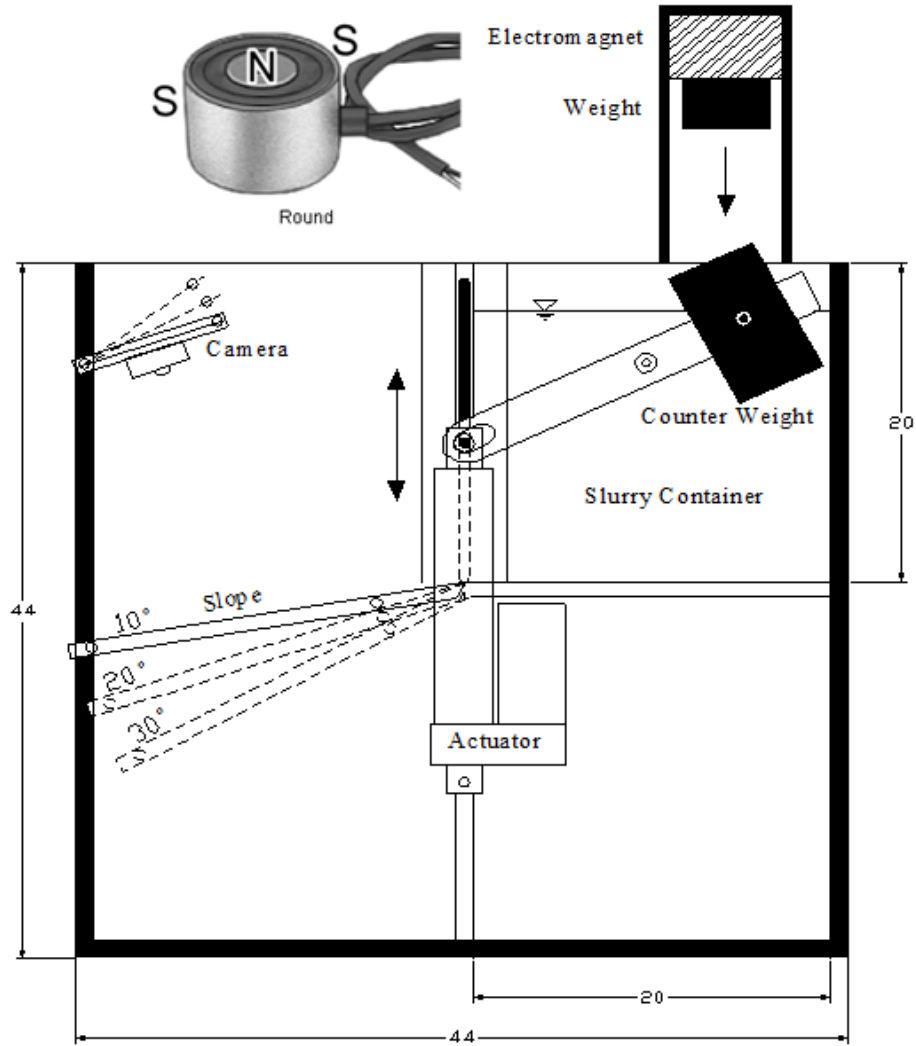


Figure 4-8 Design of centrifuge model test under impact loading

4.3 Model Preparations and Test Procedures

A group of centrifuge model tests were performed on the two samples collected from Kentucky and West Virginia. The design of the model container for the flow tests is discussed in Section 4.2.3. To begin each test, the door of the container was closed and grease was applied along the container's bottom and sides. As shown in Figures 4-5 and 4-8, approximately one gallon of slurry with different initial water contents simulated the prototype coal waste impoundment pool.

The filled container was placed on the centrifuge arm and the model was gradually spun up to a centrifugal acceleration of 50g. Centrifuge scaling laws shown in Table 4-1 were applied to the flow measurements to calculate the corresponding flow behavior of the slurry as it should occur in a prototype impoundment. As the stress field increased with the centrifuge acceleration, it increased the consolidation (or drainage) process and consequently the water content of the sample ended up lower than its initial water content. There was a small amount of water accumulated on the surface as the result of consolidation but this had no influence on the flow failure as the amount of free water was small. Based on the results of a few trial tests, it was found that the water content was reduced by 5 to 7% when initial water content was higher than 65% and about 3% when it was lower than 65%. Accordingly, the coal waste slurry samples in the centrifuge tests were intentionally prepared with the initial water contents slightly higher than the designed values.

In general, the procedure of the centrifuge model test followed that of the small-scale model test. Due to the limited quantity of slurry samples, the centrifuge tests were only conducted with the slope angles of 10° and 30°. Impoundment flow failure was simulated by rapidly opening the container door. If a flow failure was initiated the slurry flowed down the slope. A Gopro Hero3 high speed video camera installed facing the slope recorded the results of the test. The slope was scaled in order to determine flow velocity and distance.

4.4 Test Results and Analysis under Static Loading

The centrifuge model tests were conducted under 50g centrifugal acceleration and simulated the flow behavior of coal waste slurry from the bottom of a slurry impoundment pool 10 m long, 7.5 m wide and 10 m deep. In the static loading tests, the flow of the slurry was

driven by the material's self-weight in the direction parallel to the slope. The KY and WV samples were prepared at different initial water contents and their flow was tested using the two slope angles. Their movements were recorded by the high-speed video camera and then analyzed frame by frame using film processing software in order to determine the velocity and travel distance of the slurry flow. According to the centrifuge scaling laws shown in Table 4-1, the scaling factor for velocity converts the velocity measured in the model to that in the prototype.

The variation of flow velocity with the water content of the slurry and slope angle are graphically exhibited in Figure 4-9. The flow velocities of the two slurry samples decreased as the water content and slope angle decreased. This correlation agrees well with the recorded results from small-scale model tests. The flow of the KY and WV samples ceased down the 30° slope at water contents of 40% and 50% respectively. As shown in Table 4-3, the increased stress field in the centrifuge has lowered the critical water contents of both samples. However, the critical water contents were still above the corresponding liquid limit of each sample. In the opinion of the authors, establishing and maintaining a water content of slurried fine coal refuse below its liquid limit is a reasonably conservative practice during the expansion of upstream-constructed impoundments and in cases where the potential for a breakthrough into an underground mine exists.

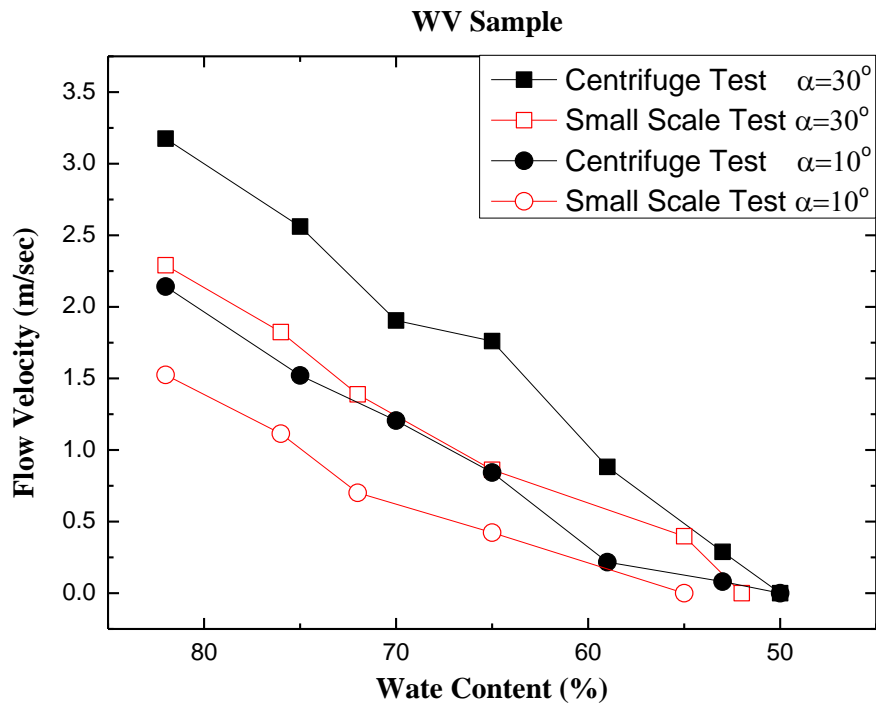
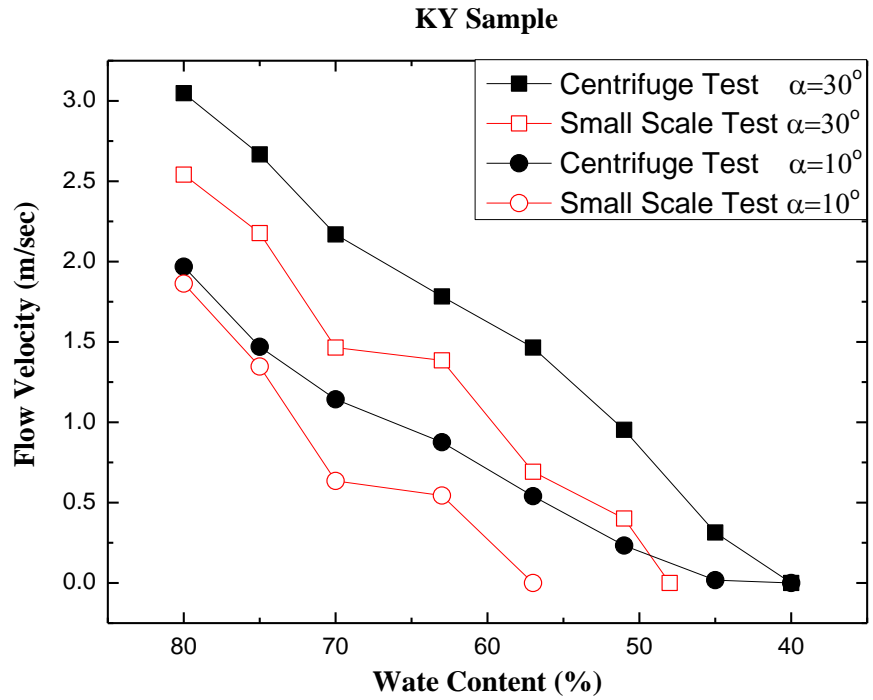


Figure 4-9 Centrifuge test results for two coal slurry samples (prototype scale)

Table 4-3 Comparison of liquid limit with critical water content in centrifuge tests

Critical Water Content	KY Sample	WV Sample
Liquid Limit	38.1%	42.5%
Small-Scale Tests	51%	52%
Centrifuge Tests	40%	50%

The travel distance and the depth of flow normal to the slope in the midstream were also recorded and scaled to a prototype impoundment environment. As shown in Table 4-4, the impounded coal waste slurry traveled more than 80 m once the flow was initiated. At the slope angle of 10°, the transition from the non-flowable to flowable state seemed quite sensitive to water content. Only a slight increase of water content triggered extensive flow of the slurry. With respect to both slope angles, an increase of flow depth was observed from less than 0.05 m to between 0.55 and 1.75 m as the initial water content decreased from 80% to less than 50%.

Table 4-4 Recorded travel distances and flow depths of two samples in the centrifuge tests.

(Data scaled to a prototype impoundment environment, total distance for the model is 81.28m in prototype scale)

Water content (%)	KY Sample				Water content (%)	WV Sample			
	30°		10°			30°		10°	
	L (m)	D (m)	L (m)	D (m)		L (m)	D (m)	L (m)	D (m)
80	>81.28	<0.05	>81.28	<0.05	80	>81.28	<0.05	>81.28	<0.05
75	>81.28	<0.05	>81.28	0.075	75	>81.28	<0.05	>81.28	0.1
70	>81.28	0.075	>81.28	0.175	70	>81.28	0.125	>81.28	0.25
63	>81.28	0.1	>81.28	0.3	65	>81.28	0.15	>81.28	0.38
57	>81.28	0.2	>81.28	0.425	59	>81.28	0.3	>81.28	0.43
51	>81.28	0.35	>81.28	0.65	53	>81.28	0.55	76.2	0.9
45	>81.28	1.25	60.96	1.75					

(L: extent of flow; D: flow depth in the midstream; dimensions in prototype scale)

The flow behavior of coal waste slurry at various water contents and slope angles in the centrifuge tests are exhibited in Figure 4-10. At an initial water content of 80%, a shallow and smooth layer of slurry flowed down the slope with depth less than 5mm. As the water content was reduced, the flow viscosity increased. A solid plug on top of the flow (where there was no velocity gradient) thickened. As discussed in the small-scale model tests, the flow of the coal waste slurry transitioned from Newtonian to non-Newtonian (Bingham Plastic) from higher to lower water contents.



Figure 4-10 Flow of KY coal refuse sample in the centrifuge tests

The flow velocities measured in the centrifuge model tests were also compared with those measured in the small-scale model tests. As shown in Figure 4-9, the solid dots represent data from centrifuge model tests while the hollow dots represent data from small-scale model tests. Although the data are in the same order of magnitude, the flow velocities in the centrifuge tests were faster than those in the small-scale model tests due to the increased stress field. The small centrifuge model in the high stress field was equivalent to a sample with larger mass and volume in the prototype.

The above results correspond with the findings from work performed by Kailey et al. (2011) on debris flows. The effect of mass volume and water content were assessed via a series of centrifuge tests. They concluded that increases in both mass and water content increased the peak flow velocity. However, the effect of water content was much more pronounced than that of mass.

The determination of flow regime in this current study followed the identical procedure as that in the small-scale model tests in Section 3.3.2 but was also scaled to the prototype impoundment. As shown in Table 4-5, the flows of both the KY and WV samples were calculated to be laminar in nature even at the highest water contents. The calculated Reynolds numbers in the centrifuge model tests were larger than those in the small-scale model tests due to the increased stress field and, consequently, the faster flow rates. In addition, the Reynolds numbers of WV sample were found to be smaller than those of KY samples due to its greater viscosity.

Table 4-5 Determination of flow regime in the centrifuge tests

Kentucky Sample							
Water Content %	ρ <i>kg / m³</i>	v <i>m/sec</i>	R <i>m</i>	η <i>Pa·sec</i>	Re	Re_c	Regime
80	1393	3.05	0.05	0.1	2094	2180	Laminar
75	1408	2.67	0.05	0.16	1158	2145	Laminar
70	1425	2.17	0.07	0.21	1082	2166	Laminar
63	1451	1.78	0.1	0.34	741	2209	Laminar
57	1477	1.47	0.19	0.47	874	2343	Laminar
51	1506	0.95	0.32	0.54	850	2743	Laminar
West Virginia Sample							
Water Content %	ρ <i>kg / m³</i>	v <i>m/sec</i>	R <i>m</i>	η <i>Pa·sec</i>	Re	Re_c	Regime
80	1420	3.18	0.05	0.33	674	2105	Laminar
75	1438	2.56	0.05	0.43	422	2104	Laminar
70	1456	1.91	0.12	0.52	645	2121	Laminar
65	1477	1.76	0.14	0.69	548	2124	Laminar
53	1534	0.29	0.48	0.95	224	2565	Laminar

4.5 Test Results and Analysis under Impact Loading

The configuration of centrifuge model tests under impact loading is shown in Figure 4-11. An aluminum tube was installed right above the slurry sample with an electromagnet attached at the top. The electromagnet can generate sufficient power to hold a one pound mass. The mass was dropped during the spin at 50g by turning off the electromagnetic power. The height of the mass could be adjusted in order to generate different impact energies. Each impact loading test represents a single-cycle event such as the frontal wave of a blast vibration, a sudden failure of a mine barrier or subsidence event. A pore water pressure transducer was buried in the middle of

the slurry sample. The recorded development of excess pore water pressure was helpful in evaluating whether the sample liquefied under impact loading.

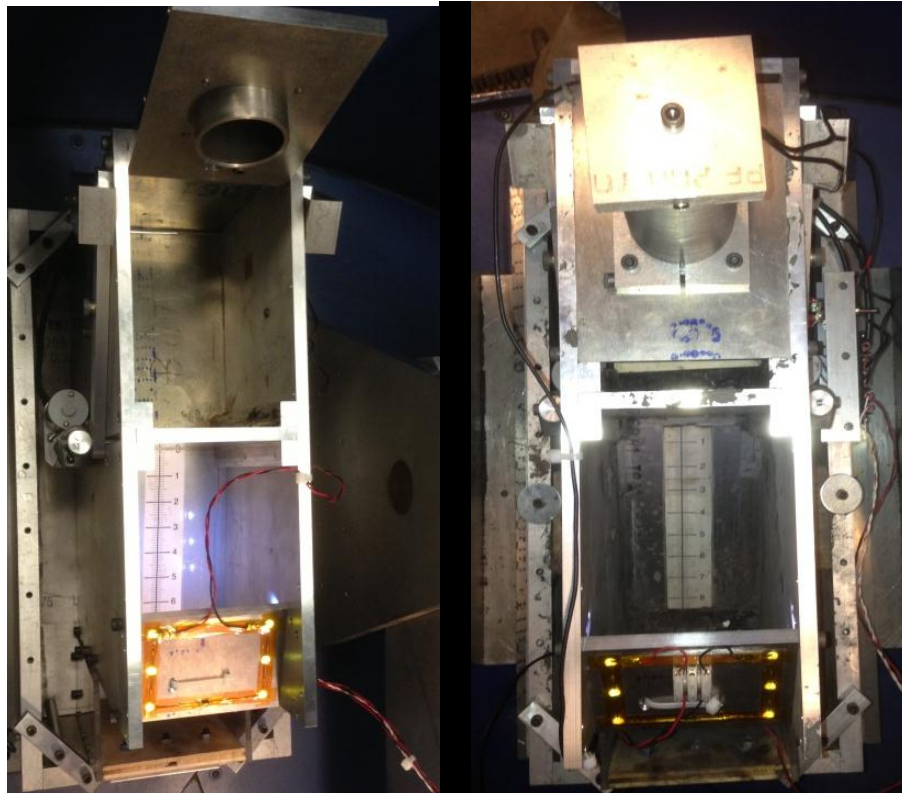


Figure 4-11 The centrifuge model test under impact loading

The samples were tested at the water content at which the flow ceased under static loading. The results of the centrifuge tests under impact loading are summarized in Table 4-6 and exhibited in Figure 4-12. Figure 4-13 illustrates the development of excess pore water pressure after the mass was dropped. The vertical axis represents the pore water pressure ratio which is the ratio of the excess pore water pressure to the initial effective stress at the measuring point

$\frac{\Delta u}{\sigma'}$. Liquefaction would take place when the pore pressure ratio reaches the value of one.

Different compressive strains were induced by dropping the mass from different heights. As shown in Table 4-6, no flow was triggered under 3% compressive strain. For the KY sample

at 40% water content, the flow was initiated under 5% compressive strain with extremely slow velocity. The flow stopped after it traveled less than one meter (see Figure 4-12). The recorded pore water pressure in Figure 4-13 indicated that the liquefaction of the KY coal waste slurry sample occurred when compressive strain increased up to 8%. Although the existing Data Acquisition System on the centrifuge could not collect sufficient data to display the entire development of pore water pressure, the peak value at the end of the curve was very close to one, indicating that the coal refuse lost its effective stress and the fine particles were behaving as if suspended in a liquid. Accordingly, the flow velocity and the extent of flow were greatly increased at this water content. When water content was lower than the liquid limit, the flow could hardly be triggered. At 36% water content, the recorded pore pressure ratio was smaller than 0.5 under 10% compressive strain. The value of flow velocity was too small to be measured.

For the WV coal waste slurry sample, the centrifuge tests started at 50% water content. The flow ceased at this water content under static loading in spite of a large amount of pore water in the sample. At the slope angle of 30° , the fine refuse was liquefied when the compressive strain reached 6% with the recorded pore pressure ratio in Figure 4-13 approaching one. As shown in Figure 4-12, the solid sample changed into a highly viscous fluid and flowed at the velocity of 0.176 m/sec. The flow initiated by impact loading traveled more than 10 meters in prototype scale (see Table 4-6). At 45% water content, more evident flow was observed under 10% compressive strain than under 6% strain with the pore pressure ratio as high as 0.8. Even though the coal waste slurry did not liquefy, the flow travelled more than 5 meters at the speed of 0.061 m/sec. No flow was observed when the initial water content was lower than its liquid limit of 42.5%.

Table 4-6 The summarized results of centrifuge tests under impact loading ($\alpha = 30^\circ$)

Kentucky Sample				
Water Content (%)	Compressive Strains ε (%)	Drop Height (m)	Extent of Flow (m)	Flow Velocity (m/s)
40	3	2.5	0	0
40	5	4	0.64	0.0047
40	8	5	3.56	0.02
36	10	7.5	≈ 0	≈ 0
33	10	8	0	0
33	13	9.5	0	0
West Virginia Sample				
Water Content (%)	Compressive Strains ε (%)	Drop Height (m)	Extent of Flow (m)	Flow Velocity (m/s)
50	3	2	0	0
50	6	4	>10	0.176
45	6	4	1.27	0.0013
45	10	6	5.1	0.061
40	10	7.5	0	0
40	13	9	0	0

(Dimensions in prototype scale under 50g)

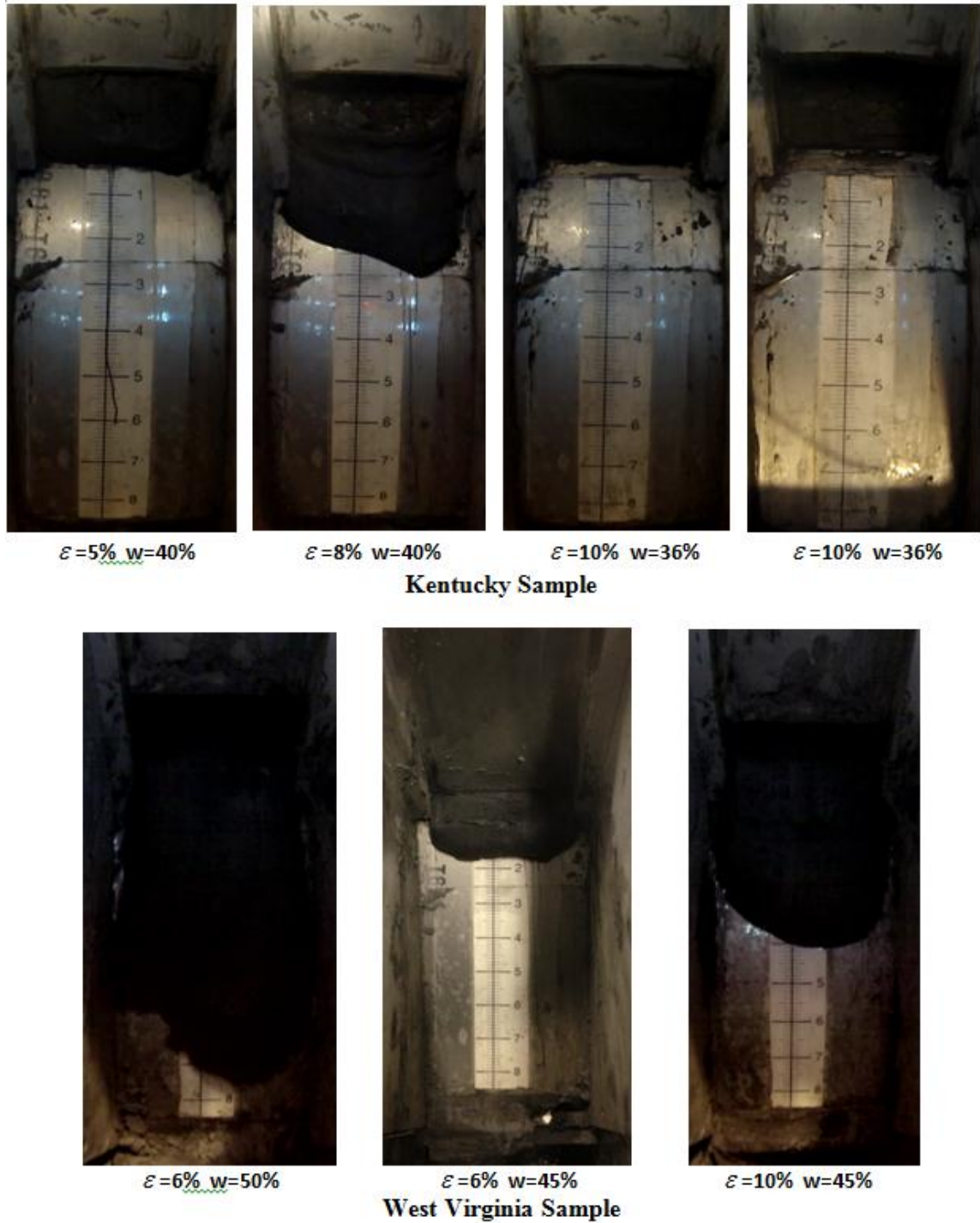


Figure 4-12 Flow of coal refuse in the centrifuge tests under impact loading ($\alpha = 30^\circ$)

In conclusion, the results of centrifuge model tests were consistent with those obtained from the small scale tests although the flow velocity was 20 percent higher due to the increased

stress field. Some minor discrepancies might exist in the data resulting from the slightly higher water content employed at the beginning of each centrifuge test.

The results also demonstrate the effect of a high void ratio in the fine refuse even at full consolidation. In the event of impact or dynamic loading excess pore water pressure in the material can quickly build up and cause severe reduction, if not elimination, of the effective strength of the material. Liquefaction of impounded fine refuse can produce a dangerously large pressure increase against an embankment that is improperly designed or constructed. However, the results from both the small-scale model tests and centrifuge model tests also indicate that the impounded fine coal refuse will have sufficient resistance to flow under impact loading as long as its water content is lower than its liquid limit.

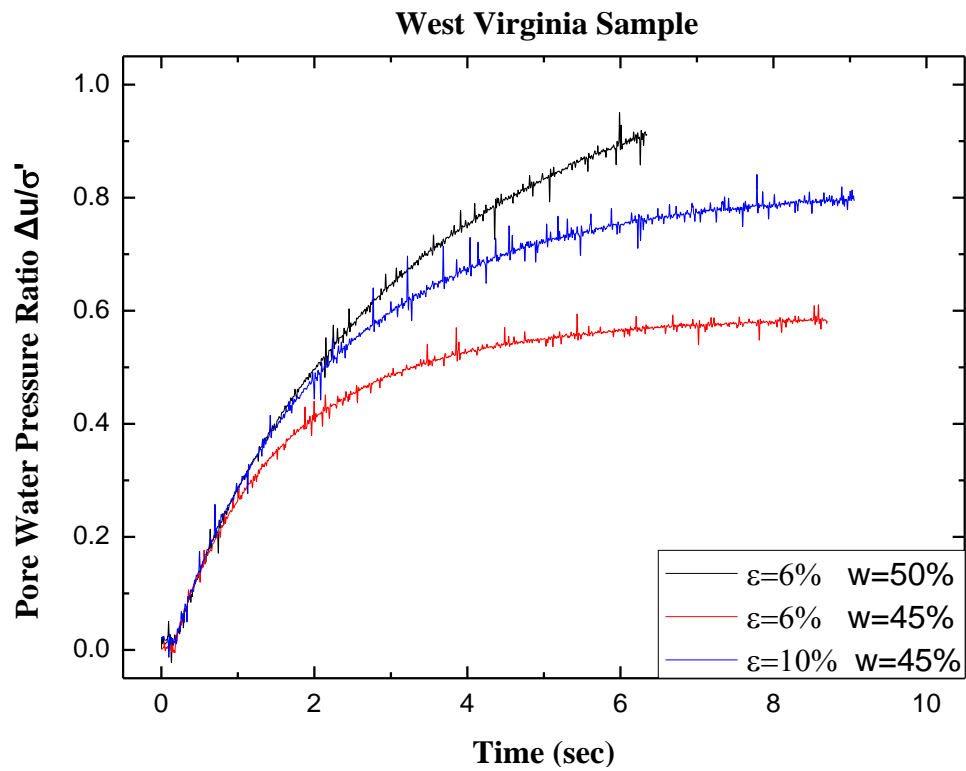
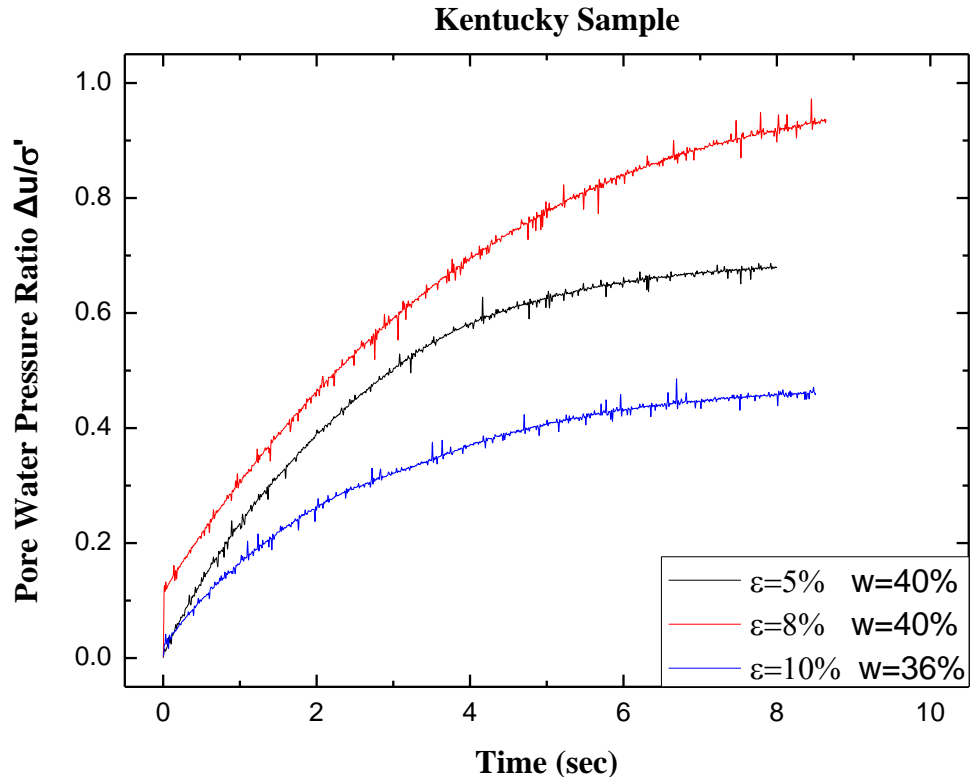


Figure 4-13 Recorded pore water pressure under impact loading (The drop of mass occurred at time zero)

4.6 Evaluation of Slurry Cells as a Countermeasure

4.6.1 Review of Coal Waste Slurry Cells

The slurry cell is widely considered to be one of the viable alternatives to the conventional coal slurry impoundment. Slurry cells are groups of small impoundments containing typically less than 20 acre-feet of coal slurry (Committee on Coal Waste Impoundments, 2002; and Craynon, 2013). The cells are separated from each other by dikes comprising compacted coarse refuse. They can be constructed in layers and the entire sequence can reach a total depth that approximates or even exceeds that of conventional impoundments (Michael et al., 2010). The construction of slurry cells is more suitable in flatter terrain than on sites consisting of steep slopes and narrow valleys (Gardner et al., 2003) although they are also been constructed in rugged topography in recent years. As shown in Figure 4-14, each cell is small and self-contained so that it limits the potential for flow failure by holding much less slurry within the impounding structure. Flow potential is further diminished by the internal drainage and geotechnical strength provided by the dikes. However, Michael et al. (2010) warned that slurry cell construction does not completely mitigate the potential for breakthrough into a proximate underground mine if the cells are constructed above a capped conventional impoundment. The extra surcharge onto the capped impoundment from stacked slurry cells can generate enough hydrostatic pressure to induce failure in a mine barrier or in rock strata above a mine.

In this study, the design of slurry cell is endorsed as a countermeasure to flow-failure potential under impact loading. In practice, slurry cells are constructed with compacted and high strength coarse refuse dikes that provide additional stability to impounding structure. Coarse refuse also has much higher permeability than its finer counterpart, rendering it less susceptible

to liquefaction. Moreover, the dikes act as drains for the fine refuse slurry and consequently speed up the consolidation process. Since coarse refuse is a by-product of coal mining and thus locally available slurry cell, construction should be an economical as well as effective deterrent to both embankment breaches and underground mine breakthroughs.

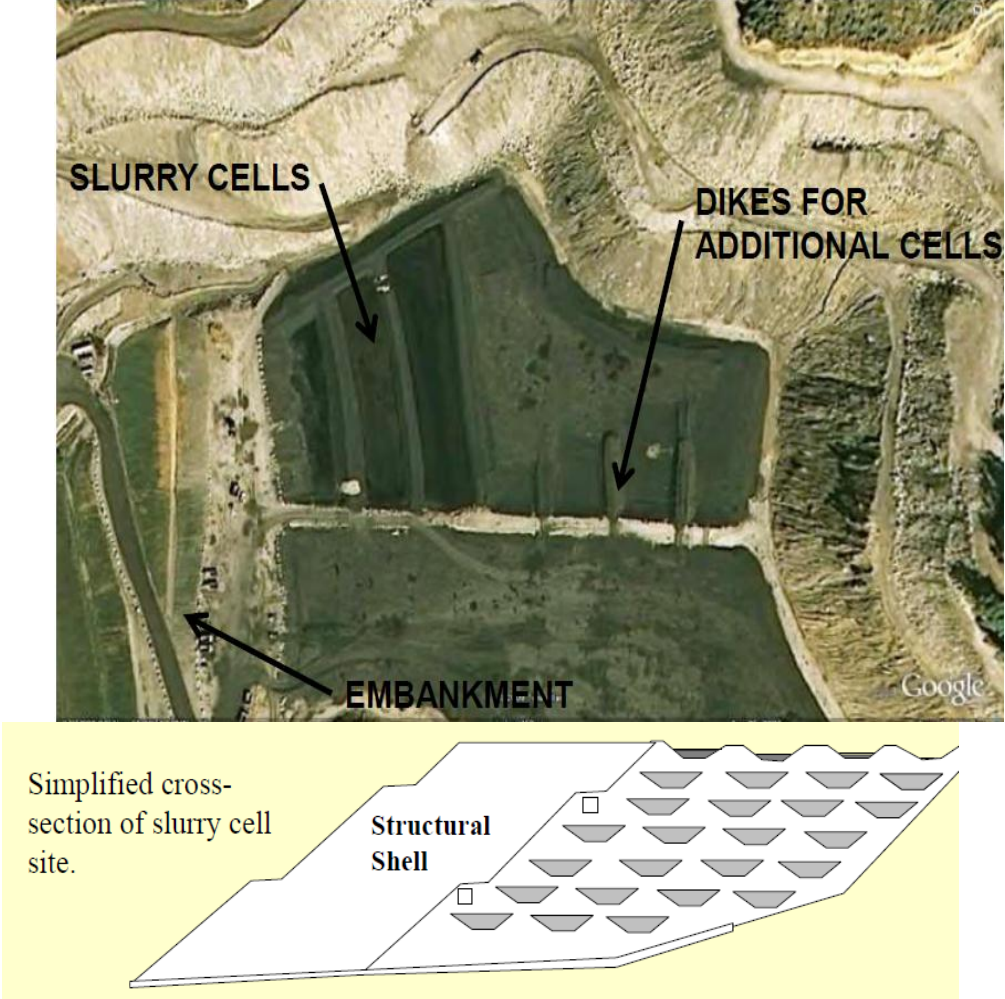


Figure 4-14 Coal refuse slurry cells (after Wu et al., 2003; and Michael et al. 2010)

4.6.2 Centrifuge Model Preparations

A series of centrifuge model tests were performed in order to validate the effectiveness of the slurry cell design. The miniature model of an arrangement of four slurry cells is shown in

Figure 4-15. The dikes were constructed with crushed stone with particle sizes between 2.0 and 4.75 mm. The sample was prepared in two 8 cm thick layers. Each layer comprised a 2 cm continuous sheet of crushed stone beneath slurry cells 6 cm thick. The centrifuge testing procedure was identical to the one used for impact loading (as described in Section 4.3).



Figure 4-15 Centrifuge model with coarse refuse build cells

Since no flow was observed under impact loading when water content of the samples was lower than liquid limit, the centrifuge model tests with slurry cells were performed at the water contents of 40% and 50%, and under the highest compressive strain of 10%. The pore pressure transducer was embedded at the bottom of the upper layer to record the development of excess pore water pressure.

4.6.3 Test Results and Analysis

The summarized results are listed in Table 4-7. The mass was dropped from a height of 7 m height to induce 10% compressive strain. No flow was triggered in either sample. Only a small amount of stones and water traveled down the slope when the door was lifted. Flow was not observed in two additional tests with the same water content and slurry cell configuration.

As shown in Figure 4-16, the generated pore pressure ratio of both samples under impact loading was less than 0.5, which was significantly less than the ratios recorded in the centrifuge tests on the specimens of pure slurry. In contrast to the latter tests, dissipation of excess pore water pressure was observed after a peak value was reached (Figure 4-16). Water flowing down the flume during the tests is interpreted to have resulted from drainage through the hydraulically conductive dikes. The results support the hypothesis that slurry cell construction is an effective means of improving the stability of an impoundment against impact loading.

Table 4-7 The summarized results of centrifuge tests with slurry cells ($\alpha = 30^\circ$)

Kentucky Sample				
Water Content (%)	Compressive Strains (%)	Drop Height (m)	Extent of Flow (m)	Flow Velocity (m/s)
40	10	7	0	0
West Virginia Sample				
Water Content (%)	Compressive Strains ε (%)	Drop Height (m)	Extent of Flow (m)	Flow Velocity (m/s)
50	10	7	0	0

(dimensions in prototype scale under 50g)

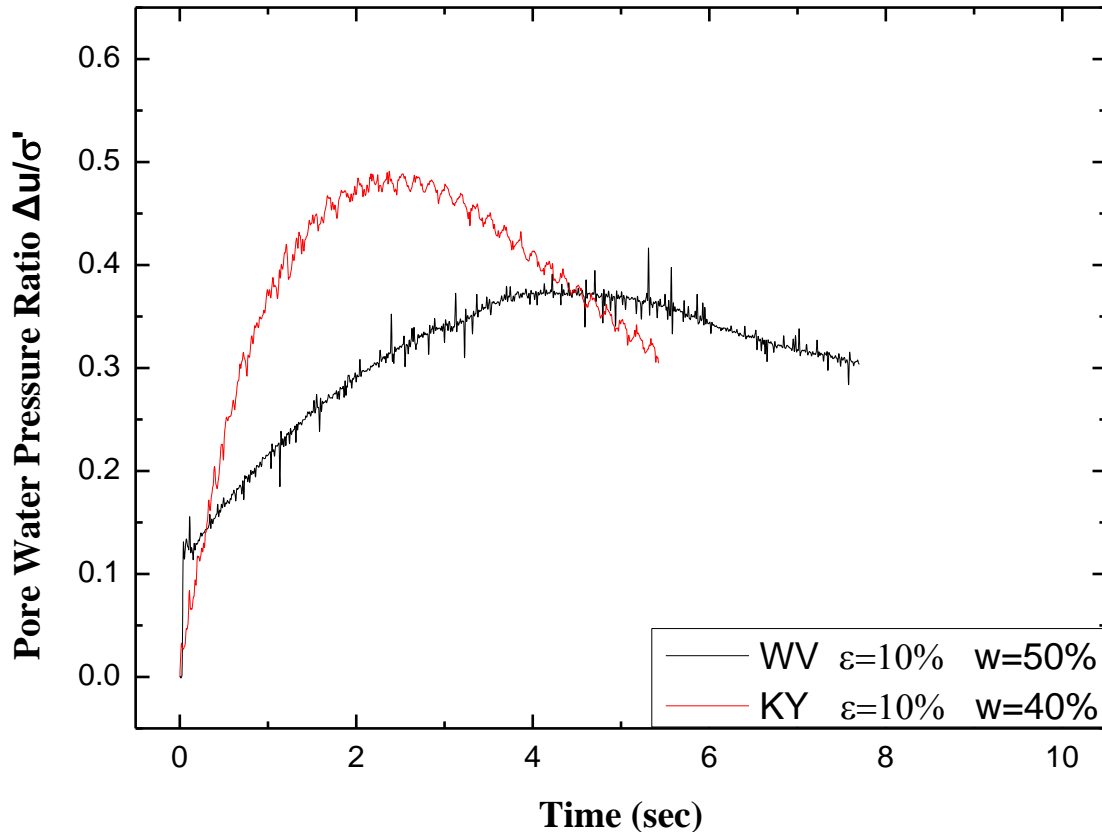


Figure 4-16 Recorded pore water pressure under impact loading by using slurry cells

4.7 Conclusions

A group of centrifuge model tests were performed on the two representative coal waste slurry samples. The flow behavior of the coal waste slurry was studied under both static and impact loading. In addition, the results of centrifuge tests were compared with the results obtained in the small-scale model tests. Finally, slurry cell construction was evaluated as a potential countermeasure to the effect of impact loading. Based on the results, the following conclusions are drawn:

- 1) Consistent results were obtained between the tests of the two coal waste slurry samples. The results matched well with those measured in small-scale model tests.
- 2) Centrifuge tests can generate accurate data on the flow behavior of coal waste slurry under a prototype impoundment stress field.

3) A special model container was designed and successfully used for centrifuge flow tests under both static loading and impact loading.

4) By comparing the results of the small scale model test and centrifuge test, it was found that the increase of mass or volume of slurry sample would increase the flow velocity. However, the influence of mass was less important than that of water content.

5) Under static loading in both small-scale and centrifuge tests, the flow velocity and travel distance of coal waste slurry decreased as the water content and slope angle decreased. The flow of coal waste slurry ceased at a water content higher than liquid limit. In addition, the critical water content was a little higher than that in the small-scale model test due to the increased stress field.

6) Although the recorded flow velocities and Reynolds number increased, the coal waste slurry flow can still be classified as laminar.

7) Based on the recorded pore water pressure ratio, the liquefaction of coal waste slurry was observed under compressive strains larger than 5%. Extensive flow was initiated as liquefaction occurred. However, coal waste slurry should have sufficient resistance to flow under impact loading as long as its water content is lower than its liquid limit.

8) The incorporation of slurry cells in impounding structures was validated as an effective and economical countermeasure to flow failure under impact loading due to (1) the high strength and permeability of compacted, coarse-grained dikes and (2) local availability of coarse refuse.

9) No flow was observed when slurry cell samples were subjected to impact loading (at 10 % compressive strain) in the centrifuge tests. The pore water pressure ratios were

significantly less than those recorded in tests on the pure slurry samples. In addition, Rapid dissipation of the pore water pressure occurred after the impact loading.

CONCLUSIONS AND RECOMMENDATIONS

5.1 Introduction

The potential of flow failures from coal waste impoundments have been a major concern for federal agencies such as the OSMRE and MSHA, geotechnical engineering consultants, and the coal industry. Failures of coal waste impoundments and other types of tailings dams have occurred several times in the past few decades. In the worst cases, millions tons of slurry flowed into waterways at high speed, resulted in tremendous property and environmental damages, and caused loss of life. A large number of coal waste impounding facilities are located in narrow valleys in steep-slope topography and adjacent to or above underground coal mine workings. Two mechanisms of flow failure in this setting include breaches of poorly constructed or overloaded embankments and breakthroughs into underground mines.

Impoundment breaches and breakthroughs commonly occur following heavy precipitation events. However, failures following liquefaction within impounded fluids following dynamic events such as earthquakes were also reported in the past 40 years. Casagrande (1950) found that flour-sized coal waste materials hydraulically deposited in an impoundment basin are in a very loose condition and consequently are extremely sensitive to dynamic disturbance. Up to the present time, however, very little study on the influence of dynamic impact loading on flow initiation and flow properties of coal waste slurry.

In this project, a comprehensive study was performed on the geotechnical properties and flow behavior of coal waste slurry under both static and impact loading using laboratory tests, small-scale model tests, and centrifuge model tests. Relationships have been established between the material's flow behavior and its geotechnical properties. The Bingham-Plastic conceptual flow model was employed to evaluate the results of the small-scale and centrifuge model tests.

The effectiveness of an engineering countermeasure, the construction of slurry cells, was also assessed with the centrifuge apparatus. The results of this study helped us to understand the flow behavior of impounded coal waste slurry; and will aid us and other investigators in developing tools to prevent flow failure or predict the effect of hypothetical failures on public safety, property, and the environment. The conclusions of this study may also lead to more effective impoundment designs and safer construction practices.

5.2 Summary of Conclusions

This project carried out a comprehensive study on the geotechnical properties and flow behavior of coal refuse under static loading and dynamic impact loading. Several conclusions were drawn based on the results of standard laboratory tests, small-scale model tests, and centrifuge model tests.

5.2.1 Geotechnical Properties of Impounded Coal Refuse Slurry

A group of laboratory tests was performed on two slurry samples from two different impoundments in Kentucky and West Virginia. Measured properties of the material included particle size distribution, specific gravity, Atterberg limits, permeability, compressibility, coefficient of consolidation, shear strength, and viscosity. Based on the findings stated in Chapter 2 of this report, the following conclusions can be drawn:

- 1) More than 80% of the particles of the samples passed the No.200 sieve.

The two samples have significantly different grain-size distributions which appear to have affected different consolidation rates, hydraulic conductivities, and flow velocities and distances. The fine coal refuse can be classified as low-plasticity silt (ML).

2) The specific gravity of the sampled slurry ranged between 2 to 2.15 which is generally low relative to other soils. The low specific gravity is typically associated with low levels of effective stress and shear strength. Coal waste slurry is generally known to have loose granular structure even after consolidation, which increases the potential for flow.

3) The liquid limit of the KY and WV samples occurred at 38.1 and 42.5 percent moisture, respectively. According to the results of the small scale model tests and centrifuge model tests, flow of the samples did not occur at water contents higher than their liquid limits even under impact loading. However, it is still recommended that the liquid limit be used as the critical water content to determine flowability during the construction, maintenance, and reclamation of coal waste impoundments.

4) The slurry samples had higher compressibility and lower consolidation rates at higher water contents. Relative to other fluidized materials, more settlement time is necessary for coal waste slurry to achieve significant consolidation strength.

5) Consolidation is a complex process incorporating pore water drainage, volume reduction, density increase, and buildup of effective strength. The results of consolidation tests should be used in the design and construction of impoundments, particularly upstream- and centerline-constructed impoundments, to determine the time required for the water content of the slurry to drop below its liquid limit or for the development of sufficient consolidation strength prior to expanding the facility.

6) The hydraulic conductivity of slurry samples was in the range of 10^{-4} to 10^{-9} cm/s, which is classified as very low to impervious permeability. Low permeability

impedes consolidation and consequently renders slurried fine refuse subject to liquefaction under the impact loading.

7) Triaxial tests were conducted to measure the undrained and drained shear strength of the samples at different initial water contents. Generally, the shear strength of both samples was extremely low. Significant strength buildup was observed as the water content was decreased to below the liquid limit. However, a significant amount of time for consolidation would be required for sufficient shear strength to naturally develop within the pool of an impoundment.

8) Viscosity is the internal frictional resistance of a fluid to flow. Once a flow failure of an impoundment takes place, the viscosity of the fluid influences the velocity and distance of flow. The viscosity of coal waste slurry was measured by a NDJ-8S rotational viscometer under different water contents and rotational speeds. According to the measured results, the coal waste slurry is considered to be a “shear-thinning” non-Newtonian fluid whose viscosity decreases with the rotational speed.

9) Viscosity of coal refuse was found to be very sensitive to the water content. At the high rotational speed of 60 rpm, the viscosity varied from 10^3 cP at about 40% water content to 10^2 cP at 80% water content. The increased water content mitigates interactions between the fine refuse particles and thereby reduces the resistance to the slurry flow.

5.2.2 Flow Behavior of Impounded Coal Waste Slurry under Static Loading

The rheological properties and flow behavior of impounded coal waste slurry has been studied carefully in this research. A group of small-scale model tests and centrifuge model tests

were performed on the slurry samples under the self-weight condition. The effects of initial water content, driving shear force, and other geotechnical parameters on the flow behavior of coal waste slurry have been studied. Based on the recorded results, the following conclusions can be drawn:

1) Velocity and travel distance of coal waste slurry flow decreased as the water content and applied shear stress (controlled by the slope angle) was reduced. Flow did not occur at a water content slightly higher than the liquid limit.

2) Although the flow velocities in centrifuge model tests were greater than those in small-scale model tests due to the increased stress field (equivalent to the load exerted by the weight of impounded slurry), they were still on the same order of magnitude. The effect of pool volume on flow velocity was less significant than that of water content.

3) The WV sample exhibited more viscous behavior (i.e. slower velocity and thicker flow depth) than the KY sample which likely resulted from the higher percentage of fine particles in the WV sample.

4) The applicability of different standard rheological models was evaluated. The flow of the slurry samples can be considered Newtonian with low viscosity at the higher water contents because of the negligible yield stresses and low linear slopes of the $\tau-\dot{\gamma}$ curves. As the water content was decreased the flow became heavier, more viscous, and non-Newtonian. The Bingham-Plastic model was used in the flow analysis in the interest of simplicity, however, it is noted that the Pseudo-Bingham Plastic model (or Herschel-Bulkley model) best matched the raw lab data.

5) Plastic viscosity η_p and yield stress τ_y are the two primary parameters governing the flow behavior of a Bingham-Plastic fluid, each of which can be determined based on the established $\tau-\dot{\gamma}$ curve. Both the yield stress and plastic viscosity increased as the water content was reduced.

6) The coal waste slurry flow (in the midstream where the flow velocity of the slurry is constant) can be considered as a uniform, steady, laminar flow.

7) The profile of the slurry flow can be described as a solid plug region near the free surface underlain by a parabolic gradation of flow velocity. The solid plug region thickened as the water content was reduced.

8) Although the flow ceased under static loading at a water content higher than the liquid limit, a large amount of pore water still existed in the slurry samples, making the samples susceptible to the flow failure if dynamically disturbed.

5.2.3 Flow Behavior of Impounded Coal Waste Slurry under Impact Loading

Impact loading such as from mine blasts and earthquakes can adversely affect the impoundment stability. The mechanism of flow failure can be embankment instability or mine barrier failure combined with liquefaction within the slurried fine refuse. An impact event producing a single seismic wave was added to the self-weight loading of the slurry samples during a second phase of small-scale and centrifuge model tests. The tests were applied to samples with water contents below liquid limit. Based on the recorded results, the following conclusions can be drawn:

1) Considering the cost, safety, and effectiveness, the monotonic impact loading was successfully simulated by dropping a weight onto the pond.

2) Coal waste slurry samples with water contents less than liquid limit were tested under compressive strains ranging from 0.1% to 5% in the small-scale model tests and 3% to 13% in the centrifuge model tests. Based on the results of previous experiments performed by Veyera (1985), liquefaction should take place under a single wave of compressive strain greater than 0.01% for soils with low effective stresses and low relative densities and 1% for soils with high effective stresses and high relative densities

3) Slurry flow was not triggered by impact loading until the compressive strain exceeded 1%. When the flow started, the solid sample changed into a very thick and viscous fluid.

4) The centrifuge is an effective and economical tool to investigate the flow behavior of coal waste slurry by generating similar self-weight stress fields and impact loading effects to those that may occur in a typical impoundment.

5) More extensive flow in response to the impact loading was observed in the centrifuge model tests than in the small scale model tests. According to the recorded pore water pressures, liquefaction took place under compressive strains greater than 5%, resulting in relatively extensive flows.

6) The effect of impact loading became insignificant as the water content was reduced a level slightly higher than the liquid limit. Coal waste slurry with a water content below liquid limit should have sufficient resistance to impact disturbance.

5.2.4 Effectiveness of Slurry Cells as a Countermeasure

Depending on its water content, impounded coal waste slurry can be liquefied under impact loading. Liquefaction can change the impounded fine refuse from a plastic solid into a

viscous fluid, producing a large pressure increase against an embankment or mine barrier. A separate set of centrifuge model tests were conducted to evaluate the employment slurry cells as a countermeasure to liquefaction potential within the slurry pool of an impoundment. Based on the recorded results, the following conclusions can be drawn:

- 1) The advantage of slurry cells is related to the dikes of coarse refuse separating them, i.e. their great stiffness and geotechnical strength, high permeability, and ability to engender speedy dissipation of pore water pressure within the slurried fine refuse.

- 2) No flow was observed when the samples were subjected to a compressive strain as high as 10%. The measured pore water pressure indicated that the slurry did not liquefy. In addition, the pore water pressures recorded were much less than those measured in previous experiments without the slurry cells.

5.3 Recommendations for Future Studies

Recommendations for future work include:

- 1) One of the limitations in this research was the limited amount of sampled coal waste slurry tested. Although the water content was found to be the predominant factor influencing flowability, the volume effect (experienced in the prototype impoundment) needs to be further assessed. Also, when testing larger specimens of fine refuse in a larger scale model test, steady-state flow would be better achieved and flow velocity more accurately measured. The development and application of a larger scale model tests is recommended.

- 2) All the laboratory tests and physical model tests were conducted on coal waste slurry samples obtained from two impoundments. As the properties of coal waste

slurry varies both among and within impoundments, additional samples should be tested for a more comprehensive understanding of the general flow properties of coal waste slurry. A centralized geotechnical database on fine refuse slurry properties should be established and periodically augmented in support of future research and the development of improved impoundment design and construction methodologies.

3) In the small-scale model tests, the slurry liquefaction was estimated based on measured compressive strains. The empirical work on soils that supports this approach may have limited applicability to coal waste slurry. The pore pressure transducers or other sensors suitable for a 1-g test are needed in order to identify the development of pore water pressure in impact loading tests.

4) The study of non-Newtonian flow of impounded coal waste slurry is complex. Assumptions and approximations utilized in this research to simplify the analysis should be validated or adjusted through additional physical model testing and numerical computation.

5) It has been demonstrated that impounded fine refuse with a water content higher than its liquid limit can liquefy under impact loading. Particular attention should be paid to the construction of impoundments (especially in upstream method) in areas close to active mine blasting. The response of impounded fine refuse to blast loading should be field tested.

6) Considering the extremely low permeability of fine coal refuse and the fact that the consolidation strength of the material can take many years to develop, long-term monitoring of upstream embankment deformation (e.g. settlement and sliding) and pore water pressures in the fine refuse is warranted. Insights gained from such monitoring

can be augmented with periodical in-situ tests (e.g. SPT or CPT measurements, geophysical surveys) or laboratory tests (consolidation tests, direct shear tests, triaxial tests) to assess consolidation development in the impoundment pool.

7) Although the simulated coal waste impoundment with slurry cells exhibited sufficient resistance to impact loading, the effectiveness of the cells in preventing embankment breaches or mine barrier breakthroughs should be further evaluated for various in-field site conditions. For instance, the response to impact loading of facilities comprised of stacked slurry cells lying above capped conventional impoundments should be assessed. Surcharge from the stacked slurry cells may adversely increase the hydrostatic pressure in the underlying fine refuse slurry.

8) In the interest of mitigating flow failure potential in impoundments, alternatives in addition to slurry cells should be explored in future studies. For instance, the combining of fine and coarse refuse in the impoundment should be considered.

9) An underground breakthrough scenario does not result in an open channel flow. The flow is affected by the size and depth of the breakthrough opening and the geometry and condition of the penetrated mine workings as well as the properties of the slurry. A comprehensive study on slurry flow behavior within a typical underground mine environment is needed.

10) Research should be conducted to model the effect of sinkhole subsidence on impounded fine coal refuse. For example, the tendency of the material with different geotechnical or rheological properties to bridge over vs. flow through a sinkhole of various dimensions should be assessed.

REFERENCES

- Abdali, S., Mitsoulis, E., & Markatos, N. (1992). Entry and exit flows of Bingham fluids. *Journal of Rheology*, 36(2), 389.
- Abdel-Ghaffar, M. (1990). *The Meaning and Practical Significance of the Cohesion Intercept in Soil Mechanics. Thesis*. University of Illinois, Urbana-Champaign, IL.
- Administration, M. S. (2009). Engineering And Design Manual Coal Refuse Disposal Facilities. *2nd Edition, MSHA, United States Department of Labor*.
- Agarwal, V. (2009). *Geotechnical investigation of coal mine refuse for backfill in mines*. Department of Mining Engineering, National Institute of Technology.
- Akayuli, C., & Ofosu, B. (2013). Empirical Model for Estimating Compression Index from Physical Properties of Weathered Birimian Phyllites. *The Electronic Journal of Geotechnical Engineering*, 18, 6135-6144.
- Aktas, K., & Woodburn, E. (2000). Effect of addition of surface active agent on the viscosity of a high concentration slurry of a low-rank British coal in water. *Fuel Processing Technology*, 62, 1-15.
- Aktas, Z., & Woodburn, E. (2000). Effect of addition of surface active agent on the viscosity of a high concentration slurry of a low-rank British coal in water. *Fuel Processing Technology*, 62, 1-15.
- Anonymous. (2007). *Wikipedia exploration of the consolidation tests*. Retrieved from [http://en.wikipedia.org/wiki/Consolidation_\(soil\)#mediaviewer/File:Consolidation_spring_analogy.jpg](http://en.wikipedia.org/wiki/Consolidation_(soil)#mediaviewer/File:Consolidation_spring_analogy.jpg)
- Anonymous. (2012). *ROTATIONAL VISCOMETER - diagram, schematic, and image 04*. Retrieved from http://www.faqs.org/patents/imgfull/20120210774_04
- Anonymous. (2013). *Wikipedia: exploration of the viscometer*. Retrieved from <http://en.wikipedia.org/wiki/Viscometer>.
- Anonymous. (2014). *Wikipedia exploration of Buffalo Creek Flood*. Retrieved from http://en.wikipedia.org/wiki/Buffalo_Creek_Flood
- Anonymous. (2014). *Wikipedia exploration of the Newtonian Fluid*. Retrieved from http://en.wikipedia.org/wiki/Newtonian_fluid
- Anonymous. (2014). *Wikipedia exploration of the non-Newtonian Fluid*. Retrieved from http://en.wikipedia.org/wiki/Non-Newtonian_fluid

Anonymous. (2014). *Wikipedia: exploration of the Bingham Plastic*. Retrieved from http://en.wikipedia.org/wiki/Bingham_plastic

ASTM. (1963). *Test method of particle-size analysis of soils. D422*. West Conshohocken, Pa: ASTM.

ASTM. (1985). *Practice for dry preparation of soil samples for particle size analysis and determination of soil constants. D421*. West Conshohocken, Pa.: ASTM.

ASTM. (1985). *Standard test methods for Liquid Limit, Plastic Limit and Plasticity Index of soils. D4318*. West Conshohocken, Pa: ASTM.

ASTM. (2004). *Standard test methods for measurement of hydraulic conductivity of saturated porous materials using a flexible wall permeameter, ASTM D5084-03*. West Conshohocken, PA.

ASTM. (2005). *Standard Test Methods for One-Dimensional Consolidation Properties of Soils Using Incremental Loading. D2435*. West Conshohocken, Pa: ASTM.

ASTM. (2006). *Method for Consolidated Drained Triaxial Compression Test for Soils, ASTM D7181-11*. West Conshohocken, Pa.

ASTM. (2006). *Standard Test Method for Apparent Viscosity of Adhesives Having Shear-Rate-Dependent Flow Properties Using Rotational Viscometry, ASTM*. West Conshohocken, PA.

ASTM. (2006). *Standard Test Method for Permeability of Granular Soils (Constant Head), ASTM D2434-68*. West Conshohocken, Pa.

ASTM. (2006). *Standard Test Method for Shear Viscosity of Coal-Tar and Petroleum Pitches, ASTM*. West Conshohocken, PA.

ASTM. (2006). *Standard Test Method for Viscosity Determination of Asphalt at Elevated Temperatures Using a Rotational Viscometer, ASTM*. West Conshohocken, PA.

ASTM. (2006). *Standard Test Methods for Viscosity of Adhesives, ASTM D1084*. West Conshohocken, Pa.

ASTM. (2007). *Standard Test Method for Unconsolidated-Undrained Triaxial Compression Test on Cohesive Soils, ASTM D2850-03a*. West Conshohocken.

Atesok, G., Boylu, F., Sirkeci, A., & Dincer, H. (2002). The effect of coal properties on the viscosity of coal-water slurries. *Fuel*, 81, 1855-1858.

Avegherinos, P., & Schofield, A. (1969). Drawdown failures of centrifuged models. *Proceeding, Seventh International Conference on Soils Mechanics and Foundation Engineering*, 2, 497-505.

Balmforth, N., Craster, R., & Sassi, R. (2002). Shallow viscoplastic flow on an inclined plane. *Journal of Fluid Mechanics*, 470, 1-29.

Bardet, J. (1997). *Experimental soil mechanics*. Upper Saddle River, New Jersey 07458: Prentice Hall.

Bilbao, L., Lane, D., Michael, P., Richmond, M., Stoltz, J., Stump, D., & Superfesky, M. (2011). *POTENTIAL OF IMPOUNDED-COAL-WASTE-SLURRY BREAKTHROUGHS INTO UNDERGROUND MINES*. U.S. Department of the Interior, Office of Surface Mining Reclamation and Enforcement.

Bishop, A. (1973). The stability of tips and spoil heaps. *Quarterly Journal of Engineering Geology*, 6, 335-376.

Blight, G. (1969). Waste gypsum as an embankment material. *Proceedings of Seventh International Conference on Soil Mechanics and Foundation Engineering*, 39-43.

Boger, D., Scales, P., & Sofra, F. (2006). Rheological Concepts. In *Paste and Thickened Tailings: a Guide*. Australian Centre for Geomechanics, 25-37.

Botsaris, G., & Glazman, Y. (1988). *Interfacial Phenomena in Coal Technology*. Marcel Dekker, Inc., New York.

Bowles, J. (1979). *Physical and Geotechnical Properties of Soils*. New York: McGraw Hill.

Bowles, J. (1992). *Engineering properties of soils and their measurement* (Fourth ed.). McGraw-Hill Companies.

Boylu, F., Dincer, H., & Atesok, G. (2004). Effect of coal particle size distribution, volume fraction and rank on the rheology of coal–water slurries. *Fuel Processing Technology*, 85, 241-250.

Brisson, P., Garga, V., & Vanapalli, S. (2002). *Determination of Unsaturated Flow Characteristics in Mine Tailings*. Retrieved from http://by.genie.uottawa.ca/~vanapall/papers/conference/2002/Pat_Sai_CGS2002.pdf

Brookfield. (2009). *Brookfield Viscometer Assignment*. Retrieved from <http://www.eng.auburn.edu/~drmills/mans382/Viscometer/Brookfield%20Viscometer%20Assignment.doc>

Brookfield Engineering Labs Inc. (2005). *More solutions to sticky Problems*. Retrieved from <http://www.viscometers.org/PDF/Downloads/More%20Solutions.pdf>

Bucky, P. (1931). Use of model for the study of mining problems. *American Institution of Mining and Metallurgical Engineers*, 425, 3-28.

- Burns, C., Gauglitz, P., & Russell, R. (2010). *Shear strength correlations for Kaolin/Water slurries: A comparison of recent measurements with historical data*. U.S. Department of Energy, Pacific Northwest National Laboratory, Richland, Washington.
- Busch, R.A.; Backer, R.R.; Atkins, L.A.; Kealy, C.D. (1975). *Physical Property Data on Fine Coal Refuse*. Bureau of Mines, United States Department of The Interior. Spokane, Wash: Spokane Mining Research Center.
- Carrier, W. D. (1983). Design Capacity of Slurried Mineral Waste Ponds. *Journal of the Geotechnical Engineering Division, ASCE, 109(GT5)*, 699-716.
- Casagrande, A. (1950). Notes on the design of earth dams. *Journal of Boston Society of Civil Engineering, Oct.*, 231-255.
- Casagrande, A., & Poulos, S. (1964). Fourth report on investigation of stress-deformation and strength characteristics of compacted clays. *Harvard Soil Mechanics Series No. 74*.
- Castillo, C., & Williams, M. (n.d.). Rheology of very concentrated coal suspensions. *University of California, Berkeley, Chemical Engineering Series*.
- Chan, A. (2003). Determination of the Coefficient of Consolidation Using a Least Squares Method. *Geotechnique, 53(7)*, 673-678.
- Charlie, W. (1988). Blast induced liquefaction of soils: laboratory and field tests. *Research Grant AFOSR-85-0172*.
- Charlie, W., Veyera, G., & Muzzy, M. (1982). Shock induced soil liquefaction: test facility development. *28th International Instrumentation Symposium, Instrument Society of America, Las Vegas, NV*.
- Chen, C., Bullen, A., Vitale, E., & Elnaggar, H. (1967). *Permeability and related properties of coal refuse*. Wiley, New York: Engineering Practice.
- Chhabra, R. (2010). Non-Newtonian Fluids: An Introduction. *SERC School-cum-Symposium on Rheology of Complex Fluids*. India: Indian Institute of Technology Madras.
- Chhabra, R., & Richardson, J. (2008). Non-Newtonian Flow and Applied Rheology. *2nd edition, Oxford, Butterworth-Heinemann*.
- Chhabra, R., & Richardson, J. (2008). Non-Newtonian Flow and Applied Rheology. *2nd edition, Oxford, Butterworth-Heinemann*.
- Committee on Coal Waste Impoundments. (2002). Coal Waste Impoundments: Risks, Responses, and Alternatives. *National Academy of Sciences*.

- Cooke, R. (2002). Laminar flow setting: the potential for unexpected problems. *Proceedings of 15th International Conference on Hydrotransport, Banff, Canada.*
- Corte, J. (1988). Proceedings of the International Conference on Geotechnical Centrifuge Modelling, Paris, April, Balkema.
- Coussot, P. (1994). Steady laminar flow of concentrated mud suspension in open channels. *Journal of hydraulic research*, 32(4), 535-558.
- Coussot, P. (1994). Steady, laminar, flow of concentrated mud suspensions in open channel. *Journal of Hydraulic Research*, 32(4), 535-559.
- Craig, W. (1984). The application of centrifuge modelling to design. *Proceedings of a Symposium, Manchester, April, Balkema.*
- Craig, W. (1995). Geotechnical centrifuge: past, present and future. *Geotechnical Centrifuge Technology*, 1-18.
- Craynon, J. (2013). Environmental considerations in energy production. *Society for Mining, Metallurgy, and Exploration, Inc. (SME).*
- Damitio, C. (1978). Field experience on blast-induced liquefaction. *Int. Workshop on Blast-Induced Liquefaction, Dames and Moore, AFOSR, Maidenhead, U.K.*, 137-148.
- De Kee, D., Chhabra, R., Powley, M., & Roy, S. (1990). Flow of viscoplastic fluids on an inclined plane: evaluation of yield stress. *Chemical Engineering Communications*, 96, 229-239.
- Deng, C., Nio, T., Sanada, Y., & Chiba, T. (1989). Relationship between swelling of coal particles and apparent viscosity of slurry during coal liquefaction for Akabira coal/creosote oil slurry system. *Fuel*, 68(9), 1134–1139.
- Deysarkar, A., & Turner, G. (1980). The effect of vibrations on the flow properties of a saturated paste of iron ore and water. *International Journal of Mineral Processing*, 257-276.
- Dobry, R., & Alvarez, L. (1967). Seismic failures of Chilean tailings dams. *Journal of the Soil Mechanics and Foundations Division, ASCE*, 93(SM6), 237-260.
- Elcometer. (2006). Rotational viscometers. Retrieved from www.elcometer.com
- Engin, T., Dogruer, U., Evrensel, C., Heavin, S., & Gordaninejad, F. (2004). Effect of wall roughness on laminar flow of Bingham plastic fluids through microtubes. *Journal of Fluids Engineering*, 126, 880-883.
- Engineering News-Record (1972). Failure of coal waste embankment blamed on lack of engineering, March 9, 1972, p.11.

- Engineers, U. A. (1982). Engineering and design stability for earth and rock-fill dams. *Manual 1110-2-2300*. Washington, DC.
- Ferrini, F., Battara, V., Donati, E., & Piccinini, C. (1984). Optimization of particle grading for high concentration coal slurry. Proc. *9th Int. Conference Hydraulic Transport of Solids in Pipes*. Roma.
- FHWA. (2007). *Pro46 Long Term Pavement Performance Project Laboratory Materials Testing and Handling Guide*. United States Department of Transportation - Federal Highway Administration .
- Figuroa, J., Saada, A., Dief, H., & Dietz, C. (1998). Development of the geotechnical centrifuge at Case Western Reserve University. *Centrifuge 98, Kimura, Kusakabe & Takemura (eds). Balkema, Rotterdam*, 3-8.
- Florin, V., & Ivanov, P. (1961). Liquefaction of saturated sandy soils. *5th International Conferene on Soil Mechanics and Foundation Engineering, Paris, France*, 107-111.
- Fragaszy, R., Voss, M., Schmidt, R., & Holsapple, K. (1983). Laboratory and centrifuge modeling of blast-induced liquefaction. *8th Int. Symposium on Military Application of Blast Simulation, Spiez, Switzerland, Proceedings II*, 1-20.
- Gardner, J., Houston, K., & Campoli, A. (2003). Alternatives analysis for coal slurry impoundments. *SME Annual Meeting, Feb. 24-26, Cincinnati, Ohio*.
- Garnier, J., Gaudin, C., Springman, S., Culligan, P., Goodings, D., Konig, D., . . . Thorel, L. (2007). Catalogue of scaling laws and similitude questions in geotechnical centrifuge modelling. *International Journal of Physical Modelling in Geotechnics*, 7(3), 1-23.
- Haldenwang, R. (2003). Flow of non-Newtonian fluids in open channels. *Ph.D. Thesis, Department of Civil Engineering, Cape Technikon*.
- Haldenwang, R., Kotze, R., & Chhabra, R. (2012). Determining the viscous behavior of non-Newtonian fluids in a flume using a laminar sheet flow model and ultrasonic velocity profiling (UVP) system. *J. Braz. Soc. Mech. Sci. & Eng.*, 34(3), 276-284.
- Haldenwang, R., Slatter, P., & Chhabra, R. (2010). An experimental study of non-Newtonian fluid flow in rectangular flumes in laminar, transition and turbulent flow regimes. *Journal of the South African Institution of Civil Engineering*, 52(1), 11-19.
- Haldenwang, R., Slatter, P., & Chhabra, R. (2010). An experimental study of non-Newtonian fluid flow in rectangular flumes in laminar, transition and turbulent flow regimes. *Journal of the South African Institution of Civil Engineering*, 52(1), 11-19.

- Hanks, R., & Pratt, D. (1967). On the flow of Bingham plastic slurries in pipes and between parallel plates. *Society of Petroleum Engineers Journal*, 1, 342-346.
- Hanson, A., DeMouche, L., Lesikar, B., & Dreager, A. (2013). *Onsite wastewater management: a manual for tribes*. Las Cruces, NM.: New Mexico State University .
- Hegazy, Y., Cushing, A., & Lewis, C. (2004). *Physical, Mechanical and Hydraulic Properties of Coal Refuse for Slurry Impoundment Design*. D'Appolonia Engineering, Monroeville, PA .
- Henriquez, J., Vandervoort, A., & Simms, P. (2009). Imaging and modelling of flows of gold paste tailings during deposition - laboratory study and field scale predictions. *Paste2009, Australian Centre for Geomechanics, Perth*, 31-38.
- Hough, B. (1957). *Basic Soils Engineering*. New York: The Ronald Press Company.
- Huang, Y., & Li, J. (1987). Strength and consolidation characteristics of fine coal refuse. *Report to Office of Surface Mining, Department of Interior*.
- Huang, Y., Li, J., & Gamini, W. (1987). *Strength and consolidation characteristics of fine coal refuse*. University of Kentucky Contract Report J5140126 prepared for U.S. Department of Interior Office of Surface Mining Reclamation and Enforcement, Lexington, KY.
- Hubert, A. (1963). The behavior of sand in one-dimensional compression. *Ph.D. Thesis, Dept. of Civil Engineering, University of Illinois at Urbana*.
- Idriss, I. (2003). Some considerations in the assessment of the performance of tailings dams during earthquakes. *Proceedings o International Workshop on Earthquake Simulation in Geotechnical Engineering, Dept. of Civil Engineering, Case Western Reserve University, Cleveland, Ohio*.
- Ishihara, K. (1992). Post-earthquake failure of a tailing dam due to liquefaction of the pond deposit. *Proceedings of the Internaional Conference on Case histories in Geotechnical Engineering, University of Missouri, Rolla, Missouri*, 3.
- Ivanov, P., Sinitsyn, A., & Musaelyan, A. (1981). Characteristics of soils at cyclic and shock loads. *10 Int. Conf. on Soil Mechanics and Foundation Engineering, Stockholm, Sweden*, 3, 239-243.
- Jeyapalan, J., Duncan, J., & Seed, H. (1983). Investigation of Flow Failure of Tailings Dams. *Journal of Geotechnial Engineering*, 109(2), 172-189.
- Jeyapalan, J., Duncan, M., & Seed, B. (1983). Analyses of flow failures of mine tailings dams. *Journal of Geotechnical Engineering*, 109(2), 150-171.

- Jeyapalan, K. (1980). Analyses of Flow Failures of Mine Tailings Impoundments. *Ph.D. Thesis, University of California, Berkeley.*
- Jones, A., & Uckert, R. (2006). The investigate of the use of coal mine refuse for subbase material and embankment fill in South Dakota. *Billings Land Reclamation Symposium, 3134 Montavesta Rd., Lexington, KY.*
- Justice, C. (1997). *Consolidation and Shear Strength of Coal Slurry.* Kentucky: University of Kentucky.
- Kailey, P., Bowman, E., Laue, J., & Springman, S. (2011). Modelling debris flow processes with a geotechnical centrifuge. *Italian Journal of Engineering Geology and Environment, 3,* 339-349.
- Kaji, R., Muranaka, Y., & Hishinuma, Y. (1986). Effect of electrolyte on the rheological properties of coal–water mixtures. *AIChE Spring National Meetings, C3-D1.*
- Kawatra, S., & Bakshi, A. (1995). Determination of changes in rheologic properties of coal slurries in process streams. *Coal Preparation, 15,* 165-175.
- Kimura, T. (n.d.). Lecture Presented at U.S. Japan Workshop on Liquefaction, Napa, CA, June . 1993.
- Kimura, T., Kusakabe, O., & Takemura, J. (1998). Centrifuge 98 - Proceedings of the International Conference, IS-Tokyo 98, Tokyo, Japan.
- Ko, H., & Dewoolkar, M. (1998). Modeling liquefaction in centrifuge. *Proceedings, Physics Mechanics of Soil Liquefaction, 307-322.*
- Ko, H., & McLean, F. (1991). Proceedings of the International Conference Centrifuge 1991, Boulder, Colorado, June, Balkema.
- Kok, L. (1977). The effect of blasting in water-saturated sands. *5th International Symposium on Military Application of Blast Simulation, Stockholm, Sweden, May,* 1-10.
- Koppula, S. (1978). Statistical Estimation of Compression Index. *Geotechnical Testing J, 4(2),* 68-73.
- Kotza, R. (2007). Rheological characterization of highly concentrated mineral suspensions using an ultrasonic velocity profiler. *Thesis, CAPE PENINSULA UNIVERSITY OF TECHNOLOGY.*
- Kozicki, W., & Tiu, C. (1967). Non-Newtonian flow through open channels. *The Canadian Journal of Chemical Engineering, 45,* 127-134.
- Kozicki, W., & Tiu, C. (1986). Parametric modelling of flow geometries in non-Newtonian flows. *Encyclopedia of Fluid Mechanics, 7,* 199-252.

- Krizek, R. (2004). *Slurries in geotechnical engineering*. Evanston, Illinois: The Twelfth Spencer J. Buchanan Lecture.
- Kurzeme, M. (1971). Liquefaction of saturated granular soils. *1st Australia-New Zealand Conference on Geomechanics, Australian Geomechanics Society, Melbourne, Australia, 1*, 45-53.
- Kutter, B. (1992). Dynamic Centrifuge Modeling of Geotechnical Structures. *Transportation Research Record 1336, TRB, National Research Council, Washington D.C.*, 24-30.
- Kutter, B. (1995). Recent Advances in Centrifuge Modeling of Seismic Shaking. *Third International Conference on Recent Advances in Geotechnical Earthquake Engineering and Soil Dynamics, 2*, 927-941.
- Kwak, M., James, D., & Klein, K. (2005). Flow behavior of tailings paste for surface disposal. *International Journal of Mineral Processing, 77*, 139-153.
- Lamb, H. (1879). *Hydrodynamics*. Cambridge University Press. .
- Leonards , G., & Ramiah , B. (1959). Time effects in the consolidation of clays. *ASTM STP, 254*, 117-130.
- Leong, & Boger, D. (1990). Surface chemistry effects on concentrated suspension rheology. *Journal of Colloid and Interface Science, 136*(1), 249-258.
- Leung, W., Ballard, R., & Ledbetter, R. (1994). Proceedings of the International Conference Centrifuge 94, Singapore, Balkema.
- Lewis, M. (1989). *Water in Earth Science Mapping for planning, development and conservation*. (J. A. MCCALL, & G. A. TROTMAN, Eds.)
- Lingeburg, M. (2003). *Civil Engineering Reference Manual for the PE Exam*. Professional Publications Inc., Belmont, CA.
- Liu, G. (2009). Verification of shear wave velocity based liquefaction criteria using centrifuge model. *PH.D. Thesis, Department of Civil Engineering, Case Western Reserve University* .
- Liu, J. (2003). Stability of viscoplastic flow. *Geophysical Fluid Dynamics, 232-252*.
- Liu, L., & Dobry, R. (1994). Seismic settlement and pore pressure of shallow foundations. *Centrifuge 94, Leung, Lee and Ten es, Balkema, Rotterdam, 227-232*.
- Logos, C., & Nguyen, Q. (1996). Effect of particle size on the flow properties of a South Australian coal-water slurry. *Power Technology, 88*, 55-58.
- Logos, C., & Nguyen, Q. (1996). Effect of particle size on the flow properties of a South Australian coal-water slurry. *Powder Technology, 88*, 55-58.

- Lyakhov, G. (1961). Shock waves in the ground and the dilution of water saturated sand. *Zhurnal Prikladnoy Mekhaniki i. Tckhricheskoy, Fiziki, Moscow, USSR, 1*, 38-46.
- Madabhushi, S. (1994). Effect of pore fluid in dynamic centrifuge modeling. *Centrifuge 94, Leung, Lee and Tan eds, Balkem, Rotterdam*, 127-132.
- Mekle, C., Kubota, T., & Ko, D. (1974). 'An Analytical Study of the effects of surface roughness on boundary layer transition. *AF Office of Scientific Res. Space and Missile Sys. Org., Report No. AD/A004786*.
- Melzer, L. (1978). Blast-induced liquefaction of materials. *Nuclear Technology Digest, AFWL-TR-78-110, Air Force Weapons Lab., Kirkland, Air Force Base, Albuquerque, New Mexico, August*, 21-38.
- Mesri, G., Feng, T., & Shahien, M. (1999). Coefficient of Consolidation by the Inflection Point Method. *Journal of Geotechnical and Geoenvironmental Engineering, 125(GT8)*, 716-718.
- Mezger, T. (2002). *The Rheology Handbook: For Users of Rotational and Oscillatory Rheometers*. Hannover, Germany .
- Michael, P. et al. (2005). The flowability of impounded coal refuse: a review of recent work and current ideas in the engineering profession, Technical Assitance Report to the Appalachian Region Management Council, Office of Surface Mining, U.S. Department of the Interior. *U.S. Office of Surface Mining Appalachian Region Management Council Open-File Report, Pittsburgh, PA, 25 plus appendix*.
- Michael, P., & Chavel, L. (2008). Environmental risks associated with coal refuse impoundment reclamation: an assessment of the possibility of an underground mine breakthrough occurring as a result of the impoundment reclamation process. *U.S. Office of Surface Mining Appalachian Region Management Council Open-File Report, Pittsburgh, PA, 14*.
- Michael, P., Richmond, M., Superfesky, M., Stump, D., & Chavel, L. (2010). Potential of breakthroughs of impounded coal refuse slurry into underground mines. *Environmental & Engineering Geoscience, XVI(3)*, 299-314.
- Michalek, S., Gardner, G., & Wu, K. (1996). Accidental release of slurry and water from coal impoundments through abandoned underground coal mines. *Pittsburgh, PA: Mine Safety and Health Administration, Safety and Health Technology Center*.
- Mikasa, M., & Takada, N. (1973). Significance of centrifuge model test in soil mechanics. *Proceedings, Eighth International Conference on Soil Mechanics and Foundations, 1*, 273-278.
- Mitsoulis, E., Abdali, S., & Markatos, N. (1993). Flow simulation of Herschel-Bulkley fluids through extrusion dies. *Canadian Journal of Chemical Engineering, 71(1)*, 147-160.

- Monte, J. L. (1976). One-Dimensional Mathematical Model for Large-Strain Consolidation. *Geotechnique*, 26(3), 495-510.
- Moon, A. (1984). Effective shear strength parameters for stiff fissured clays. *4th Australia-New Zealand Conference on Geomechanics*, (pp. 107-111).
- Murthy, V. (2002). *Geotechnical Engineering: Principles and Practices of Soil Mechanics and Foundation Engineering*. New Delhi, DEL, India.
- Nagase, A., Kusakabe, O., & Wong, S.-F. (1984). Centrifuge model tests on bearing capacity of clay. *J Geotech Eng Div, ASCE*, 110, 1749-1765.
- National Research Council. (2002). Coal waste impoundments: risks, responses, and alternatives. *National Academy Press, Washington, D.C.*, 185.
- Ng, C. (2014). The state-of-the-art centrifuge modelling of geotechnical problems at HKUST. *Journal of Zhejiang University-Science A (Applied Physics & Engineering)*, 15(1), 1-21.
- Office of Surface Mining Reclamation & Enforcement (2011). Technical Position Paper: Potential of Impounded-Coal-Waste-Slurry Breakthroughs into Underground Mines—Issues and Answers: *open file report, U.S. Office of Surface Mining Appalachian Region*, Pittsburgh, PA, 25 plus appendix.
- Oldroyd, J. (1947). A rational formulation of the equations of plastic flow for a Bingham solid. *Mathematical Proceedings of the Cambridge Philosophical Society*, 43(1), 100-105.
- Olson, R. (1986). State of Art: Consolidation Testing, Consolidation of Soils, Testing and Evaluation. (E. R. N.Yong and F. C. Townsend, Ed.) *ASTM STP 892*, 7-70.
- Olson, R., & Mesri, G. (1970). Mechanisms controlling the compressibility of clays. *J Am Soc Civ Engrs*, 96, 1853-1878.
- Osborne, D. (1988). *Coal Preparation Technology*. Norwell, MA: Kluwer Academic Publishers.
- Palmer, B., & Krizek, R. (1987). Thickened slurry disposal method for process tailings. *Proceedings of the ASCE Geotechnical Specialty Conference on Geotechnical Practice for Waste Disposal '87, Geotechnical Special Publication (13), ASCE, NY*, 728-743.
- Philips, C., & Davis, R. (1991). Determination rheological parameters of debris flow material. *Geomorphology*, 4, 101-110.
- Phillips, R., Guo, P., & Popescu, R. (2002). Physical Modeling in Geotechnics - ICPMG'02, July, St.John, Canada.

- Qiu, Y., & Segoo, D. (1998). Engineering properties of mine tailings. *In Proceedings of the 51st Canadian Geotechnical Conference: Canadian Geotechnical Society*, (pp. 149-154). Vancouver, B.C.
- Qu, C., Zhang, X., Chen, S., Li, Y., Pan, F., & Yao, Y. (2013). Characteristics of capillary sealing mechanism of late quaternary shallow biogenic gas in the hangzhou bay area. *Advance in Earth Science*, 28(2), 209-220.
- Rendon-Herrero, O. (1980). Universal Compression Index Equation. *Journal of Geotechnical Engineering Division, ASCE, GT11*, 1179-1199.
- Rischbieter, F. (1977). Soil liquefaction-a survey of research. *Proceedings, 5th International Symposium on Military Application of Blast Simulation, Stockholm, Sweden*, 1-24.
- Robinson, R., & Allam, M. (1998). Effect of Clay Mineralogy on Coefficient of Consolidation. *Clays and Clay Minerals*, 46(5), 596-600.
- Round, G., & Hessari, A. (1985). The effect of size distribution and pH on the rheology of coal slurries. *Part. Multiph. Process.* 3, 329-340.
- Round, G., & Hessari, A. (1985). The effect of size distribution and pH on the rheology of coal slurries. *Particular Multiphase Process*, 3, 329-340.
- Saada, A., & Townsend, F. (1981). State of the art: laboratory strength testing of soils. (R. N. Townsend, Ed.) *Laboratory shear strength of soil. ASTM STP 740*, 7-77.
- Samarasinghe, A., Huang, Y., & Drnevich, V. (1982). Permeability and consolidation of normally consolidated soils. *J Geotech Eng, ASCE*, 108, 835-850.
- Sawyer, D., Flemings, P., Buttles, J., & Mohrig, D. (2012). Mudflow transport behavior and deposit morphology: role of shear stress to yield strength ratio in subaqueous experiments. *Marine Geology*, 307-310, 28-39.
- Schaflinger, U., Acrivos, A., & Zhang, k. (1990). Viscous resuspension of a sediment within a laminar and stratified flow. *International Journal of Multiphase Flow*, 16(4), 567-578.
- Schofield, A. (1980). Cambridge geotechnical centrifuge operations. *Geotechnique*, 30(3), 227-268.
- Shinavski, L. (2006). Overview of impoundment abandonment. *Presentation at the U.S. Mine Safety and Health Administration 2006 Annual Dam Safety Seminar: National Mine Health and Safety Academy, Beaver, WV*.
- Shook, C., & Roco, M. (1991). Slurry flow: principles and practice. *Butterworth and Heinemann*.

- Singh, A. (2012). *RHEOLOGICAL INVESTIGATION OF COAL WATER SLURRIES WITH AND WITHOUT ADDITIVE*, Thesis. Department of Mechanical Engineering, Thapar University, India .
- Skempton, A. (1944). Notes on the Compressibility of Clays. *Q. J. Geol. Soc. London*, 100(1-4), 119-135.
- Skempton, A. (1964). Long-term stability of clay slopes. *Géotechnique*, 14(2), 77-102.
- Somogyi, F. (1979). *Analysis and Prediction of Phosphatic Clay Consolidation: Implementation Package*. Lakeland, Florida: Florida Phosphatic Clay Research Project.
- Sowers. (1979). *Introductory Soil Mechanics and Foundations: Geotechnical Engineering, 4th Ed.* Macmillan, New York.
- Spelay, R. (2007). Solids transportation in laminar, open channel flow of non-Newtonian slurry. *Ph.D. Thesis, University of Saskatchewan, Saskatoon, Saskatchewan, Canada.*
- Sridharan, A., & Nagaraj, H. (2004). Coefficient of Consolidation and its Correlation with Index Properties of Remolded Soils. *Geotechnical Testing Journal*, 27(5).
- Sridharan, A., & Nagaraj , H. (2003). Coefficient of Consolidation and its Correlation with Index Properties of Remolded Soils. *Geotechnical Testing Journal*, 27(5).
- Sridharan, A., & Prakash, K. (1985). Improved Rectangular Hyperbola Method for Determination of Coefficient of Consolidation. *Geotechnical Testing Journal*, 8(3), 37-40.
- Sridharan, A., & Prakash, K. (1995). Critical Appraisal of Laboratory Determination of c_v . *International Symposium on Compression and Consolidation of Clayey Soils* (pp. 567-572). Hiroshima, Japan: Balkema Publishers.
- Sridharan, A., & Rao, G. (1976). Mechanisms controlling volume change of saturated clays and the role of effective stress concept. *Géotechnique*, 32, 249-260.
- Steedman, R. Z. (1990). The seismic response of waterfront retaining walls. *Design and Performance of Earth Retaining Structures, ASCE Special Publication*(25), 872-886.
- Stewart, D., Chen, Y., & Kutter, B. (1998). Experience with the use of Methylcellulose as a viscous pore fluid in centrifuge models. *Geotechnical Testing Journal*, 21(4), 365-369.
- Stout, B., Papillo, J., McAteer, D., Childers, H., Hoover, J., Higginbotham, J., & Quaranta, J. (2004). Coal slurry impoundment location and warning system. *Tailings and Mine Waste, Taylor and Francis Group, London*, 275-278.
- Straub, L., Silberman, E., & Nelson, H. (1958). Open channel flow at small Reynolds numbers. *American Society of Civil Engineers*, 123, 685-713.

- Studer, J., & Kok, L. (1980). Blast-induced excess porewater pressure and liquefaction: experience and application. *Int. Symposium on Soils under Cyclic and Transient loading, Swansea, UK*, 581-593.
- Studer, J., & Prater, E. (1977). An experimental and analytical study of the liquefaction of saturated sands under blast loads. *Int. Conf. on Numerical Methods in Soil and Rock Mechanics, Karlsruhe, Germany*, 2, 217-238.
- Suthaker, N., & Scott, J. (1994). Large scale consolidation testing of oil sand fine tails. *In Proceedings of the International; Congress of Environmental Geotechnics: Geotechnical and Related Aspects of Waste Management Associated with Municipal, Mine, Industrial, and Nuclear Wastes: Canadian Geotechnical Society, Edmonton, AB (Canada)*, 149-154.
- Suthaker, N., Scott, J., & Miller, W. (1997). The first fifteen years of a large scale consolidation test. *Proceedings of the 50th Canadian Geotechnical Conference: Canadian Geotechnical Society, Ottawa, Ontario*, 476-483 .
- Swamee, P., & Aggarwal, N. (2011). Explicit equations for laminar flow of Bingham plastic fluids. *Journal of Petroleum Science and Engineering*, 76, 178-184.
- Sweigard, R., Hopkins, T., Justice, C., Beckman, T., Thompson, E., & Rohlf, R. (1997). *Impact of consolidation on the shear strength of coal refuse impoundments*. SME Annual Meeting, Denver, CO.
- Tani, I. (1969). Boundary Layer Transition. *Annual Reviews of Fluid Mechanics. Annual Reviews, Tiago, Palo Alta, CA*, 1.
- Taylor, D. (1948). *Fundamentals of Soil Mechanics*. New York: John Wiley and Sons.
- Taylor, R. (1995). Centrifuges in Modelling: Principles and Scale effects. *Geotechnical Centrifuge Technology, Blackie Academic and Professional, Glasgow*, 19-33.
- Ter-Stepanian, G. (1963). On the long-term stability of slopes. *Norwegian Geotech. Institute, Publication*, 52, 1-14.
- Ter-Stepanian, G., & Goldstein, M. (1969). Multistoreyed Landslides and the strength of soft clays. *Proceedings, Seventh International Conference on Soil Mechanics and Foundation Engineering*, 2, 693-700.
- Terzaghi, K. (1931). The static rigidity of plastic clays. *Journal of Rheology*, 2(3), 253-262.
- Terzaghi, K., & Peck, R. (1967). *Soil Mechanics in Engineering Practice*. New York: John Wiley and Sons.

- Thacker, B., Ullrich, C., Athanasakes, J., & Smith, G. (1988). Evaluation of a refuse impoundment built by the upstream method. *ASCE Geotechnical Special Publication, No.21*, 730-749.
- Thomson, S., & Kjartanson, B. (1985). Study of delayed failure in a cut slope in stiff clay. *Canadian Geotechnical Journal*, 22(2), 286-297.
- U.S. Energy Information Administration (2015). Power generation from coal and natural gas expected to temporarily converge this spring. <http://www.eia.gov/todayinenergy/detail.cfm?id=21232>.
- U.S. Mine Safety and Health Administration. (2001). Report of Investigation: Noninjury Impoundment Failure/Mine Inundation Accident. *Mine Safety and Health Administration, Arlington, VA, 71 pp. plus appendices*.
- Vallejo, L., & Scovazzo, V. (2003). Determination of the shear strength parameters associated with mudflows. *Soils and Foundations*, 43(2), 119-133.
- Van Der Kogel, H., Van Loon-Engels, C. H., & Ruygrok, P. (1981). Wave propagation in porous media, shock tube experiments. *10th International Conference on Soil Mechanics and Foundation Engineering, Stockholm, Sweden*, 253-256.
- Veyera, G. (1985). Transient porewater pressure response and liquefaction in a saturated sand. *Ph.D. Thesis, Department of Civil Engineering, Colorado State University, Fort Collins, Colorado*.
- Vlachopoulos, J., & Strutt, D. (2003). The Role of Rheology in Polymer Extrusion. *In: Proceedings of New Technologies for Extrusion. Milan: SPIE*, (pp. 1-25).
- Volpe, R. (1979). Physical and engineering properties of copper tailings. *Current Geotechnical Practice in Mine Waste Disposal, ASCE Monograph*.
- Wakeley, L., & Peterson, R. (2004). *comments to Peter Michael of the U.S. Office of Surface Mining Comments on the OSM Draft Report Entitled "The Flowability of Impounded Coal Refuse"*. Vicksburg, MS.: U.S. Army Engineer R&D Center Geotechnical and.
- West, T. (1995). *Geology applied to engineering*. Prentice Hall.
- Whitman, R., & Lambe, P. (1988). Earthquake like shaking of a structure founded on saturated sand. *Centrifuge 88, Corte ed, Balkema, Rotterdam*, 529-538.
- Whitman, R., & Ting, N. (1993). Experimental results for tilting wall with saturated backfill. *Verification of Numerical Procedures for the Analysis of Soil Liquefaction Problems*, 2, 1515-1528.

- Whitney, E., Moudgil, B., & Onoda, G. (1977). Dewatering of phosphatic clay wastes. *Report of Department of Material Science and Engineering, University of Florida.*
- Widodo, S., & Ibrahim, A. (2012). Estimation of Primary Compression Index (Cc) Using Physical Properties of Pontianak Soft Clay. *International Journal of Engineering Research and*, 2(5), 2232-2236.
- Wilson, S., & Marsal, R. (1979). Current trends in design and construction of embankment dams. *prepared for International Commission on Large Dams and Geotechnical Division of the American Society of Civil Engineers . New York: American Society of Civil Engineers.*
- Wilson, S., & Taylor, A. (1996). The channel entry problem for a yield stress fluid. *Journal of Non-Newtonian Fluid Mechanics*, 65, 165-176.
- Worth, C., & Wood, D. (1978). The correlation of Index Properties with Some Basic Engineering Properties of Soils. *Canadian Geotechnical Journal*, 15, 137-145.
- Woskoboenko, F., Siemon, S., & Creasy, D. (1989). The rheology of Victorian brown coal slurries: 2. Effect of pH. *Fuel*, 68, 120-124.
- Wu, K., Owens, H., & Fredland, J. (2003). MSHA's Review of Impoundment Plans. *Presentations, International Workshop on Seismic Stability of Tailings Dams.*
- Xia, Y., Wang, W., & Xu, Z. (2009). Numerical Computation of Laminar Flow Pipeline Transport Axial Flow Field. *Information Technology and Computer Science*, 2, 196-199.
- Zeng, X. (2003). Challenges in seismic stability analysis of tailings dams. *International Workshop on Seismic Stability of Tailings Dams, Case Western Reserve University, Cleveland, OH.*
- Zeng, X. W. (1998). Influence of viscous fluids on properties of sand. *Geotechnical Testing Journal*, 21(1), 45-51.
- Zeng, X., Wu, J., & Rohlf, R. (1998a). *Modeling the seismic response of coal-waste tailings dams.* Geotechnical News, 29-32.
- Zeng, X., Wu, J., & Rohlf, R. (1998b). *Seismic stability of coal-waste tailings dams.* Geotechnical Earthquake Engineering and Soil Dynamics III, 951-961.
- Zeng, X., Wu, J., & Rohlf, R. (1998c). Response of coal-waste tailings dams under simulated earthquake loading. *Proceedings of Centrifuge 98, Tokyo, Japan*, 255-260.
- Zhang, H., & Ren, Z. (1982). Discussion of resistance of hyperconcentrated flow in open channels. *Scientia Sinica (Series A)*, 1332-1342.

Zook, R., Olup, B., & Pierre, J. (1974). *Engineering evaluation of coal refuse slurry impoundments*. AIME Annual Meetingm Dallas, Texas.